A Bayesian Statistics Approach to Updating Finite Element Models with Frequency Response Data

by

Brian E. Lindholm

Dissertation submitted to the Faculty of the
Virginia Polytechnic Institute and State University
in partial fulfillment of the requirements for the degree of

Doctor of Philosophy
in
Mechanical Engineering

APPROVED:

Dr. Robert L. West, Jr.

Dr. Rakesh K. Kapania

Dr. Charles E. Knight

Dr. Larry D. Mitchell

Dr. Alfred L. Wicks

August, 1996
Blacksburg, Virginia

Keywords: bayesian, regression, parameter estimation, model updating

LD
5655
V856
1996
L563
c.2

A BAYESIAN STATISTICS APROACH TO UPDATING FINITE ELEMENT MODELS WITH FREQUENCY RESPONSE DATA

by

Brian E. Lindholm

Dr. Robert L. West, Jr. Chairman
Mechanical Engineering

(ABSTRACT)

This dissertation addresses the task of updating finite element models with frequency response data acquired in a structural dynamics test. Standard statistical techniques are used to generate statistically qualified data, which is then used in a Bayesian statistics regression formulation to update the finite element model. The Bayesian formulation allows the analyst to incorporate engineering judgment (in the form of prior knowledge) into the analysis and helps ensure that reasonable and realistic answers are obtained. The formulation includes true statistical weights derived from experimental data as well as a new formulation of the Bayesian regression problem that reduces the effects of numerical ill-conditioning.

Model updates are performed with a simulated free-free beam, a simple steel frame, and a cantilever beam. Improved finite element models of the structures are obtained and several statistical tests are used to ensure that the models are improved.

Acknowledgements

Many thanks are owed to my advisor, Dr. Robert West, for his unfailing support and belief in what I was doing. His ability to see "the bigger picture" helped me go further than I ever thought possible.

I thank Dr. Larry Mitchell for his guidance on the experimental work, and I thank Dr. Rakesh Kapania, Dr. Charles Knight, and Dr. Alfred Wicks for helping me keep some perspective on what I was trying to do. I also thank all of them for helping me make sure that my work applied to the tricky cases as well as the friendly ones.

Special thanks are also due to Dr. Jeffrey Birch, who taught me so much of the statistics that I use, and to Dr. Calvin Ribbens, who taught me how to do *big* matrix problems on the computer. I also thank Dr. David Montgomery, who got me started on the signal processing statistics, and Randall Mayes of Sandia National Labs, who helped me try out my ideas on a "real-world" structure.

And finally, I would like to thank my friends Elizabeth Besteman and David Coe for their friendship and emotional support during the crunch at the end.

This material is based upon work supported in part under a National Science Foundation Graduate Fellowship. Any opinions, findings, conclusions, or recommendations expressed in this publication are those of the author and do not necessarily reflect the views of the National Science Foundation.

Table of Contents

Abstract ii
Acknowledgements iii
Table of Contents iv
List of Figures viii
List of Tables x
Nomenclature xii

Part I: Introduction and Literature Review

Chapter 1: Introduction 2
1.1: Model Updating 2
1.2: Research Goals 4
1.3: Research Hypothesis 4
1.4: Research Objectives 5
1.5: Scope of Research 7
1.6: Contributions of Research 9
1.7: Structure of the Dissertation 11

Chapter 2: Literature Review 14
2.1: Model Update Categorization 14
2.2: Recent Work in the Literature 19
2.3: Comments on the Literature 29
2.4: Other Relevant Work 32

Part II: Basic Statistical Theory

Chapter 3: Bayesian Statistics 35
3.1: Ordinary Least-Squares 35
3.2: Maximum Likelihood Estimation 37
3.3: Maximum a Posterior Estimation 42
3.4: Additional Comments on Statistics 47
3.5: The Core Equations 50

Chapter 4: Update Parameters 51
4.1: Model Update Parameters 51
4.2: Bayesian Priors 53

Chapter 5: Sine-Dwell Statistics 56
5.1: Sine-Dwell Test Data 56
5.2: Relative Response Statistics 60
5.3: Is Sine-Dwell Data Normally Distributed? 65
5.4: Assembling Sine-Dwell Data 70

Chapter 6: Frequency Response Function Statistics 73
6.1: FRF Test Data 73
6.2: FRF Statistics 75
6.3: The FRF Data Normally Distributed? 81
6.4: Assembling FRF Data 82

Chapter 7: Finite Element Predictions 85
7.1: Finite Element Modeling 85
7.2: Generating the Prediction Vector 87
7.3: Generating the Sensitivity Matrix 91
7.4: Concluding Remarks 93

Part III: "Quality Control" Issues

Chapter 8: Computational Issues 95
8.1: Matrix Decompositions 96
8.2: Parameter Rescaling 97
8.3: Bayesian Regression Reformulation 99
8.4: Step Size Determination 101
8.5: Convergence Testing 102
8.6: Computation Time 103
8.7: Concluding Remarks on Numerical Issues 104

Chapter 9: Model Update Verification 106
9.1: Time-Invariance Testing 106
9.2: Lack-of-Fit Testing 110
9.3: Parameter Consistency Testing 113
9.4: Cross-Validation Testing 115

Chapter 10: Visualization Statistics 117
10.1: Sine-Dwell Visualization Statistics 117
10.2: FRF Visualization Statistics 119

Part IV: Case Studies

Chapter 11: The Simulated Beam 121
11.1: Simulation Overview 121
11.2: Simulation Results 124

Chapter 12: The Sandia Test Frame 129
12.1: Preliminary Issues 129
12.2: Sine-Dwell Study 134
12.3: FRF Study 144
12.4: Concluding Remarks on Sandia Test Frame 152

Chapter 13: The Cantilever Beam 154
13.1: Preliminary Issues 154
13.2: Model Updating Results 163
13.3: Concluding Remarks on the Cantilever Beam 171

Part V: Conclusions and Recommendations

Chapter 14: Conclusions and Recommendations 174
14.1: Conclusions 174
14.2: Recommendations for Future Work 176

References 180

Appendices

Appendix A: Estimation Methodologies 190
Maximum Likelihood Estimation (MLE) 190
Maximum a Posterier (MAP) Estimation 191

Appendix B: FFT Orthogonality 194

Appendix C: Model Update Algorithm 197

Appendix D: Using the Scanning LDV 199

Appendix E: Cantilever Beam Priors 201
Clamp Stiffnesses 201
Beam Thickness and Width 202
Tip Inertias 202
Stinger Stiffness 204

Vita 205

List of Figures

Figure 2.1: Categories of Model Updating Algorithms 15
Figure 2.2: Regression Analysis Choices 18
Figure 2.3: Model Updates Using Modal Data 29
Figure 2.4: Model Updates Using FRF Data 31

Figure 3.1: Ordinary Least-Squares Solutions 40
Figure 3.2: Weighted Least-Squares Solutions 41
Figure 3.3: Confidence Region from Weighted Regression 45
Figure 3.4: Confidence Region from Prior Knowledge 45
Figure 3.5: Confidence Region from Bayesian Regression 46

Figure 5.1: Sample Time-Series Data 57
Figure 5.2: Monte Carlo Simulations, Set #1 66
Figure 5.3: Monte Carlo Simulations, Set #2 68
Figure 5.4: Sample y Vector from Sine-Dwell Data 71
Figure 5.5: Sample f Vector from Sine-Dwell Data 72

Figure 6.1: FRF Monte Carlo Results 78
Figure 6.2: FRF Variance Comparison 78
Figure 6.3: Sample y Vector from FRF Data 83
Figure 6.4: Sample f Vector from FRF Data 84

Figure 7.1: Sensor Orientation Example 88

Figure 9.1: Force Amplitude Residuals 108

Figure 11.1: Analytical Beam Model 121
Figure 11.2: Visualization Statistics before Update 125
Figure 11.3: Visualization Statistics after Update 126

Figure 12.1: Sandia Test Frame 129
Figure 12.2: NASTRAN Model of Frame 131
Figure 12.3: Variances of Sine-Dwell Data 136
Figure 12.4: Visualization Statistics from Initial Model 138
Figure 12.5: Visualization Statistics after Preliminary Update 139

Figure 12.6: Visualization Statistics after Intermediate Update . . . 140
Figure 12.7: Visualization Statistics after Final Update 141
Figure 12.8: Variances of FRF Data 146
Figure 12.9: Initial Model FRF Comparison 147
Figure 12.10: Additional Initial Model FRF Comparison 148
Figure 12.11: Final Model FRF Comparison 149
Figure 12.12: Additional Final Model FRF Comparison 149

Figure 13.1: Cantilever Beam Setup 155
Figure 13.2: Clamp Schematic 155
Figure 13.3: FE Model of Cantilever Beam 156
Figure 13.4: Data Acquisition Pattern 159
Figure 13.5: Variances of Data from Cantilevered Beam 160
Figure 13.6: Evidence of Time-Variation in 450 Hz Data 162
Figure 13.7: Visualization Statistics from Initial Model 166
Figure 13.8: Visualization Statistics after Final Update 167
Figure 13.9: Low Frequency Response Shape 168
Figure 13.10: High Frequency Response Shape 168

Figure E.1: Test Configuration for Effective Mass Testing 203

List of Tables

Table 1.1: Key Questions for Model Updating 4

Table 3.1: Data for Weighted Regression Example 39
Table 3.2: Priors for Regression Example 44

Table 4.1: Example of Prior Information 54

Table 5.1: The Multivariate Delta Method 62

Table 9.1: Durbin-Watson Critical Values 109
Table 9.2: Critical Chi-Squared Values 115

Table 11.1: Update Parameter Target Values 122
Table 11.2: Excitation Frequencies 122
Table 11.3: Prior Knowledge about Parameters 123
Table 11.4: Simulation Results 124
Table 11.5: Improved Prior Knowledge 128
Table 11.6: Update Results from Improved Priors 128

Table 12.1: Sandia Test Frame Update Parameters 132
Table 12.2: Excitation Frequencies 135
Table 12.3: Parameter Estimates from Sine-Dwell Test 142
Table 12.4: Reduced Parameter Results: Sine-Dwell 143
Table 12.5: Parameter Estimates from FRF Test 150
Table 12.6: Reduced Parameter Results: FRF 151

Table 13.1: Cantilever Beam Update Parameters 157
Table 13.2: Excitation Frequencies 158
Table 13.3: Time-Invariance Testing Results 161
Table 13.4: Parameter Estimates from Cantilever Beam 164
Table 13.5: Reduced Parameter Results: Cantilever Beam 165
Table 13.6: Cantilever Beam Natural Frequencies 170

Table B.1: FFT / Least-Squares Equivalency Script 194
Table B.2: Equivalency Script Output 195
Table C.1: Model Update Algorithm 197
Table D.1: LDV Registration Results 200

Nomenclature

n_y	number of total data points
n_m	number of measurements locations (with index i)
n_e	number of excitation locations (with index j)
n_f	number of fundamental excitation frequencies (with index k)
n_h	number of total harmonics fitted (with index l)
n_t	number of time-samples in a data block
n_a	number of averages used in FRF estimation

Bayesian Statistics

$\boldsymbol{p}$	vector of modeling parameters
$\boldsymbol{p}_0$	vector of prior estimates of modeling parameters
$\hat{\boldsymbol{p}}$	vector of updated parameter estimates
$\boldsymbol{W}_p$	prior weighting matrix
$\boldsymbol{y}$	data vector
$\hat{\boldsymbol{y}}$	predicted data vector
$\boldsymbol{W}_y$	data weighting matrix
$\boldsymbol{z}$	vector for additional quantities
$\hat{\boldsymbol{z}}$	predicted vector for additional quantities
$\boldsymbol{W}_z$	weighting matrix for additional quantities
$\boldsymbol{X}$	prediction sensitivity matrix

Modal Parameters

ϕ_r	mode shape of rth mode at point s
$\omega_{r,s}$	natural frequency of rth mode
ζ_r	viscous damping ratio of rth mode

Sine-dwell Statistics

$\boldsymbol{e}$	time-series data vector from excitation signal
$\boldsymbol{r}$	time-series data vector from response signal
$\boldsymbol{X}$	regressor matrix
$\boldsymbol{a}$	vector of excitation coefficients
$\boldsymbol{A}$	vector of excitation amplitudes
$\boldsymbol{b}$	vector of response coefficients
$\boldsymbol{B}$	vector of response amplitudes
$\boldsymbol{c}$	vector of <u>relative</u> response coefficients signal

FRF Statistics

F_k	FFT of excitation data
X_k	FFT of response data
$G_{ff,k}$	excitation autospectrum estimate
$G_{xx,k}$	response autospectrum estimate
$G_{xf,k}, G_{fx,k}$	cross-spectrum estimates
H_k	FRF estimate (usually H_1)
γ_k	coherence function

Finite Element Modeling

$\boldsymbol{K}$	finite element stiffness matrix
$\boldsymbol{M}$	finite element mass matrix
$\boldsymbol{C}$	finite element viscous damping matrix
γ	structural damping ratio
$\boldsymbol{u}$	dynamic response vector
$\boldsymbol{F}$	dynamic force vector
$\boldsymbol{g}$	dynamic force residual vector

Matrix Decompositions

$\boldsymbol{Q}, \boldsymbol{R}$	matrices from the QR matrix decomposition
$\boldsymbol{C}$	matrices from the Cholesky decomposition

Simulated Beam

k_t	translational stiffness
c_t	translational viscous damping
k_r	rotational stiffness
c_r	rotational viscous damping

Sandia Test Frame

$k_{t,x}$	translational joint stiffness
$k_{t,y}$	translational joint stiffness
$k_{t,z}$	translational joint stiffness
$k_{r,x}$	rotational joint stiffness
$k_{r,y}$	rotational joint stiffness
$k_{r,z}$	rotational joint stiffness
A	cross-section area
I_1	major area moment of inertia
I_2	minor area moment of inertia
J	torsional moment of inertia
γ	structural damping ratio

Cantilever Beam

k_r	translational clamp stiffness
k_t	rotational clamp stiffness
E	modulus of rigidity
ρ	density
γ	structural damping ratio
t	thickness of beam
w	width of beam
m_t	effective transducer mass
I_t	effective transducer rotatory inertia
k_s	stinger rotational stiffness

PART I:

Introduction and Literature Review

Chapter 1: Introduction

1.1 Model Updating

When accounting for the dynamic behavior of a structure in engineering design, it is helpful to have a finite element model of the structure available for prediction purposes. This enables the designer to determine the effects of *changes* made to the structure without having to actually build a modified structure. Indeed, this is one of the main objectives of using the finite element method.

However, finite element models of structures do not always accurately predict the behavior of the structure. This can happen if there are modeling errors present in the finite element model. Examples of such errors include the use of inaccurate estimates of material properties, the use of poor thickness or dimension estimates, or improper modeling of the boundary conditions of the system. If errors are present in the model, then errors will be present in *predictions* made by the model. The model will not be suited for *quantitative* behavior prediction; at best, it can only be used for *qualitative* behavior prediction. In extreme cases, it may not even be good for qualitative prediction purposes.

Unfortunately, it is not easy for the analyst to create a sufficiently accurate finite element model of a given structure. This is especially true when there is considerable uncertainty present in the modeling parameters used to build the finite element. For example, the elastic modulus of the structure material may not be precisely known, or

the boundary condition model that should be used to model a clamp holding the structure may not be known.

One method of dealing with these difficulties is to *update* the modeling parameters using data from a structural dynamics test. An effective model update procedure will cause the revised model to better predict the experimental data acquired in the test. Additionally, the model update procedure should provide evidence that the model has genuinely been *improved*, as opposed to having been manipulated to fit only the *specific* set of data used to perform the model update.

Using *Bayesian statistics* with *frequency response data* is a particularly suitable framework for performing such model updates. Bayesian statistics provides a formal methodology for incorporating prior knowledge about a system into the model update process, and it also provides a framework for describing *how good* the results of the model update process are. These considerations help ensure that reasonable and realistic changes are made to the finite element model.

A significant amount of research has been dedicated to this problem in the past, but most of it has been oriented around approaches utilizing the results of experimental modal analysis. An overview of relevant literature on the FE update problem is presented in Chapter 2. While most of the techniques in the literature work with modal test data, the use of frequency response data lends itself more easily to a formal statistical analysis, as will be shown in Part II of the dissertation.

1.2 Research Goals

The primary goal of the research presented in this dissertation is to substantially *improve* the predictive capability of a finite element model by updating the model with frequency response data acquired in a structural dynamics test. However, the process of updating a model with test data is not simple, and there are a number of questions that must be addressed. A list of these questions is given in Table 1.1.

Table 1.1: Key Questions for Model Updating

How can the test data be used most effectively?
How can the quality of the model update be described?
Is there a way to compensate for highly variable noise levels in the data?
How can "engineering judgement" be included?
Is there a way to ensure that the predictive capabilities of the model go beyond simply predicting the specific data set used to update the model?
Does the model update procedure provide unique/consistent answers?
Does the model update reflect physical reality?

The issues of Table 1.1 comprise the secondary goals of this dissertation. If the answers to these questions are incorporated into the model update process, the analyst will be much more confident that the model has been truly improved.

1.3 Research Hypothesis

The fundamental hypothesis of this research is that analytical models of structures can be effectively updated if the update problem is formulated as a *Bayesian* regression problem in which estimates of *modeling parameters* are updated. Comparisons are made *directly* between frequency response measurements and analytical predic-

tions of those same measurements, with statistical weights being used to make the comparison as efficient as possible (minimizing errors in the final parameter estimates). *Prior* information concerning the design parameters is also incorporated, helping ensure that parameter estimates are reasonable and realistic. The Bayesian formulation also provides a framework for describing the quality of the updated parameter estimates and for performing statistical tests that help ensure the validity of the model update.

1.4 Research Objectives

In order to meet the goals of this research, a number of objectives must be achieved. The bulk of the work is oriented around the model update problem formulation with a Bayesian statistics framework. Also, consideration is given to the parameter selection and modeling process.

Identify Design Parameters

The identification of erroneous modeling parameters is perhaps the most important part of the model update process. These modeling parameters typically concern structure size and shape, material properties, and boundary conditions. Unfortunately, there are no simple guidelines for selecting the parameters to be updated, and the issue must be addressed on a case-by-case basis.

Comparing Test Results to Analysis

The method used to compare test data to finite element model predictions is the defining characteristic of a model update algorithm. In this research, Bayesian statis-

tical theory is used to develop a weighted sum-of-squares error term that represents the differences between the test and analysis. The resulting formulation for estimating modeling parameter values is called a *Bayesian regression formulation*.

Incorporate Sources of Uncertainty

The model update formulation will be most effective if it accounts for as many sources of uncertainty into the process as possible. These sources include variable noise levels on the data and uncertainty in parameter estimates used to generate the initial model. Statistical tools such as the multivariate delta method are used to generate estimates of mean and variance for the data, while Bayesian priors contain estimates of the mean and variance of the initial parameter estimates used to generate the model. A lack-of-fit analysis is used to compensate for sources of uncertainty that may have been neglected, such as miscalibration errors or model form errors.

Describe Quality of Results

The Bayesian regression formulation provides standard methods for computing confidence intervals and correlation matrices for the updated parameter estimates. Visualization techniques are also developed in order to demonstrate how well the model predicts the *shape* and *amplitude* of the dynamic response of the structure.

Verify Results

Methods of verifying the model update include performing data quality tests and cross-validation tests. Specifically, time-invariance tests are performed *before* the model update to ensure that the data used is valid. Cross-validation techniques are

used *after* the model update to ensure that the updated mode is capable of fitting other data sets beyond the specific set used to perform the model update. Parameter consistency checks are also performed after the model update to help ensure that reasonable and realistic parameter estimates have been obtained.

Perform Model Updates on Actual Problems

The Bayesian regression formulation developed in this dissertation is used on three different model update problems. The first problem is a simulated beam in which boundary condition parameters are updated. The second is a steel frame in which joint stiffness and beam cross-section parameters are updated. The third problem is a cantilever beam in which boundary condition parameters representing a clamp are updated.

1.5 Scope of Research

The potential scope of research involving model updating is very broad. However, the research performed for this dissertation was strategically restricted in order that the most relevant research items could be investigated thoroughly.

Structure complexity

The test articles used in this research were of relatively simple geometry, i.e., beams or simple frames. Updating a finite element model of a more complex structure would have been more interesting and intellectually satisfying, but for purposes of testing a new model update methodology, it was best to start with simple and well-understood problems.

Modeling technique

The only modeling technique used in this research was the finite element method. Transfer matrix methods or Rayleigh-Ritz methods could also have been used, but the basic model update formulation would not have changed.

Testing methodology

Data was obtained from the test structures using broad-band FRF testing (accomplished with an impact from a modal test hammer) and single frequency sine-dwell testing (accomplished with a sinusoidally driven electromagnetic shaker). Other testing techniques such as swept-sine testing or burst-random testing could have been used, but these would not have changed the model update formulation.

Transducer types

Data was acquired from structures using either accelerometers or a scanning laser-Doppler vibrometer (SLDV). Other types of experimental data, such as strain gauge measurements, could have been incorporated but were not due to time considerations.

Parameter types

The update parameters included isotropic material properties, beam cross-section properties, and structural damping coefficients. Boundary condition parameters were also included. While this is a fairly complete list, most of these parameters focus on global properties of the structure. An element-by-element model update (requiring one or more parameters for each element) would be very useful for damage detection purposes, as would a thickness-profiling study based on spline control-point parameters,

but these problems are large and complex enough to be addressed in dissertations of their own. They are not addressed here.

1.6 Contributions of Research

Development of a True Bayesian Statistics Formulation

The Bayesian statistics regression formulation has appeared in numerous papers in the literature. However, many of these methods are done only in a Bayesian statistics "style" rather than in a true Bayesian formulation. Specifically, the Bayesian statistics approach requires weighting matrices for both data and prior information. In much of the literature, arbitrary weighting matrices such as $W = I$ are used, or the issue of weighting matrices is ignored entirely. In this research, the data weighting matrix comes from the initial signal processing done on the raw time signals, while the weighting matrix for the Bayesian priors comes from variance estimates describing the initial quality of the parameters used to model the system under study. Other measurements taken from the system can also be incorporated into the analysis.

Using a data-based weighting matrix is statistically optimal in the sense that it uses the data as efficiently as possible, providing *minimum variance* parameter estimates. Additionally, it allows the analyst to use data with highly variable noise levels without user intervention. This capability is particularly useful with working with scanning laser-Doppler vibrometer (SLDV) data and shaker-based FRF data. In the case of SLDV data, time-domain response signal drop-outs can be a problem, while

frequency-domain force autospectrum drop-outs can be a problem in shaker-based FRF data.

Statistics for Multi-Frequency Sine-Dwell Data

A second major contribution of this work is the development of statistically qualified response coefficients that are used to describe time-series data coming from a structural dynamics test in which *multiple* excitation frequencies are used. Prior work has focused on cases in which only a single excitation frequency is used.

Reformulation of the Bayesian Statistics Problem

In order to implement the Bayesian regression formulation on a computer, the problem has to be reformulated to alleviate the effects of ill-conditioning. This is accomplished with the use of modern matrix decompositions and a reformulation of the Bayesian regression problem that makes it numerically equivalent to an ordinary least-squares problem.

Development of a Lack-of-fit Testing and Compensation

A third contribution of the work presented in this dissertation is the lack-of-fit test. This test provides a statistically rigorous method of determining whether or not it is possible to better fit the data. If the test statistic comes out as insignificant, the analyst can conclude that the model fits the model as well as can *possibly* be expected, and that there is no point in trying to further refine the model. However, a significant test statistic indicates that there may still be a model that better matches the data.

Additionally, it is possible to downweight data residuals in the Bayesian regression formulation to *compensate* for the presence of lack-of-fit. This ensures that the prior information provided by the analyst still has an effect in the analysis and that unrealistically small confidence interval sizes are not computed. This is particularly important in evaluating the model in cases where the number of data points overwhelmingly outnumbers the number of pieces of prior information.

Model Update Verification Procedures

A fourth area of contribution includes two model verification tests used to ensure that the model update is valid. The first test is a time-invariance test performed on the test data before the model update, which helps ensure that the data are valid. The second is a cross-validation test performed after the model update to ensure that the model has predictive capabilities that go beyond the specific data set used to update the model.

1.7 Structure of The Dissertation

This dissertation is broken into five major parts: (I) introduction and literature review; (II) basic statistical theory used to update models; (III) issues concerning "quality control," including computer implementation issues and statistical techniques used to verify the model update; (IV) model update case studies, both simulated and experimental; and (V) conclusions and recommendations.

Part I of the dissertation consists of Chapter 1 (this introductory chapter) and Chapter 2, the literature review. In the literature review, an overview of the many

model update algorithms that exist is presented. Particular attention is paid to those algorithms that address statistical issues.

Part II deals with the basic statistical theory used to update finite element models. Specifically, Chapter 3 provides an introduction to the use of Bayesian statistics in regression problems, which is the basic framework on which this dissertation is based. Chapter 4 provides an explanation of the update parameters typically used in a model update approach based on Bayesian statistics. This chapter also explains what statistical *priors* are and how they are obtained. Chapter 5 discusses how time-series data from a sine-dwell test is processed to generate statistically-qualified (having both mean and variance information available) frequency response data to be used by the model update algorithm. Chapter 6 presents similar results for broad-band frequency response function (FRF) data. Finally, Chapter 7 discussed how the finite element method is used to compute analytical predictions of the test data along with parameter sensitivities of the predictions.

Part III of the dissertation deals with "quality control" issues, both numerical and statistical. Chapter 8 discusses a number of computational and numerical concerns relating to the computer-based implementation of the Bayesian statistics model update formulation. Chapter 9 presents a number of statistics-based tools for testing the quality of the input data and for determining whether or not the updated model has been *improved*. Finally, Chapter 10 presents a number of visualization statistics that help provide insight into the changes made to the model.

Part IV of the dissertation presents three case studies, one using simulated data and two using experimental data. Chapter 11 presents a simulated study in which boundary condition parameters are estimated using sine-dwell data. A Monte Carlo study is also performed to confirm variance estimates. Chapter 12 presents an experimental study in which joint stiffness parameters used in a finite element model of a frame are updated using both sine-dwell data and FRF data. Chapter 13 presents an experimental study in which boundary condition parameters representing the effects of a steel clamp on a cantilever beam are estimated using sine-dwell data. This study is more complete than the steel frame study of Chapter 12, as more of the statistical tests of Chapter 9 are used here.

Part V, consisting of only Chapter 14, provides a brief summary of conclusions and a list of recommendations for future work.

Chapter 2: Literature Review

INTRODUCTION

The subject of updating finite element models using experimental test data is well represented in the literature, with hundreds of papers being available on the subject. In this chapter, a general overview of these various model update techniques is presented, followed by a more detailed discussion concerning recent work in this area. The chapter concludes with references to other works relating to the research presented in this dissertation.

2.1 MODEL UPDATE CATEGORIZATION

The numerous model update procedures discussed in the literature can be categorized according the *type* of algorithms used. Specifically, there are three basic characteristics that can be used to categorize a model update algorithm: (1) the type of test data used; (2) the means by which test data are compared to analysis; and (3) the methodology used to updating the finite element (FE) model. The primary options for each of these selections is shown below in Figure 2.1. Highlighted in gray are the options used in this disseration.

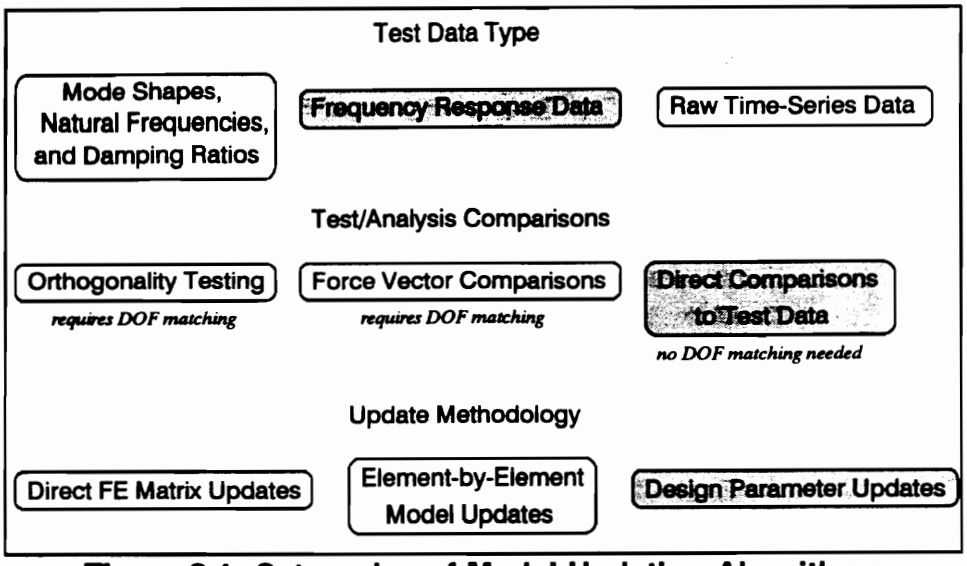

Figure 2.1: Categories of Model Updating Algorithms

Types of Test Data

Modal test data, typically coming in the form of the modal parameters ω_r (natural frequency), ξ_r (viscous damping ratio), and $\phi_{r,s}$ (mode shape) are perhaps the most common type of data used in model updating. Modal parameters are usually obtained from a polynomial-based fit of FFT-based frequency response function (FRF) data. Many other model update algorithms work directly with the FRF data. Finally, a few algorithms work directly with raw time-series data. This last category of algorithms is much less common and is typically restricted to problems found in controls.

Test-Analysis Comparison Techniques

If the data to be used in the model update is comprised of modal parameters, there are a number of options for comparing the model to the test data. An older technique (less commonly used now except for visualization purposes) is the cross-orthogonality matrix $\boldsymbol{Z}$ given in Eq. (2.1). If the test and analysis match perfectly, the matrix $\boldsymbol{Z}$

will equal an identity matrix. A model update algorithm used here would have the objective of minimizing the differences between $\boldsymbol{Z}$ and $\boldsymbol{I}$ (most often in a Frobenius norm sense, i.e., minimize $SSE = \sum_{i=1}^{n_r} \sum_{j=1}^{n_r} (z_{ij} - \delta_{ij})^2$, where $\delta_{ij} = 1$ for $i = j$ and $\delta_{ij} = 0$ for $i \neq j$).

$$\boldsymbol{Z} = \boldsymbol{\Phi}_{test}^{\mathrm{T}} \boldsymbol{M} \boldsymbol{\Phi}_{FEM} \tag{2.1}$$

It should be noted that using Eq. (2.1) requires that the test and analysis degrees-of-freedom (DOF) be matched, since there are normally many more analytical DOF (which include both translation and rotation values at FE nodes) than experimental DOF (which typically include only translation measurements from small number of accelerometer locations). Degree-of-freedom matching is accomplished with either modal expansion, which expands the test data to match the analysis DOF, or with the use of model reduction, which collapses the finite element DOF to match those of the test. This will be discussed in more detail in Section 2.3.

Another comparison technique that can be used is the dynamic force residual. This comparison takes advantage of the fact that the excitation force and system response are related by the fundamental equation of motion of the system. For modal parameter data there are no applied loads, since modes correspond to free vibration. Thus, the force residual vector $\boldsymbol{g}_r$, defined in Eq. (2.2) for mode r, should be zero. Force residuals can also be computed for dynamic response shapes $\boldsymbol{u}_k$, which can be extracted directly from the FRF at frequency ω_k with an applied force of $\boldsymbol{F}_k$ at the appropriate location. This response-based force residual is defined in Eq. (2.3).

$$g_r \equiv \left(K - \omega_r^2 M\right)\phi_r \approx 0 \tag{2.2}$$

$$g_k \equiv \left(K + i\omega_k C - \omega_k^2 M\right)u_k - F_k \approx 0 \tag{2.3}$$

As with the cross-orthogonality matrix of Eq. (2.1), the objective of a model update algorithm would be to minimize the vector g, typically by minimizing $(g^T g)$ in a least-squares fashion. Again, degree-of-freedom matching is required via either modal expansion or model reduction.

A third approach to comparing test data to the finite element model is to *directly* compare model predictions to the test data, typically in a sum-of-squares error fashion. In a modal approach, this might involve direct comparisons between natural frequencies, e.g., $\sum_{r=1}^{n_r}\left(\omega_{data} - \hat{\omega}_{FEM}\right)^2$, or a more generalized approach involving direct comparisons between natural frequencies, mode shapes, and damping ratios simultaneously. With FRF data, analytical FRFs predicted using the model would be directly compared to the measured FRFs. Time-series data can compared to analysis in this fashion as well. In many direct comparison techniques, the residuals are weighted.

Model Update Methodologies

The final option used to categorize model update methods is the means by which the finite element model is updated. Many of the simplest update methods make *direct* modifications to individual entries of the FE mass and stiffness matrices. These methods are usually very efficient computationally, but have fallen somewhat out of favor because the results of direct matrix updates are difficult to interpret. The ever-

increasing power of computers has also reduced the need for such computationally efficient algorithms.

An alternative to direct mass and stiffness matrix updates are methods that update models at the finite element level. These algorithms are most often used for damage detection purposes. The computational expense is increased, but the results are easier to understand.

A final approach to updating finite element models is to update *modeling parameters* such as material modulus or thickness. Many different algorithms for parameter estimation exist, but most involve the use of an optimization algorithm or a regression algorithm to solve a least-squares type minimization problem. There are three types of least-squares formulations possible, as shown in Figure 2.2, with the research choices used in this dissertation being highlighted in grey.

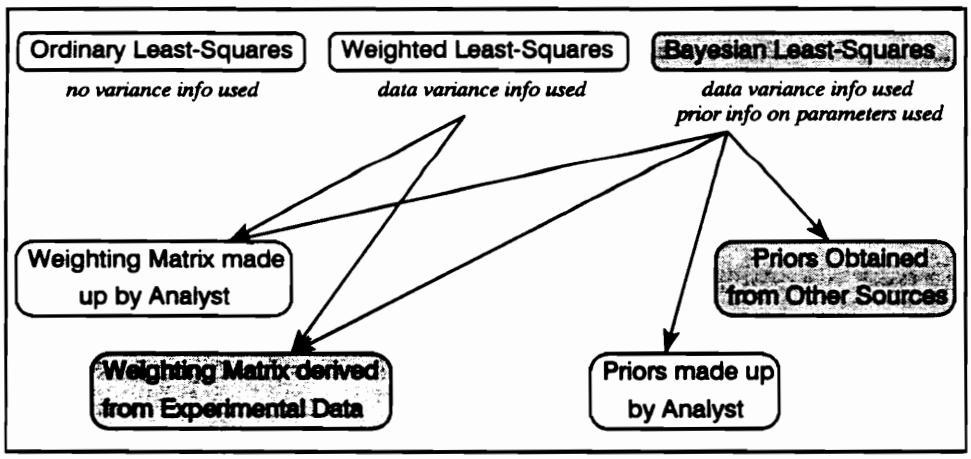

Figure 2.2: Regression Analysis Choices

Ordinary least-squares has been used a number of times in the literature, but a weighted least-squares analysis can be used if data variance information (necessary for

computing weights) is available. Furthermore, if prior information is available for the parameters being estimated, a *Bayesian* statistics analysis can be used.

2.2 Recent Work in the Literature

Overviews of Model Updating

Imregun and Visser [1] presented an extensive overview of model updating that began with common comparison techniques such as the modal assurance criterion (MAC) [2] and the coordinate modal assurance criterion (COMAC) [3], along with different model reduction and data expansion techniques. Direct FE matrix update methods were discussed, followed by methods using force residuals and orthogonality, and then by sensitivity-based parameter update methods. A preference for FRF-based parameter update approaches was indicated, since the FRF contains information on out-of-band modes and the lengthy modal analysis procedure is eliminated.

Baker [4] presented an overview that included test-analysis comparison techniques, model reduction techniques, direct matrix update algorithms, and parameter update algorithms. The bulk of the methods discussed involve the use of modal data, but reference was also made to methods using FRF data. The paper concluded with a number of practical suggestions for performing model updates with modal test data and recommended that model updates be used with simple, rapidly-solved models rather that large, detailed models.

Mottershead and Friswell [5] provided a very extensive survey of model updating that included direct matrix updates and various least-squares type analyses for use with both modal and FRF data (including the Bayesian statistics approach). The

survey also included discussions of *error localization* techniques, which are used to identify erroneous parameters or regions in a finite element model; *incompleteness* issues, where effective linear dependencies present in the data can interfere with effective parameter estimation; and *weighting matrices* to be used in weighted and Bayesian regression techniques. The paper ended with recommendations that more research be performed with larger, complex models, along with more research concerning the selection of a "most suitable" initial model from a set of candidate models. A slight preference for parameter estimation approaches that utilitize regularization and error localization techniques was indicated.

Link [6] provided an extensive list of possible sources of error in model update procedures. Experimental errors can arise from wrong measurements (perhaps caused by defective or miscalibrated tranducers), the influence of test equipment on results (such as tranducer mass-loading effects), inaccurate measurements (caused by random noise), and incomplete measurements (typically caused by insufficient spatial DOF or excitation frequencies). Modeling errors can arise from discretization errors, invalid element connectivity, improper modeling of a non-linear system as linear, physical modeling errors (such as incorrect material properties, inertias, and stiffnesses), and mismatched boundary conditions between the test and the model. All of these problems must be eliminated if good results are to be obtained, and statistics techniques can deal only with random noise in measurements and physical modeling errors.

Dascotte [7] discussed some of the issues that must be addressed in updating finite element models using modal test data. The importance of matching mode shapes from

test and analysis was stressed. A preference for model update methods that use design parameters instead of direct matrix updates was also indicated, as these methods provide more physical insight into the changes made. It was also recommended that sensitivity analyses be performed with the modeling parameters in order to determine which parameters should be excluded from the model update process.

Natke [8] presented an overview of model update techniques based on Bayesian statistics. Data types included FRF data, FRF-based dynamic force residuals, modal test data, and mode-based dynamic force residuals. The importance of having statistical weights was stressed, but no discussion of where weighting matrices might come from was included. Zhang [9] showed how update methods based on direct comparisons of modal data or FRF data can be formulated similarly, and how other approaches based on dynamic force residuals and orthogonality coefficients can also be formulated in a consistent fashion.

Degree-of-Freedom Matching

Although the research presented in this dissertation does not utilitize a degree-of-freedom (DOF) matching technique, many model update algorithms do and they are thus discussed here. DOF matching typically is needed for algorithms utilize cross-orthogonality measurements or dynamic force residuals, as mentioned in the previous section. The DOF matching techniques can be broken into two categories: (1) finite element model *reduction* techniques, and (2) experimental mode shape *expansion* techniques.

Model reduction techniques generate reduced finite element matrices that are called *test-analysis models* (TAMs), referring to the fact that the reduced model has degrees-of-freedom that correspond exactly with the test. The oldest model reduction method is the static TAM, developed by Guyan [10]. This method produces exact results for static loads, but errors are generated for dynamic loads. Kammer [11] developed the modal TAM, in which the analyst picks mode shapes from the original analytical model that the reduced model will match exactly. Kammer later updated the modal TAM to account for mode shapes not included in the reduced model by including mode shapes from the static TAM [12]. O'Callahan [13] developed the improved-reduced system (IRS) TAM, which is similar to the static TAM but includes correction terms that account for the inertial effects of the missing DOF. Gordis [14] studied the IRS TAM and concluded that it was most effective when the natural frequencies of the omitted DOF are higher than those of the DOF included in the reduced model.

Freed and Flanigan [15] compared the static, modal, hybrid, and IRS TAMs using two numerical and two experimental case studies. They concluded that the IRS and hybrid TAMs work best, achieving accuracy and robustness more often than the other two. The topic of test-analysis models was studied further by Avitabile and Foster [12], who investigated test-analysis models in the context of performing comparisons with the MAC, COMAC, enhanced COMAC [16], and cross-orthogonality matrix.

An alternative approach to model reduction is mode shape expansion, where the DOF of the test data are expanded to match those of the finite element model. Lieven

and Ewins [17] discussed three expansion techniques: (1) using cubic splines for interpolation; (2) modeling the test modes as linear combinations of FEM modes; and (3) inverting the static reduction process. The inverted static reduction process proved most effective. O'Callahan *et al* [18] later developed the System Equivalent Reduction Expansion Process (SEREP), which is a more generalized procedure that can be used for either data expansion or model reduction. The process was later extended such that expanded mode shapes were smoothed consistently [19].

Update Methods using Modal Data

Model update techniques which use modal test data are the most common. Earlier techniques performed direct updates of the finite element mass and stiffness matrices, resulting in very efficient algorithms that often matched the test data perfectly. Baruch and Bar Itzhack [20] developed one of the earliest direct matrix update algorithms, which did not preserve the structure of the original FE matrices. Kabe [21] developed an improved technique that preserved the connectivity of the finite element model but sometimes resulted in a loss of positive definiteness in the FE matrices. O'Callahan [22] presented four different direct matrix update techniques which updated mass and stiffness matrices based on various combinations of mode shape and natural frequency data. Aiad *et al* [23] used simulated complex-valued mode shapes and natural frequencies to perform global updates of finite element matrices. Conti and Bretl [24] developed a direct matrix update approach for using experimental modal data to determine the rigid-body properties in addition to mount stiffnesses. A more recent

work by Ahmadian *et al* [25] utilized a formulation that preserves the connectivity between nodes and retains the positive definiteness of the FE system matrices.

Analysts using orthogonality-based model update approaches include Niedbal and Luber [26], who combined orthogonality products and energy methods with substructuring techniques to perform model updates.

Analysts using least-squares type analyses (sometimes called inverse eigensensitivity techniques) include Jung and Ewins [27], who updated design parameters using direct eigenvalue and eigenvector comparisons. Ladeveze *et al* [28] used a similar approach, except that the residuals were downweighted by response magnitudes. Nobari and Ewins [29] discussed the effectiveness of using only natural frequencies in a least-squares type analysis rather than using both natural frequency and mode shape information. Lindholm and West [30] used only mode shape information in an ordinary least-squares context to determine boundary condition parameters.

Farhat and Hemez [31] used a least-squares type analysis with mode-based dynamic force residuals. FE models were updated using an element-by-element approach designed for damage detection purposes. Hemez [32] later updated the approach to use FRF data, and then extended the approach further [33] to also include static test data.

Bayesian Approaches using Modal Data

As shown in Figure 2.2, an alternative to the ordinary least-squares regression formulation is the Bayesian regression formulation, which is sometimes called *extend-*

ed weighted least-squares, *regularized least-squares*, or *maximum a posterior* estimation. Hasselman [34] provided an explanation of the philosophy behind Bayesian statistics in addition to providing detailed guidelines for interpreting the results of a Bayesian statistical analysis. Topics discussed included model improvement vs. manipulation, uniqueness of solutions, and qualification of the model for future use. Beliveau [35] provided formulations for using Bayesian statistics with modal data, FRF data, and raw time-series data. Sensitivity results were developed for all three data types. Link [36] discussed some issues concerning the Bayesian statistics formulation, including discretization errors, faulty modeling assumptions, and inconsistent boundary conditions. Dascotte *et al* [37] presented a number of different options for weighting matrices to use in a Bayesian statistics style formulation.

Hasselman and Chrostowski [38] used the Structural System Identification (SSID) code (developed at Sandia National Laboratories to update models with a Bayesian statistics formulation [39]) to perform model updates with modal test data coming from a large space truss. Martinez *et al* [40] discussed the use of different optimization algorithms within SSID to perform parameter estimation using Bayesian statistics. Other work using the SSID code was performed by Nefske and Sung [41], who updated joint stiffness parameters in a model of an engine cradle.

Antonacci and Vestroni [42] used the Bayesian statistics approach to update lumped-mass models of civil engineering structures. Link *et al* [43] updated a bridge model using a Bayesian statistics formulation with modal test data. Alvin [44] generalized the element-by-element formulation of Farhat and Hemez [31] to a

Bayesian statistics parameter update approach. Variance estimates on the original modal data were carried through the modal expansion procedure and transformed to determine variance estimates for the computed dynamic force residuals.

Update Methods using FRF Data

As shown in Figure 2.1, FRF data can be used for model updating instead of modal test data. Authors using direct FE matrix updates with FRF data include Larsson and Sas [45], who used a reduced model to generate a dynamic stiffness matrix (DSM) which was compared to the inverse of an FRF matrix generated from multi-frequency FRF data. Kritzen and Kiefer [46] used QR decomposition techniques with FRF data to localize errors in the FE mass and stiffness matrices. A more recent direct matrix update method presented by Zimmerman *et al* [47] uses rank-one modifications of the FE stiffness matrix for purposes of damage detection.

Berger *et al* [48] used dynamic force residuals, as given in Eq. (2.3), with expanded mode shapes to localize and correct errors in substructures. Missing DOF in the experimental data were filled in using static deflections in an expansion approach similar to an inverse of Kammer's hybrid TAM [12]. Also using FRF-based force residuals were Yang and Brown [49], who used a model reduction technique to study different methods of reducing the sensitivity of the model update process to the presence of damping in the structure, which is often difficult to model accurately. Schulz *et al* [50] used dynamic force residuals coming from FRF data in a weighted least-squares formulation to update a model of a truss. A similar formulation was presented by Schulz *et al* [51] for purposes of structural damage detection.

Friswell and Penny [52] used FRF data with the Kammer's modal TAM in a weighted least-squares problem in which damping and joint stiffness parameters were updated. A similar technique was developed by Conti and Donley [53], who used a TAM with FRF data to develop a linear least-squares model update formulation.

Imregun [54] compared model update results obtained with modal test data (using the inverse eigensensitivity technique of Zhang *et al* [55]) to model update results obtained with FRF data (using the dynamic force residual method of Visser and Imregun [56]). The effectiveness of each method was dependent on which modes or FRF lines were selected for use as data. Hybrid approaches, in which one technique was used to find preliminary parameter estimates for the other, were also investigated. The approach was expanded by Imregum *et al* [57] to utilize complex-valued FRF data in an element-by-element approach and was tested by Imregum *et al* [58] in a joint stiffness parameter estimation problem.

Cogan *et al* [59] presented a least-squares approach to updating finite element models with FRF data in which residuals were scaled by the original FRF magnitudes. This approach is equivalent to a weighted least-squares formulation in which noise levels are assumed to be proportional to magnitude. The importance of having a good initial model was particularly stressed.

Reix *et al* [60] predicted global damping coefficients using a two-staged weighted least-squares formulation that directly compared measured FRF data to the analytically predicted FRF. In the first stage, global mass and stiffness properties such as modulus and density were manually updated to make the model match the results of modal

parameters fitted from the FRF. The FRF data was then *directly* used in a weighted least-squares analysis to obtain the damping coefficients.

Bayesian Approaches using FRF Data

A couple of the papers using modal data in a Bayesian formulation also discussed how FRF data would be used in a Bayesian formulation. These included the works by Beliveau [35] and Link *et al* [43]. Additionally, Mottershead and Foster [61] used the Bayesian statistics approach with FRF data to improve the conditioning of a weighted least-squares process developed to estimate element stiffnesses in a cantilever beam.

Update Methods using Time-Series Data

Ibrahim *et al* [62] developed a method which used displacement, velocity, and acceleration measurements at a few instants in time to directly update the system matrices of the FE model. Harmonic excitation is used in order that velocity and displacement data can be derived directly from acceleration data. Bronowicki *et al* [63] proposed a Bayesian statistics formulation in which time-series data was directly used to update a model. Eigensolutions coming from the finite element model were used to predict the time-series data. Koh and See [64] use the extended Kalman filter (a controls-based time-series formulation that is equivalent to the Bayesian statistics formulation [65]) to estimate structural parameters from time-series data. Their procedure incorporated an adaptive filter that adjusted data variance estimates to ensure statistical consistency and to prevent underestimation of confidence interval sizes.

Model Updates with Other Types of Data

Mahnken and Stein [66] used *strain* measurements instead of displacement measurements for purposes of estimating viscoplastic damping parameters. The problem was initially formulated as a weighted least-squares problem, but regularization terms were then added that made the problem equivalent to a Bayesian statistics formulation.

2.3 Comments on the Literature

To summarize, there are *many* different model update methodologies described in the literature. However, there does seem to be a "common" model update technique that is used most often. A schematic of this approach is given below in Figure 2.3.

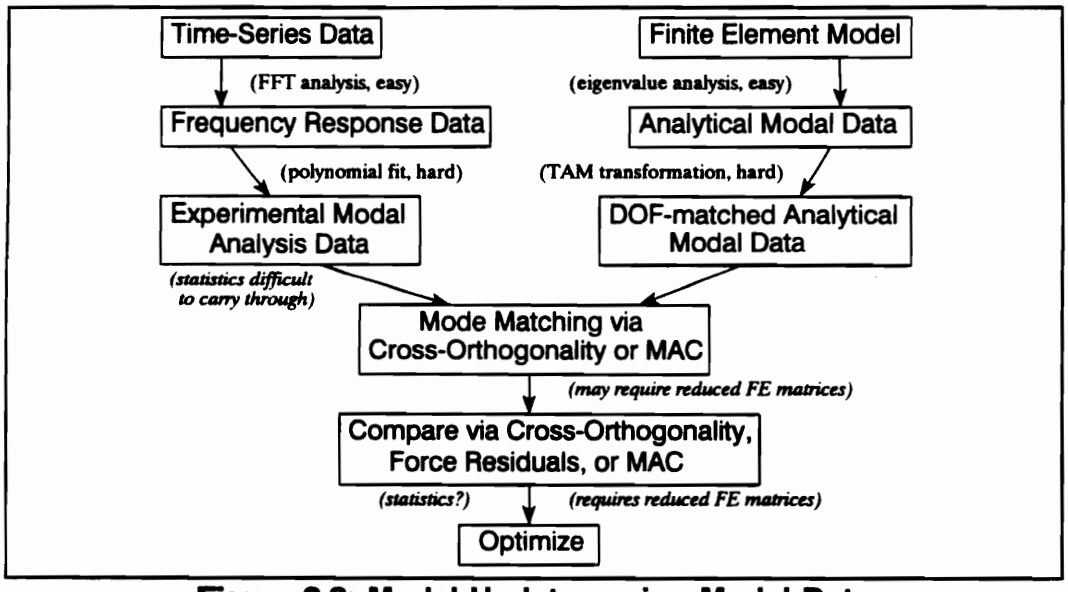

Figure 2.3: Model Updates using Modal Data

In Figure 2.3, the term "easy" means that a small number of well-understood algorithms are available for the purpose required. This does *not* mean that obtaining

unbiased FRF estimates from time-series data and computing eigensolutions for massive FE system matrices are trivial tasks. Indeed, there are several methods for estimating FRFs and several algorithms for computing the eigenvalues of large scale matrices, and these must be used properly. However, a competent analyst should be able to obtain correct results for these parts of the problem for almost any system.

The "hard" tasks, on the other hand, can become intractably difficult for certain systems. Extraction of modal parameters is typically performed with a polynomial-based fit, and a large number of algorithms exist for the purpose of performing that fit. These algorithms work quite well for many systems, but systems that have densely packed modes, nearly coupled modes, or heavy/non-proportional damping can cause modal analysis algorithms to fail. Additionally, only a few modal analysis algorithms carry through the statistics necessary to describe of the *quality* of the modal parameters extracted. One algorithm that does so was presented by Yoshimura and Nagamatsu [67].

Likewise, performing effective model reductions or test mode expansions can be very difficult for real-world structures. A poorly implemented TAM can fail to predict the natural frequencies and mode shapes of the original model; it can even introduce spurious modes into the analysis. This is particularly likely to happen if data is not acquired at a sufficient number of spatial locations or at improper locations. Mode shape expansion algorithms have similar problems. A final difficulty with the "common" approach is that it is difficult to carry statistical measures of quality all the way through the update process.

The approach being presented in this dissertation is somewhat simpler, as shown in Figure 2.4. The steps of experimental modal analysis, FE model reduction, and mode matching have all been eliminated. Additionally, it is relatively straightforward to carry statistics through the entire analysis.

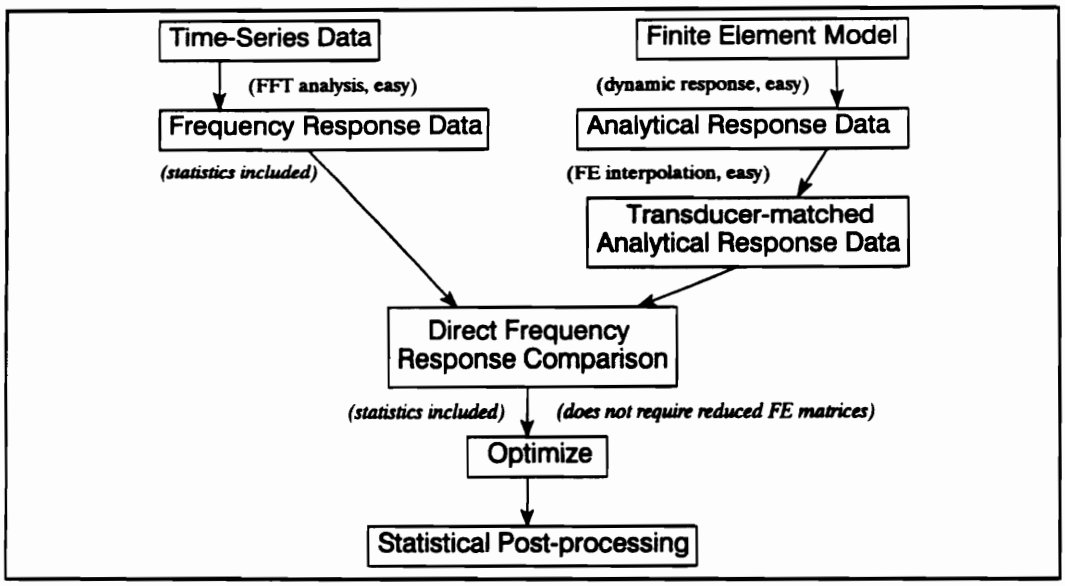

Figure 2.4: Model Updates using FRF Data

Many of the works presented in this literature review also utilitize a similar approach. Many analysts even use the same Bayesian statistics formulation that is used as the basis for the work of this dissertation. However, it appears that *nobody* (to the best of the author's knowledge) has used *estimated* weights for the purpose of updating a model, though Yoshimura and Nagamatsu [67] did use estimated weights for the purpose of estimating *modal parameters* from FRF data. Indeed, many authors simply assume $W_{data} = I$, while others do not address the issue at all. A number of authors, such as Beliveau [35], Dascotte *et al* [37], Link *et al* [43], Alvin [44], Schulz

et al [50], and Koh and See [64], address the issue of weighting matrices in considerable detail and present a number of schemes for generating them, but none describe how to estimate weights *directly* from experimental data.

2.4 Other Relevant Work

A key step in obtaining experimentally estimated weights is a statistical analysis of frequency response data. For sine-dwell data, this was addressed by Montgomery and West [68], who developed a method of variance estimation for frequency response coefficients coming from a sine-dwell test. Excitation and response signals are analyzed separately and then combined into statistically qualified *relative* response coefficients using the multivariate delta method. Montgomery *et al* [69] later verified the results using Monte Carlo simulations. Zeng and Wicks [70] compared the use of discrete Fourier transform techniques and linear regression techniques to fit sine-dwell data. Lopez Dominguez [71] also studied the issue of fitting sine-dwell data, using robust regression techniques to deal with time-domain drop-outs in time-series data coming from a laser Doppler vibrometer. A triggering strategy was used to estimate phase angle information.

Other authors have addressed the issue of estimating variances for FRF data. Bendat [72] developed a large number of formulae for estimating variances for FRF magnitude, phase angle, and coherence for the H_1 FRF estimator. Yoshimura and Nagamatsu [67] derived similar variance estimators for the H_v FRF estimator, though only for magnitude. The results were used as a source of statistical weights in a weighted least-squares modal parameter estimation procedure. Cobb [73] studied the

statistics of a three-channel FRF estimator in addition to providing guidelines on when certain variance estimators broke down.

Deaton *et al* [74] wrote a significant work on the use of estimated error variances in regression problems. They provided guidelines for when estimated weights *should* be used in a regression analysis and when they *should not* be used. Other works on this subject include papers by Williams [75] and Jacquez and Morusis [76]. Both provide guidelines for using estimated weights in least-squares problems.

Other basic references used in this work include a reference on basic statistics by Walpole and Myers [77], a reference on statistical regression techniques by Myers [78], a reference on parameter estimation by Beck and Arnold [79], a reference on large-scale matrix computations by Golub and Van Loan [80], a reference on signal processing techniques by Bendat [81], a reference on modal analysis by Ewins [82], a reference on the Monte Carlo method by Rubinstein [83], and references on the finite element method by Przemieniecki [84] and Bathe [85].

PART II:

Basic Statistical Theory

Chapter 3: Bayesian Statistics

INTRODUCTION

As discussed in the introduction, this dissertation is concerned with the task of updating finite element models with experimental data. More specifically, modeling parameters are to be updated using direct comparisons between experimentally acquired frequency response data and FEM-based analytical predictions of that same data. To this end, there are three common regression techniques that can be used to obtain statistically qualified parameters estimates: (1) ordinary least-squares regression; (2) maximum likelihood estimation (which is also known as weighted least-squares regression); and (3) maximum a posterior estimation (which is also known as Bayesian regression or regularized regression).

3.1 ORDINARY LEAST-SQUARES

Basic Theory

Ordinary least-squares estimation is the most common regression technique used in statistical parameter estimation. The objective of this methodology is to find the vector of parameter values $\hat{\boldsymbol{p}}$ that minimize a sum-of-squares error function, given in Eq. (3.1) in both scalar and vector form. The data vector $\boldsymbol{y}$ comes from the experiment, and the prediction vector $\hat{\boldsymbol{y}}$ (a function of $\hat{\boldsymbol{p}}$) comes from the FE model.

$$SSE = \sum_{i=1}^{n_y} (y_i - \hat{y}_i)^2 = (\boldsymbol{y} - \hat{\boldsymbol{y}})^{\mathrm{T}}(\boldsymbol{y} - \hat{\boldsymbol{y}}) \tag{3.1}$$

Clearly, it is preferable that the *SSE* quantity be small rather than large, since this indicates less difference between experimental measurements and predictions based on the analytical model. The $\hat{\boldsymbol{p}}$ vector that minimizes the *SSE* quantity is known as the *least-squares estimate*.

To solve for this estimate, the parameter iteration of Eq. (3.2) can be used. The matrix $\boldsymbol{X}$ is a sensitivity matrix, where $x_{ij} = \partial y_i / \partial p_j$. Gauss-Newton iteration can converge quite quickly, particularly if $\boldsymbol{X}$ is nearly constant or if the initial guess for $\hat{\boldsymbol{p}}$ is close to the minimizing least-squares estimate.

$$\Delta\hat{\boldsymbol{p}} = (\boldsymbol{X}^{\mathrm{T}}\boldsymbol{X})^{-1}(\boldsymbol{X}^{\mathrm{T}}(\boldsymbol{y} - \hat{\boldsymbol{y}})) \tag{3.2}$$

If the statistical properties of the errors present in the data are known or are assumed to be known, it is possible to make inferences concerning the estimated parameters $\hat{\boldsymbol{p}}$. Specifically, if measurement errors on the data values are independent of each other and come from a common normal distribution (with zero mean and standard deviation σ), then the *variance-covariance matrix* $\mathrm{Var}[\hat{\boldsymbol{p}}]$ that describes potential errors in the *parameter estimates* is given in Eq. (3.3). The true error variance σ^2 is usually unknown, but the estimated error variance s^2, given in Eq. (3.4), can be used in its place.

$$\mathrm{Var}[\hat{\boldsymbol{p}}] = \sigma^2(\boldsymbol{X}^{\mathrm{T}}\boldsymbol{X})^{-1} \tag{3.3}$$

$$s^2 = \frac{\sum_{i=1}^{n_y} (y_i - \hat{y}_i)^2}{(n_y - n_p)} \tag{3.4}$$

The diagonal elements of Eq. (3.3) consist of *variances* that describe the amount of potential error in each individual parameter estimate. The off-diagonal elements are *covariances* that describe how much the potential errors are related *between* different parameter estimates. The diagonal elements can be used to generate confidence intervals for the true values of each parameter, e.g., $p_{true,i} \in \hat{p}_i \pm 1.96\sqrt{\mathrm{Var}[\hat{\boldsymbol{p}}]_{ii}}$ for standard 95% confidence intervals on normally distributed parameters. Clearly, it is preferable for the entries of $\mathrm{Var}[\hat{\boldsymbol{p}}]$ to be as small as possible.

It is also possible to generate a correlation matrix describing the relationships between the various parameters. This is accomplished by pre- and post-multiplying $\mathrm{Var}[\hat{\boldsymbol{p}}]$ by a diagonal rescaling matrix, $\boldsymbol{Q}$, given in Eq. (3.5). The resulting correlation matrix is given in Eq. (3.6).

$$q_{ii} = 1/\sqrt{\mathrm{Var}[\hat{\boldsymbol{p}}]_{ii}} \qquad q_{i \neq j} = 0 \tag{3.5}$$

$$\mathrm{Corr}[\hat{\boldsymbol{p}}] = \boldsymbol{Q}\,\mathrm{Var}[\hat{\boldsymbol{p}}]\boldsymbol{Q} \tag{3.6}$$

3.2 Maximum-Likelihood Estimation

Basic Theory

Ordinary least-squares is a very powerful parameter estimation technique, but it can perform poorly when the data do not meet the assumptions of independent and identically distributed normal errors. In particular, if a subset of the data has errors that are significantly larger than the errors in other data, then the ordinary least-squares loses *efficiency*, meaning that potential errors on the estimated *parameters* become larger than ideal. Additionally, the ability to accurately estimate the variance-covariance matrix $\mathrm{Var}[\hat{\boldsymbol{p}}]$ of the parameter estimates is adversely affected.

The solution to this problem is to use *weighted* least-squares. Appendix A shows how weighted least-squares is derived using maximum likelihood theory. This theory shows that a weighting matrix should be used, as defined in Eq. (3.7), where $\mathrm{Var}[y]$ is the variance-covariance matrix describing errors on the data.

$$\boldsymbol{W}_y = \mathrm{Var}^{-1}[\boldsymbol{y}] \tag{3.7}$$

The weighting matrix fits into the sum-of-squares expression, as shown in Eq. (3.8), and fits into the parameter iteration process as shown in Eq. (3.9). The estimated parameter vector $\hat{\boldsymbol{p}}$ generated by this iteration is called the *maximum likelihood* estimate. The variance-covariance matrix given in Eq. (3.10) describes the quality of this estimate.

$$SSE = \sum_{i=1}^{n_y} \frac{(y_i - \hat{y}_i)^2}{\sigma_{y_i}^{\ 2}} = \sum_{i=1}^{n_y} w_{ii}(y_i - \hat{y}_i)^2 = (\boldsymbol{y} - \hat{\boldsymbol{y}})^{\mathrm{T}} \boldsymbol{W}_y (\boldsymbol{y} - \hat{\boldsymbol{y}}) \tag{3.8}$$

$$\Delta\hat{\boldsymbol{p}} = \left(\boldsymbol{X}^{\mathrm{T}} \boldsymbol{W}_y \boldsymbol{X}\right)^{-1} \left(\boldsymbol{X}^{\mathrm{T}} \boldsymbol{W}_y (\boldsymbol{y} - \hat{\boldsymbol{y}})\right) \tag{3.9}$$

$$\mathrm{Var}[\hat{\boldsymbol{p}}] = \left(\boldsymbol{X}^{\mathrm{T}} \boldsymbol{W}_y \boldsymbol{X}\right)^{-1} \tag{3.10}$$

Regression Example

To demonstrate the effectiveness of using weighted least-squares, the data set given in Table 3.1 is used. It should be noted that the variances in this data set are *not* uniform, with the last data point having a variance 100 times as large as the variance of the errors in the other data.

Table 3.1: Data for Regression Example

$y_{true,i}$	$x_{1,i}$	$x_{2,i}$	$\sigma_{y,i}^2$
7.8	0.0	2.6	0.1
11.6	1.0	3.2	0.1
15.4	2.0	3.8	0.1
19.2	3.0	4.4	0.1
23.0	4.0	5.0	0.1
28.0	5.0	6.0	0.1
34.2	6.0	7.4	0.1
40.4	7.0	8.8	0.1
46.6	8.0	10.2	0.1
52.8	9.0	11.6	10.0

The ten data points are used to estimate two parameters $\hat{p}_1$ and $\hat{p}_2$ using both ordinary least-squares regression and weighted least-squares regression. The model used to fit the data is given below in Eq. (3.11), which can alternatively be expressed in matrix form as given in Eq. (3.12).

$$\hat{y}_i = \hat{p}_1 x_{1,i} + \hat{p}_2 x_{2,i} \tag{3.11}$$

$$\hat{\boldsymbol{y}} = \begin{bmatrix} \boldsymbol{x}_1 & \boldsymbol{x}_2 \end{bmatrix} \begin{bmatrix} \hat{p}_1 \\ \hat{p}_2 \end{bmatrix} = \boldsymbol{X}\hat{\boldsymbol{p}} \tag{3.12}$$

A Monte Carlo study was performed with these numbers. In each trial, the data points y_i were created by adding Gaussian random numbers (with zero mean and variance $\sigma_{y,i}^2$) to the true solution, i.e., $y_i = y_{true,i} + \mathrm{N}\left[0, \sigma_{y,i}^2\right]$. This "noisy" data was then used to estimate the parameters p_1 and p_2. This process was repeated 2000 times, and 2000 sets of parameter estimates were obtained. Equations (3.2), (3.3),

and (3.4) were used for the ordinary least-squares analysis, while Eqs. (3.8), (3.9), and (3.10) were used for the weighted least-squares analysis.

Figure 3.1 below shows a scatter plot of the solutions obtained using ordinary least-squares. The scatter around the true solution $p_{true,1} = 2.00$ and $p_{true,2} = 3.00$ is caused by the noise in the data. The expression $(\boldsymbol{p} - \hat{\boldsymbol{p}})^{\mathrm{T}} \mathrm{Var}^{-1}[\hat{\boldsymbol{p}}](\boldsymbol{p} - \hat{\boldsymbol{p}}) = \chi^2_{2,0.99}$ defines a 99% confidence region that shows where the scatter points *should* be according to the estimate of $\mathrm{Var}[\hat{\boldsymbol{p}}]$ computed using Eq. (3.3). It can clearly be seen that the confidence ellipse does *not* overlap the scatter points.

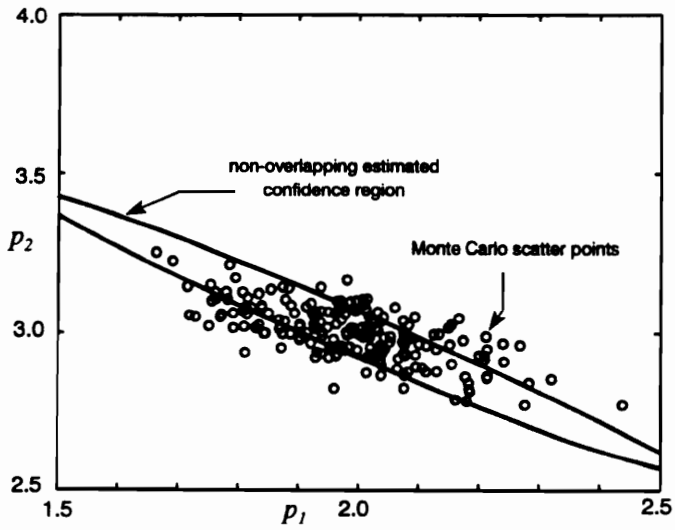

Figure 3.1: Ordinary Least-Squares Solutions

This discrepancy can be quantified by determining a "measured" variance-covariance matrix from the Monte Carlo trials [83], which can be compared to the estimate computed using Eq. (3.3). As shown in Eqs. (3.13) and (3.14), the estimate does *not* match the results provided by the Monte Carlo study. Individual entries in the matrix of Eq. (3.14) are off by more than a factor of five.

$$\mathrm{Var}\begin{bmatrix}\hat{p}_1\\ \hat{p}_2\end{bmatrix}_{Monte\ Carlo} = \begin{bmatrix}+0.0207 & -0.0093\\ -0.0093 & +0.0080\end{bmatrix} \tag{3.13}$$

$$\mathrm{Var}\begin{bmatrix}\hat{p}_1\\ \hat{p}_2\end{bmatrix}_{estimated} = s^2(X^{\mathrm{T}}X)^{-1} = \begin{bmatrix}+0.1316 & -0.0998\\ -0.0998 & +0.0777\end{bmatrix} \tag{3.14}$$

If a weighted regression analysis is used according to Eq. (3.9), different results are obtained. A scatter plot of weighted regression solutions is shown in Figure 3.2. It is apparent that the scatter around the true solution $p_{true,1} = 2.00$ and $p_{true,2} = 3.00$ has been substantially reduced. This is indicative of an improved estimation process. Additionally, the 99% confidence ellipse computed using the estimate of $\mathrm{Var}[\hat{p}]$ from Eq. (3.10) overlaps the scatter points.

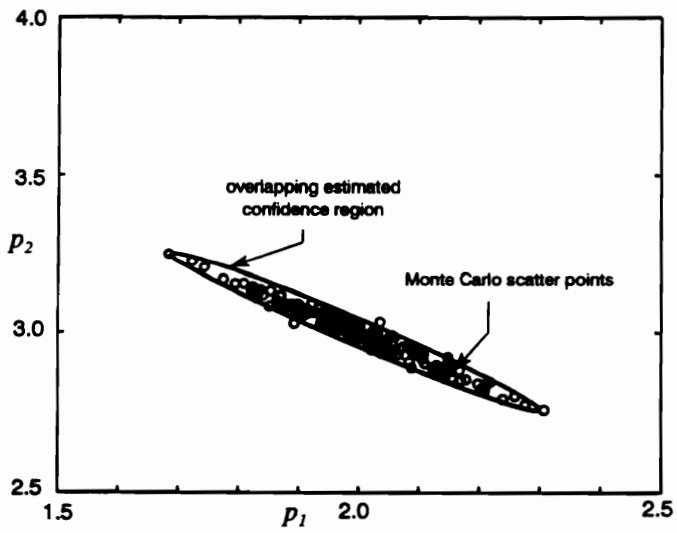

Figure 3.2: Weighted Least-Squares Solutions

As with the ordinary least-squares solutions, it is possible to determine a "measured" variance-covariance matrix using the Monte Carlo trials, which can be

compared to the estimated variance-covariance matrix obtained using Eq. (3.10). Equations (3.15) and (3.16) below provide the resulting comparison. Here, the estimated matrix matches the "measured" matrix to nearly the fourth decimal place.

$$\mathrm{Var}\begin{bmatrix}\hat{p}_1\\ \hat{p}_2\end{bmatrix}_{Monte\ Carlo} = \begin{bmatrix}+0.0135 & -0.0101\\ -0.0101 & +0.0079\end{bmatrix} \tag{3.15}$$

$$\mathrm{Var}\begin{bmatrix}\hat{p}_1\\ \hat{p}_2\end{bmatrix}_{estimated} = \left(X^{\mathrm{T}} W_y X\right)^{-1} = \begin{bmatrix}+0.0136 & -0.0102\\ -0.0102 & +0.0080\end{bmatrix} \tag{3.16}$$

Clearly, using weighted regression provided a substantial improvement over ordinary least-squares in this case. The larger variance of the 10th data point of Table 3.1 caused a noticeable increase in the variance of the parameter estimates obtained using ordinary least-squares, which can be clearly seen when Figure 3.1 is compared to Figure 3.2. Additionally, the parameter variance-covariance matrix computed using Eq. (3.3) was incorrect, meaning that the effects of the 10th point variance were not even properly accounted for.

3.3 Maximum a Posterior Estimation

Basic Theory

An additional improvement that can be made to weighted regression is the inclusion of prior knowledge concerning the parameters. When this is done, the parameter estimation problem becomes a *Bayesian statistics* problem, which provides three benefits: (1) reduced variances in parameter estimates; (2) reducing instability in

the update process caused by ill-conditioning; and (3) reduced correlation between the final parameter estimates.

To use Bayesian statistics, the analyst must have prior information concerning the parameters. Strictly speaking, this prior information comes in the form of a probability distribution function, but for normally distributed parameters the information can be summarized with an estimated means and variances, which together are called *priors*. In some cases the analyst may know little or nothing at all about the likely value of some of the parameters. In this case, *non-informative priors* should be used for the poorly understood parameters, meaning that the corresponding estimates of variance are set to infinity.

The *SSE* quantity for a Bayesian statistics analysis is given below in Eq. (3.17). The data weighting matrix is defined as $\boldsymbol{W}_y = \mathrm{Var}[\boldsymbol{y}]^{-1}$ and the weighting matrix for the vector of priors $\boldsymbol{p}_0$ is $\boldsymbol{W}_p = \mathrm{Var}[\boldsymbol{p}_0]^{-1}$. The iteration that minimizes *SSE* is given in Eq. (3.18). The estimated parameter vector $\hat{\boldsymbol{p}}$ generated by this iteration is called the *maximum a posterior* estimate, as discussed in Appendix A. The variance-covariance matrix describing the quality of this estimate is given in Eq. (3.19). Both data and priors are assumed to come from multivariate normal distributions.

$$SSE = \sum_{i=1}^{n_y} \left(\frac{y_i - \hat{y}_i}{\sigma_{y_i}} \right)^2 + \sum_{m=1}^{n_p} \left(\frac{p_{0,m} - \hat{p}_0}{\sigma_{p_{0,m}}} \right)^2 \tag{3.17}$$

$$= (\boldsymbol{y} - \hat{\boldsymbol{y}})^{\mathrm{T}} \boldsymbol{W}_y (\boldsymbol{y} - \hat{\boldsymbol{y}}) + (\boldsymbol{p}_0 - \hat{\boldsymbol{p}})^{\mathrm{T}} \boldsymbol{W}_p (\boldsymbol{p}_0 - \hat{\boldsymbol{p}})$$

$$\Delta \hat{\boldsymbol{p}} = \left(\boldsymbol{X}^{\mathrm{T}} \boldsymbol{W}_y \boldsymbol{X} + \boldsymbol{W}_p \right)^{-1} \left(\boldsymbol{X}^{\mathrm{T}} \boldsymbol{W}_y (\boldsymbol{y} - \hat{\boldsymbol{y}}) + \boldsymbol{W}_p (\boldsymbol{p}_0 - \hat{\boldsymbol{p}}) \right) \tag{3.18}$$

$$\mathrm{Var}[\hat{\boldsymbol{p}}] = \left(\boldsymbol{X}^{\mathrm{T}} \boldsymbol{W}_y \boldsymbol{X} + \boldsymbol{W}_p \right)^{-1} \tag{3.19}$$

Regression Example

In this regression example, the data of Table 3.1 is used again along with prior knowledge concerning the two parameters. Table 3.2 provides the mean and variance estimates that summarize the prior information distributions. This information can also be expressed using the vector/matrix notation of Eq. (3.20).

Table 3.2: Priors for Regression Example

parameter	mean	variance	confidence bounds
p_1	2.05	0.001	±0.062
p_2	3.25	0.020	±0.277

$$\boldsymbol{p}_0 = \begin{bmatrix} 2.05 \\ 3.25 \end{bmatrix} \qquad \mathrm{Var}[\boldsymbol{p}_0] = \begin{bmatrix} +0.001 & 0.0 \\ 0.0 & +0.020 \end{bmatrix} \tag{3.20}$$

It should be noted that the prior estimates $\boldsymbol{p}_0$ do *not* match the true solution $p_{true,1} = 2.00$ and $p_{true,2} = 3.00$. This will usually be the case. If the prior knowledge was always perfect, there would be no point is using experimental data to obtain new estimates of the modeling parameters in the first place.

Figure 3.3 below shows results from a *single* weighted least-squares regression analysis obtained using Eqs. (3.9) and (3.10). The parameter estimates, given in Eq. (3.21), do not match the true solution, which is not unexpected since there is noise present in the data. A 99% confidence region is again defined by the expression $(\boldsymbol{p}_{true} - \hat{\boldsymbol{p}})^{\mathrm{T}} \mathrm{Var}^{-1}[\hat{\boldsymbol{p}}](\boldsymbol{p}_{true} - \hat{\boldsymbol{p}}) = \chi^2_{2,0.99}$. Note that the shape of the ellipse in Figure 3.3 is the same as that shown in Figure 3.2, and that the true answer *does* lie within the ellipse.

$$\hat{p}_{wls} = \begin{bmatrix} 2.1185 \\ 2.8660 \end{bmatrix} \qquad \mathrm{Var}[\hat{p}]_{wls} = \begin{bmatrix} +0.0136 & -0.0102 \\ -0.0102 & +0.0080 \end{bmatrix} \tag{3.21}$$

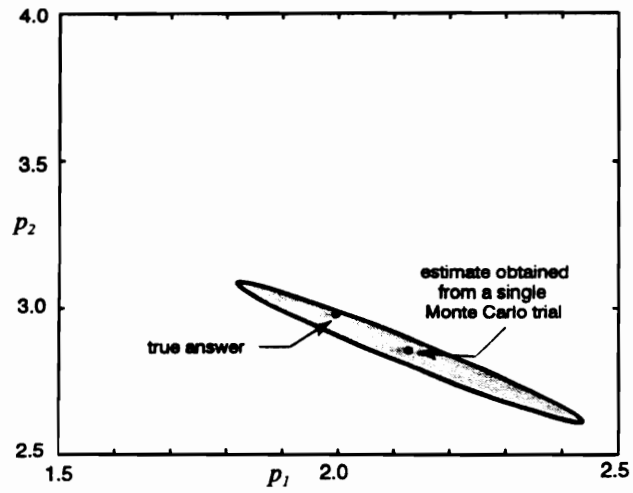

Figure 3.3: Confidence Region from Weighted Regression

A similar ellipse can be plotted for the priors using the definition of $\mathrm{Var}[p_0]$ from Table 3.2. This ellipse, plotted along with the ellipse generated from the weighted regression results, is shown in Figure 3.4.

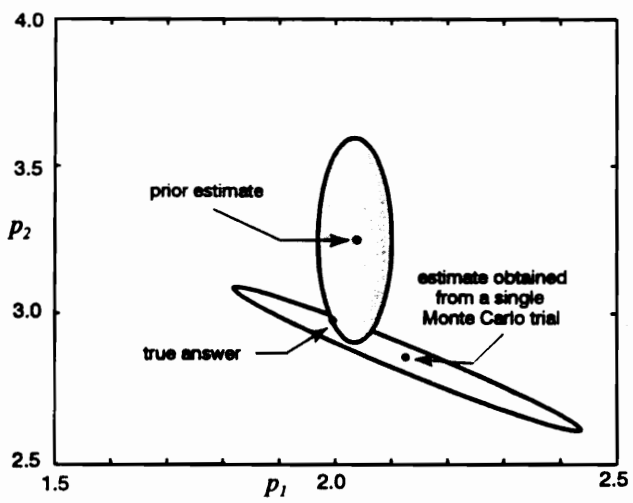

Figure 3.4: Confidence Region from Prior Knowledge

In Figure 3.4, it can be seen that there is a region where the confidence region based on the prior information distribution overlaps the estimated confidence region coming from the regression results. The true answer lies within this overlap region.

If a Bayesian statistics solution is computed using Eqs. (3.18) and (3.19), the results of Eq. (3.22) are obtained. It is worth noting that the variances are much smaller and that the parameter estimate is much closer to the true solution than either the prior estimate or the estimate obtained using weighted least-squares alone. This is particularly evident when the estimate and confidence region coming from the Bayesian regression analysis are plotted on top of the other two confidence regions, as shown in Figure 3.5.

$$\hat{p}_{bayes} = \begin{bmatrix} 2.0434 \\ 2.9271 \end{bmatrix} \qquad \mathrm{Var}[\hat{p}]_{bayes} = \begin{bmatrix} +0.00091 & -0.00067 \\ -0.00067 & +0.00078 \end{bmatrix} \tag{3.22}$$

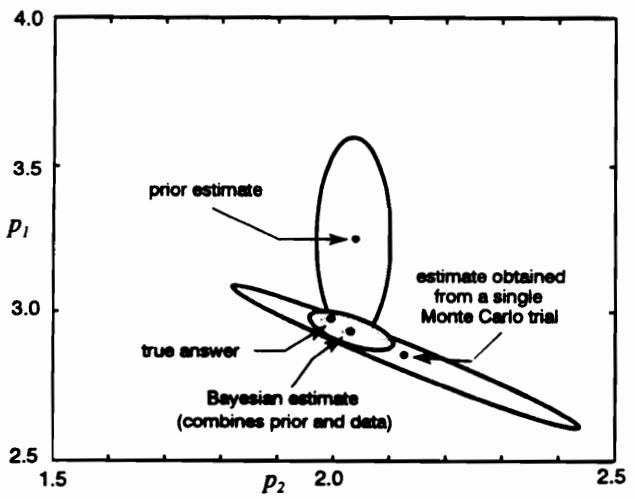

Figure 3.5: Confidence Region from Bayesian Regression

It is interesting to note that the estimated confidence region coming from the Bayesian regression analysis is located where the two other confidence regions over-

lap. This means that the Bayesian estimate is consistent with both the prior information and the data-based information coming from the weighted regression analysis.

Conclusions

Clearly, using Bayesian regression can be an improvement over even weighted least-squares, particularly if there is ill-conditioning present in the problem. Ill-conditioning can be characterized by computing the condition number of the correlation matrix of Eqs. (3.5) and (3.6). A high condition number indicates the presence of ill-conditioning in the problem, which tends to inflate parameter estimate variances, as seen in Eq. (3.21). It is also the source of the high degree of eccentricity seen in the confidence region ellipse of Figure 3.3.

For the weighted regression example, this condition number turned out to be 109.1, which is quite high for a two-parameter problem. For the Bayesian statistics analysis, however, the condition number is only 8.9, which resulted in the substantially reduced variances of Eq. (3.22) and the less eccentric ellipse of Figure 3.5.

3.4 Additional Comments on Statistics

Data and Parameter Scaling

A major advantage of using Bayesian statistics is that weighting matrices make the entire formulation independent of data and parameter scaling. Thus, switching from S.I. units to English units would have no effect on the analysis, nor would scalings used to convert from acceleration data to velocity data have any effect on the analysis. Also, the use of statistical weights provides the proper balance between data and

priors. Without the weights, the analyst would have to assign a scaling coefficient to the residuals from the priors to ensure that they influence the analysis sufficiently.

Normality of Data

In all three types of parameter estimation (ordinary least-squares, weighted regression, and Bayesian regression), the errors on the data are assumed to come from a multivariate normal (Gaussian) distribution. If this assumption is not met, it decreases the efficiency of the estimation process and renders the parameter variance-covariance matrix estimators of Eqs. (3.3), (3.10), and (3.19) inaccurate. Rarely do we have any guarantees that the errors on raw time-series data meet this assumption.

However, if a large amount of data is available (as is the case with structural dynamics testing results), the central limit theorem [77] indicates that statistical quantities based on *linear combinations* of the data will approach normality, even if errors on the data are not normally distributed. Typically, 30 or more data points must be used for this approximation to hold.

As will be described in later chapters, the data used in the model update procedure described in this dissertation are not actually raw time-series data, but are rather the *results* of signal processing performed on the time-series data. In this signal processing, a large amount of time-series data is condensed into a few numbers that effectively describe the time-series data. For low noise levels, this data condensation process is effectively linear, meaning that the results of signal processing become normally distributed. This normality of the signal processing results indicates that a sum-of-squares error is the appropriate quantity to use for comparison purposes.

Other Measurable Quantities

Typically, the data used for parameter estimation consists of processed dynamic response data. However, there may be other measurable quantities that can be included as well. For example, if the mass of the test structure is known to weigh 15.05 ± 0.05 kg, then the FE model should predict a weight within that range. Strain gauge measurements could be used as well. These additional quantities, z, can be included in the problem as shown in Eq. (3.23). The data weighting matrix is defined by $W_y = \mathrm{Var}^{-1}[y]$, the weighting matrix for prior information is defined by $W_p = \mathrm{Var}^{-1}[p_0]$, and the weighting matrix for the *additional* measurements is defined by $W_z = \mathrm{Var}^{-1}[z]$.

$$\begin{aligned} SSE &= \sum_{i=1}^{n_y}\left(\frac{y_i - \hat{y}_i}{\sigma_{y_i}}\right)^2 + \sum_{m=1}^{n_p}\left(\frac{p_{0,m} - \hat{p}_0}{\sigma_{p_{0,m}}}\right)^2 + \sum_{k=1}^{z_k}\left(\frac{z_k - \hat{z}_m}{\sigma_{z_k}}\right)^2 \\ &= (y - \hat{y})^{\mathrm{T}} W_y (y - \hat{y}) + (p_0 - \hat{p})^{\mathrm{T}} W_p (p_0 - \hat{p}) + (z - \hat{z})^{\mathrm{T}} W_z (z - \hat{z}) \end{aligned} \tag{3.23}$$

Of course, measurements of quantities can be considered simply as additional data, as the y vector does not have to be restricted to signal processing results. Therefore, the z vector can be appended to the y vector, and the W_z matrix can be appended to the W_y, forming a generalized y vector and W_y matrix pair as shown in Eq. (3.24). This means that Eq. (3.17) can be used in place of Eq. (3.23).

$$y_{generalized} = \begin{Bmatrix} y \\ z \end{Bmatrix} \qquad \mathrm{Var}[y_{generalized}] = \begin{bmatrix} \mathrm{Var}[y] & 0 \\ 0 & \mathrm{Var}[z] \end{bmatrix} \tag{3.24}$$

Comparing Different Models

The Bayesian statistics formulation for solving regression problems is also well-suited for comparing how *different* models fit the same data. This can be accomplished by simply determining which model provides the smallest *SSE* value, as defined in Eq. (3.17). The model with the smallest *SSE* value will be the model that best fits the data.

3.5 THE CORE EQUATIONS

To summarize this chapter, there are four equations that describe the Bayesian statistics approach for updating parameters in a model. As mentioned in Section 3.1, the FEM-based $\hat{y}$ data prediction vector is computed using the parameter estimate vector $\hat{p}$. A vector f of force amplitudes (to be described in Chapters 5 and 6) is also required. Equation (3.17) gives the objective function that is to be minimized. Equation (3.18) provides the basic iteration that is used to perform the function minimization/parameter estimation. Equation (3.19) gives the variance-covariance matrix that describes the quality of the resulting parameter estimates.

At the beginning of each chapter in this section, these four equations will be listed again, along with a description of which vectors/matrices have already been derived, which ones are being derived in that particular chapter, and which ones remain to be derived in later chapter.

Chapter 4: Update Parameters

THE CORE EQUATIONS

data vector:

$$\hat{y} = \hat{y}(\hat{p}, f)$$

objective function:

$$SSE = (y - \hat{y})^{\mathrm{T}} W_y (y - \hat{y}) + (p_0 - \hat{p})^{\mathrm{T}} W_p (p_0 - \hat{p})$$

iteration for parameter estimation:

$$\Delta\hat{p} = \left(X^{\mathrm{T}} W_y X + W_p\right)^{-1} \left(X^{\mathrm{T}} W_y (y - \hat{y}) + W_p (p_0 - \hat{p})\right)$$

variance-covariance matrix for parameters:

$$\mathrm{Var}[\hat{p}] = \left(X^{\mathrm{T}} W_y X + W_p\right)^{-1}$$

To be derived here:	$\hat{p}$	updated parameters estimates
	p_0	prior estimates of parameters
	W_p	weighting matrix for priors
Remaining to be derived:	y	data vector
	f	excitation vector
	W_y	data weighting matrix
	$\hat{y}$	FE prediction of data vector
	X	sensitivity matrix of FE prediction vector

4.1 MODEL UPDATE PARAMETERS

As discussed in the introduction of Chapter 1, the subject of this research is a parameter-based methodology for updating finite element (FE) models with frequency response data. The primary advantage of using a parametric approach is that the

updated parameters provide insight into the changes made to the model. Clearly, one of the main tasks the analyst initially has (in addition to building the initial FE model) is to pick the parameters that are to be updated. The parameter vector p contains one entry for each parameter to be updated. The *updated* parameter estimates that come from the regression analysis are designated $\hat{p}$, with the "hat" indicating that they are *estimated* quantities.

Since finite element models can be used to model a wide range of systems, there are virtually no restrictions on what constitutes a valid parameter, aside from the fact that they must be independent. For example, if the analyst is modeling a beam with a solid rectangular cross-section, he cannot select width b, thickness h, and cross-section area A, since $A = bh$. Unfortunately, this lack of independence will not always be obvious to the analyst.

Additionally, it is preferable that the parameters consist of values that are easily measured or interpreted. Parameters such as these include material parameters such as density and elastic modulus, global geometric properties such as length and thickness, and boundary condition values such as effective mass and effective stiffness. An example of parameters that are difficult to measure or interpret are individual entries in the finite element mass and stiffness matrices.

Trade-offs can sometimes be made between parameter ease-of-use and intuitiveness. For example, when working with a rectangular cross section of a beam (with a fixed width), it is easier to work with the area moment of inertia I, since the FE stiffness matrix is linear with respect to I. However, it is more intuitive to work with

thickness t and width w, since these are the parameters that the analyst can actually measure and are the quantities that would be modified in a design change. Parameters that required remeshing of the FE model should be avoided, since repeatedly remeshing the FE model greatly increases the expense of performing the model update. In the research of this dissertation, choices between intuitiveness and ease-of-use went both ways.

Ideally, the set of parameters will be as small as possible, while being complete enough to include the dominant sources of uncertainty in the model. Thus, when the parameters are properly updated, the uncertainty in the model will have been significantly reduced and the predictive capability of the model will have been improved.

4.2 Bayesian Priors

An additional benefit of using design parameters is that the update problem can be formulated as a *Bayesian statistics* problem. In this statistical framework, any *prior* knowledge the analyst has concerning the values of the design parameters can be formally incorporated into the update process. This knowledge, usually consisting of independent measurements of the the parameters, is called *prior information*.

In the Bayesian statistics approach, prior information is described by the *a priori* probability distribution function (PDF). This PDF is typically summarized with estimates of mean and variance for parameters coming from a normal distribution. The estimated mean and variance together are called a *prior*.

If the update parameters are selected properly, priors can be easily obtained. For example, if one of the parameters is thickness, the analyst can *measure* the thickness

with a ruler, perhaps obtaining a prior of 0.25 ± 0.03 in. (assuming that measurements are accurate to the nearest half increment on the measuring device). Alternatively, the analyst could measure the thickness with a micrometer, obtaining a much more accurate prior of 0.2605 ± 0.0005 in.. Material property priors can sometimes be obtained from reference books.

In cases involving estimation of joint stiffness or boundary condition parameters, the analyst may know little or nothing at all about the likely value of a parameter. In this case, prior information is not included in the analysis for the parameter. This can alternately be expressed as a *non-informative prior*, which is a prior having a variance estimate of infinity.

The actual quantities used in the Bayesian statistics analysis are the vector of initial parameter estimates $\boldsymbol{p}_0$ and the weighting matrix $\boldsymbol{W}_p$ that represents the quality of the initial parameter estimates. $\boldsymbol{W}_p$ is the inverse of the variance-covariance matrix $\mathrm{Var}[\boldsymbol{p}_0]$ that directly describes the distribution of potential parameter values.

Table 4.1 below shows an example of prior information for three parameters: thickness t, width w, and joint stiffness k. In this particular example, the first two parameters can be measured directly to obtain the priors, but no prior information is available on the third. It is thus expressed as a non-informative prior.

Table 4.1: Example of Prior Information

parameter	mean	confidence interval
t	0.050 m	±0.002 m
w	1.200 m	±0.020 m
k	??	??

If the confidence intervals are interpreted as 95% confidence intervals on normally distributed variables, this implies that the standard deviation for parameter p_i can be computed as $\sigma_i = \frac{\text{C.I. size}}{1.96}$ [77]. This implies that $\sigma_h = 0.001$ m and $\sigma_L = 0.010$ m. Since no prior value is available for k, a value should arbitrarily be assigned to it, such as $k = 1.0 \times 10^5$ N/m. The standard deviation assigned to it should be much larger, representing the fact that the value assigned to the parameter is very uncertain. Perhaps $\sigma_k = 1.0 \times 10^8$ N/m could be used.

At this point, the vector $\boldsymbol{p}_0$ and matrix $\mathrm{Var}[\boldsymbol{p}_0]$ should be assembled. Equations (4.1) and (4.2) provide these quantities for the sample data given in Table 4.1. The weighting matrix $\boldsymbol{W}_p$ given in Eq. (4.3) is simply the inverse of $\mathrm{Var}[\boldsymbol{p}_0]$.

$$\boldsymbol{p}_0 = \begin{bmatrix} h_0 \\ L_0 \\ k_0 \end{bmatrix} = \begin{bmatrix} 0.020 \text{ m} \\ 1.200 \text{ m} \\ 1.0 \times 10^5 \text{ N/m} \end{bmatrix} \tag{4.1}$$

$$\mathrm{Var}[\boldsymbol{p}_0] = \begin{bmatrix} \sigma_h^2 & 0 & 0 \\ 0 & \sigma_L^2 & 0 \\ 0 & 0 & \sigma_k^2 \end{bmatrix} = \begin{bmatrix} 1.0 \times 10^{-6} \text{ m}^2 & 0 & 0 \\ 0 & 1.0 \times 10^{-4} \text{ m}^2 & 0 \\ 0 & 0 & 1.0 \times 10^{16} \text{ N}^2/\text{m}^2 \end{bmatrix} \tag{4.2}$$

$$\boldsymbol{W}_p = \mathrm{Var}^{-1}[\boldsymbol{p}_0] = \begin{bmatrix} 1.0 \times 10^6 \text{ m}^{-2} & 0 & 0 \\ 0 & 1.0 \times 10^4 \text{ m}^{-2} & 0 \\ 0 & 0 & 1.0 \times 10^{-16} \text{ m}^2/\text{N}^2 \end{bmatrix} \tag{4.3}$$

Chapter 5: Sine-Dwell Statistics

THE CORE EQUATIONS

data vector:

$$\hat{y} = \hat{y}(\hat{p}, f)$$

objective function:

$$SSE = (y - \hat{y})^{\mathrm{T}} W_y (y - \hat{y}) + (p_0 - \hat{p})^{\mathrm{T}} W_p (p_0 - \hat{p})$$

iteration for parameter estimation:

$$\Delta\hat{p} = \left(X^{\mathrm{T}} W_y X + W_p\right)^{-1} \left(X^{\mathrm{T}} W_y (y - \hat{y}) + W_p (p_0 - \hat{p})\right)$$

variance-covariance matrix for parameters:

$$\mathrm{Var}[\hat{p}] = \left(X^{\mathrm{T}} W_y X + W_p\right)^{-1}$$

Already derived:	$\hat{p}$	updated parameters estimates
	p_0	prior estimates of parameters
	W_p	weighting matrix for priors
To be derived here:	y	data vector for sine-dwell data
	f	excitation vector for sine-dwell data
	W_y	data weighting matrix for sine-dwell data
Remaining to be derived:	$\hat{y}$	FE prediction of data vector
	X	sensitivity matrix of FE prediction vector

5.1 SINE-DWELL TEST DATA

This chapter discusses how linear regression techniques are used to compute elements of the data vector y and how the multivariate delta method is used to generate elements of the weighting matrix W_y. The chapter concludes with a

discussion of when the multivariate delta method approximation breaks down, along with the acceptance criterion used to determine whether or not a data point should be incorporated into the model update analysis.

Sine-dwell testing

Sine-dwell testing is a technique often used in structural dynamics testing. In this technique, a sinusoidally applied excitation force is applied at a specific frequency to the structure, usually with an electromagnetic shaker. The resulting response (either a displacement, velocity, or acceleration) is then measured at one or more points on the structure. If the structure exhibits *linear* behavior, the response of the structure will also be sinusoidal. Sample time-series data from excitation signal $e(t)$ and response signal $r(t)$ are shown below in Figure 5.1.

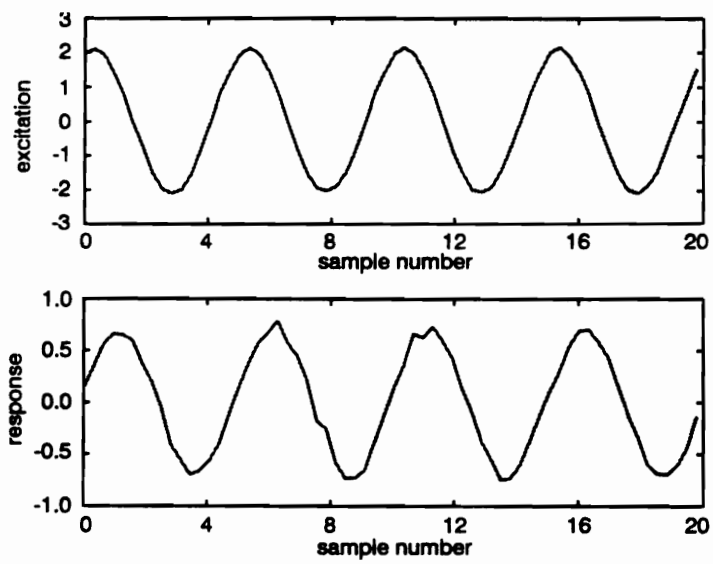

Figure 5.1: Sample Time-Series Data

From Figure 5.1, it can be seen that the force signal has an amplitude of about 2.1 units zero-to-peak, while the response signal has an amplitude of about 0.7 units zero-to-peak. Furthermore, the response signal *lags* the excitation signal by a 60° phase angle, or about 2.5 time units.

Single Frequency Time-Series Modeling

The statistics resulting from the signal processing of the time-series data is a key part of updating modeling parameters using a proper Bayesian statistics analysis, as they are the source of the data and weighting matrices used in the regression formulation. Equations (5.1), (5.2), and (5.3) show the equations used to model time-series data from single-frequency excitation signal $e(t)$, response signal $r(t)$, and *relative* response signal $r_{rel}(t)$. Allowances for DC offset are included. The real-valued scalars c_1 and c_2 are the *real* and *imaginary* components, respectively, of a complex-valued representation of the frequency response of the system. Measured time-series data blocks $\boldsymbol{e}$, $\boldsymbol{r}$, and $\boldsymbol{r}_{rel}$ are assumed to be equal to time samples of the true signals *plus* random errors coming from a Gaussian distribution of unknown variance.

$$e_{true}(t) = a_0 + A\cos(\omega t - \phi_0) = a_0 + a_1\cos(\omega t) + a_2\sin(\omega t) \tag{5.1}$$

$$r_{true}(t) = b_0 + B\cos(\omega t - \phi_0 - \phi_{rel}) = b_0 + b_1\cos(\omega t) + b_2\sin(\omega t) \tag{5.2}$$

$$r_{rel,true}(t) = c_0 + C\cos(\omega t - \phi_r) = c_0 + c_1\cos(\omega t) + c_2\sin(\omega t) \tag{5.3}$$

Multi-frequency Time-Series Modeling

The formulation of Eqs. (5.1), (5.2), and (5.3) can be expanded to account for multiple frequency components in the time-series data. This allows the analyst to test for harmonic distortion in a single frequency experiment, or perhaps to acquire data more quickly by using several frequencies in the excitation signal simultaneously. Equations (5.4), (5.5), and (5.6) show how the time-series data (excitation and response) is modeled for a signal containing n_h total harmonics.

$$e_{true}(t) = a_0 + \sum_{i=1}^{n_h} A_i \cos(\omega_i t - \phi_{0,i}) = a_0 + \sum_{i=1}^{n_h} a_{2i-1} \cos(\omega_i t) + a_{2i} \sin(\omega_i t) \tag{5.4}$$

$$r_{true}(t) = b_0 + \sum_{i=1}^{n_h} B_i \cos(\omega_i t - \phi_{0,i} - \phi_{rel,i}) = b_0 + \sum_{i=1}^{n_h} b_{2i-1} \cos(\omega_i t) + b_{2i} \sin(\omega_i t) \tag{5.5}$$

$$r_{rel,true}(t) = c_0 + \sum_{i=1}^{n_h} C_i \cos(\omega_i t - \phi_{rel,i}) = c_0 + \sum_{i=1}^{n_h} c_{2i-1} \cos(\omega_i t) + c_{2i} \sin(\omega_i t) \tag{5.6}$$

Of course, the "perfect" time signals, $e_{true}(t)$ and $r_{true}(t)$, are not available in an actual experiment, which means that the true coefficient values cannot be obtained. However, *estimates* of these parameters can be found using linear regression techniques. The estimated coefficient vector $\hat{\boldsymbol{c}} = \{\hat{c}_0, \hat{c}_1, \hat{c}_2, \ldots, \hat{c}_{2n_h}\}$ (along with a variance-covariance matrix $\mathrm{Var}[\hat{\boldsymbol{c}}]$ describing its quality) becomes the data for the Bayesian regression formulation used to perform the FE model update.

To obtain the estimates of $\hat{\boldsymbol{c}}$ and $\mathrm{Var}[\hat{\boldsymbol{c}}]$ (one set for each combination of data acquisition location, fundamental excitation frequency, and excitation location), the excitation and response time-series data must first be analyzed separately using

ordinary linear regression. The results of each analysis are then combined together using the multivariate delta method, as described in Section 5.2.

5.2 Relative Response Statistics

Individual Time Signal Analysis

To obtain estimates of $\hat{\boldsymbol{c}}$ and $\mathrm{Var}[\hat{\boldsymbol{c}}]$, the time-series data blocks acquired from excitation and response signals (each of length n_t) must first be analyzed individually. This is accomplished using ordinary least-squares, as described in Chapter 3. This provides the estimated vectors $\hat{\boldsymbol{a}} = \{\hat{a}_0, \hat{a}_1, \hat{a}_2, \ldots, \hat{a}_{2n_h}\}$ and $\hat{\boldsymbol{b}} = \{\hat{b}_0, \hat{b}_1, \hat{b}_2, \ldots, \hat{b}_{2n_h}\}$ representing excitation and response, respectively, along with variance-covariance matrices describing the quality of the estimated vectors.

To perform the regression for n_h harmonics, the regressor matrix $\boldsymbol{X}$ is first defined as given in Eq. (5.7). Since the problem is linear, the iteration of Eq. (3.2) is not required. Vectors $\boldsymbol{a}$ and $\boldsymbol{b}$ can be directly computed using Eqs. (5.8) and (5.9) using excitation data vector $\boldsymbol{e}$ and response data vector $\boldsymbol{r}$, respectively.

$$\boldsymbol{X} = \begin{bmatrix} 1 & \cos(\omega_1 t_1) & \sin(\omega_1 t_1) & \cdots & \cos(\omega_{n_h} t_1) & \sin(\omega_{n_h} t_1) \\ 1 & \cos(\omega_1 t_2) & \sin(\omega_1 t_2) & \cdots & \cos(\omega_{n_h} t_2) & \sin(\omega_{n_h} t_2) \\ \vdots & \vdots & \vdots & & \vdots & \vdots \\ 1 & \cos(\omega_1 t_{n_t}) & \sin(\omega_1 t_{n_t}) & \cdots & \cos(\omega_{n_h} t_{n_t}) & \sin(\omega_{n_h} t_{n_t}) \end{bmatrix} \tag{5.7}$$

$$\hat{\boldsymbol{a}} = \begin{bmatrix} \hat{a}_0 \\ \hat{a}_1 \\ \vdots \\ \hat{a}_{2n_h} \end{bmatrix} = (\boldsymbol{X}^{\mathrm{T}}\boldsymbol{X})^{-1}\boldsymbol{X} \begin{bmatrix} e(t_1) \\ e(t_2) \\ \vdots \\ e(t_{n_t}) \end{bmatrix} = (\boldsymbol{X}^{\mathrm{T}}\boldsymbol{X})^{-1}\boldsymbol{X}\boldsymbol{e} \tag{5.8}$$

$$\hat{\boldsymbol{b}} = \begin{bmatrix} \hat{b}_0 \\ \hat{b}_1 \\ \vdots \\ \hat{b}_{2n_h} \end{bmatrix} = (\boldsymbol{X}^{\mathrm{T}}\boldsymbol{X})^{-1}\boldsymbol{X} \begin{bmatrix} r(t_1) \\ r(t_2) \\ \vdots \\ r(t_{n_t}) \end{bmatrix} = (\boldsymbol{X}^{\mathrm{T}}\boldsymbol{X})^{-1}\boldsymbol{X}\boldsymbol{r} \tag{5.9}$$

As described in Chapter 3, estimated variance-covariance matrices for $\hat{\boldsymbol{a}}$ and $\hat{\boldsymbol{b}}$ can be computed using Eqs. (3.3) and (3.4). This provides the results of Eqs. (5.10) and (5.11).

$$\hat{\boldsymbol{e}} = \boldsymbol{X}\hat{\boldsymbol{a}} \qquad s_e^2 = \frac{(\boldsymbol{e} - \hat{\boldsymbol{e}})^{\mathrm{T}}(\boldsymbol{e} - \hat{\boldsymbol{e}})}{n_t - 2n_h - 1} \qquad \mathrm{Var}[\hat{\boldsymbol{a}}] = s_e^2(\boldsymbol{X}^{\mathrm{T}}\boldsymbol{X})^{-1} \tag{5.10}$$

$$\hat{\boldsymbol{r}} = \boldsymbol{X}\hat{\boldsymbol{b}} \qquad s_r^2 = \frac{(\boldsymbol{r} - \hat{\boldsymbol{r}})^{\mathrm{T}}(\boldsymbol{r} - \hat{\boldsymbol{r}})}{n_t - 2n_h - 1} \qquad \mathrm{Var}[\hat{\boldsymbol{b}}] = s_r^2(\boldsymbol{X}^{\mathrm{T}}\boldsymbol{X})^{-1} \tag{5.11}$$

Relative Response and Amplitude

With the individual analyses of the excitation and response time-series data available, it becomes possible to compute *amplitude* vectors $\hat{\boldsymbol{A}}$ and $\hat{\boldsymbol{B}}$, for excitation and response respectively, as given in Eqs. (5.12) and (5.13). The coefficient vector $\hat{\boldsymbol{c}}$ that represents the frequency response of the system *relative* to excitation, is computed as given in Eq. (5.14).

$$\hat{\boldsymbol{A}} = \begin{bmatrix} \hat{A}_0 \\ \hat{A}_1 \\ \vdots \\ \hat{A}_{n_h} \end{bmatrix} = \begin{bmatrix} \hat{a}_0 \\ \sqrt{\hat{a}_1^2 + \hat{a}_2^2} \\ \vdots \\ \sqrt{\hat{a}_{2n_h-1}^2 + \hat{a}_{2n_h}^2} \end{bmatrix} \tag{5.12}$$

$$\hat{\boldsymbol{B}} = \begin{bmatrix} \hat{B}_0 \\ \hat{B}_1 \\ \vdots \\ \hat{B}_{n_h} \end{bmatrix} = \begin{bmatrix} \hat{b}_0 \\ \sqrt{\hat{b}_1^2 + \hat{b}_2^2} \\ \vdots \\ \sqrt{\hat{b}_{2n_h-1}^2 + \hat{b}_{2n_h}^2} \end{bmatrix} \tag{5.13}$$

$$\hat{\boldsymbol{c}} = \begin{bmatrix} \hat{c}_0 \\ \hat{c}_1 \\ \hat{c}_2 \\ \hat{c}_3 \\ \vdots \\ \hat{c}_{2n_h} \end{bmatrix} = \begin{bmatrix} \text{DC offset} \\ \text{Re}_1 \\ \text{Im}_1 \\ \text{Re}_2 \\ \vdots \\ \text{Im}_{n_h} \end{bmatrix} = \begin{bmatrix} \hat{b}_0 \\ \left(\hat{a}_1\hat{b}_1 + \hat{a}_2\hat{b}_2\right)/\hat{A}_1 \\ \left(\hat{a}_1\hat{b}_2 - \hat{a}_2\hat{b}_1\right)/\hat{A}_1 \\ \left(\hat{a}_3\hat{b}_3 + \hat{a}_4\hat{b}_4\right)/\hat{A}_2 \\ \vdots \\ \left(\hat{a}_{2n_h-1}\hat{b}_{2n_h} - \hat{a}_{2n_h}\hat{b}_{2n_h-1}\right)/\hat{A}_{n_h} \end{bmatrix} \tag{5.14}$$

Multivariate Delta Method

Obtaining the variance-covariance matrices for $\hat{\boldsymbol{A}}$, $\hat{\boldsymbol{B}}$, and $\hat{\boldsymbol{c}}$ is accomplished with the multivariate delta method [85]. A summary of this method is given below in Table 5.1.

Table 5.1: The Multivariate Delta Method

If there is a vector quantity $\boldsymbol{y}$ that can be written as a function of another vector quantity $\boldsymbol{x}$, then the multivariate delta method can be used to estimate the variance-covariance matrix of the new vector $\boldsymbol{y}$ in terms of the variance-covariance matrix of the original vector $\boldsymbol{x}$. Specifically, if $\boldsymbol{y} = \boldsymbol{f}(\boldsymbol{x})$, with $\Sigma = \text{Var}[\boldsymbol{x}]$, then $\text{Var}[\boldsymbol{y}] = \Delta^{\text{T}}\Sigma\Delta$ where the elements of Δ are $\delta_{ij} = (\partial y_j/\partial x_i)$. Because of the linearization used in the formulation, the results are *asymptotically correct*. This means that they are perfect for data sets containing an infinite amount of low variance data. For finite data sets with higher variance levels, the results are approximate.

In this case, variance-covariance matrices of the excitation amplitude vector $\hat{A}$, response amplitude vectors $\hat{B}$, the relative response vector $\hat{c}$ (all of which are *functions* of excitation and response estimate vectors $\hat{a}$ and $\hat{b}$) can be estimated in terms of the variance-covariance matrices of $\hat{a}$ and $\hat{b}$.

The amplitude estimate variances are easiest to compute since $\hat{A}$ is independent of $\hat{b}$ and $\hat{B}$ is independent of $\hat{a}$. The delta matrices for these two vectors are given below in Eqs. (5.15) and (5.16). Equation (5.17) shows how these delta matrices are used to compute estimates of $\mathrm{Var}[\hat{A}]$ and $\mathrm{Var}[\hat{B}]$ using the estimates of $\mathrm{Var}[\hat{a}]$ and $\mathrm{Var}[\hat{b}]$ from Eqs. (5.10) and (5.11), respectively.

$$\Delta_A = \begin{bmatrix} 1 & 0 & 0 & \dots & 0 & 0 \\ 0 & \hat{a}_1/\hat{A}_1 & 0 & \dots & 0 & 0 \\ 0 & \hat{a}_2/\hat{A}_1 & 0 & \dots & 0 & 0 \\ \vdots & \vdots & \vdots & & \vdots & \vdots \\ 0 & 0 & 0 & \dots & 0 & \hat{a}_{2n_h-1}/\hat{A}_{n_h} \\ 0 & 0 & 0 & \dots & 0 & \hat{a}_{2n_h}/\hat{A}_{n_h} \end{bmatrix} \tag{5.15}$$

$$\Delta_B = \begin{bmatrix} 1 & 0 & 0 & \dots & 0 & 0 \\ 0 & \hat{b}_1/\hat{B}_1 & 0 & \dots & 0 & 0 \\ 0 & \hat{b}_2/\hat{B}_1 & 0 & \dots & 0 & 0 \\ \vdots & \vdots & \vdots & & \vdots & \vdots \\ 0 & 0 & 0 & \dots & 0 & \hat{b}_{2n_h-1}/\hat{B}_{n_h} \\ 0 & 0 & 0 & \dots & 0 & \hat{b}_{2n_h}/\hat{B}_{n_h} \end{bmatrix} \tag{5.16}$$

$$\mathrm{Var}[\hat{A}] = \Delta_A^{\mathrm{T}}\mathrm{Var}[\hat{a}]\Delta_A \qquad \mathrm{Var}[\hat{B}] = \Delta_B^{\mathrm{T}}\mathrm{Var}[\hat{b}]\Delta_B \tag{5.17}$$

A similar process is used to compute $\mathrm{Var}[\hat{\boldsymbol{c}}]$. The delta matrix for this vector is given in Eq. (5.18), and the resulting variance-covariance matrix computation is given in Eq. (5.19).

$$\Delta_c = \begin{bmatrix} 0 & 0 & 0 & \cdots & 0 & 0 \\ 0 & -(\hat{a}_2\hat{c}_2)/\hat{A}_1^{\,2} & (\hat{a}_2\hat{c}_1)/\hat{A}_1^{\,2} & \cdots & 0 & 0 \\ 0 & (\hat{a}_1\hat{c}_2)/\hat{A}_1^{\,2} & -(\hat{a}_1\hat{c}_1)/\hat{A}_1^{\,2} & \cdots & 0 & 0 \\ \vdots & \vdots & \vdots & & \vdots & \vdots \\ 0 & 0 & 0 & \cdots & -(\hat{a}_{2n_h}\hat{c}_{2n_h})/\hat{A}_{n_h}^{\,2} & (\hat{a}_{2n_h}\hat{c}_{2n_h-1})/\hat{A}_{n_h}^{\,2} \\ 0 & 0 & 0 & \cdots & (\hat{a}_{2n_h-1}\hat{c}_{2n_h})/\hat{A}_{n_h}^{\,2} & -(\hat{a}_{2n_h-1}\hat{c}_{2n_h-1})/\hat{A}_{n_h}^{\,2} \\ 1 & 0 & 0 & \cdots & 0 & 0 \\ 0 & \hat{a}_1/\hat{A}_1 & -\hat{a}_2/\hat{A}_1 & \cdots & 0 & 0 \\ 0 & \hat{a}_2/\hat{A}_1 & \hat{a}_1/\hat{A}_1 & \cdots & 0 & 0 \\ \vdots & \vdots & \vdots & & \vdots & \vdots \\ 0 & 0 & 0 & \cdots & \hat{a}_{2n_h-1}/\hat{A}_{n_h} & -\hat{a}_{2n_h}/\hat{A}_{n_h} \\ 0 & 0 & 0 & \cdots & \hat{a}_{2n_h}/\hat{A}_{n_h} & \hat{a}_{2n_h-1}/\hat{A}_{n_h} \end{bmatrix} \tag{5.18}$$

$$\mathrm{Var}[\hat{\boldsymbol{c}}] = \Delta_c^{\mathrm{T}} \begin{bmatrix} \mathrm{Var}[\hat{\boldsymbol{a}}] & 0 \\ 0 & \mathrm{Var}[\hat{\boldsymbol{b}}] \end{bmatrix} \Delta_c \tag{5.19}$$

It is worth noting that the vector entries $\hat{A}_0$, $\hat{B}_0$, and $\hat{c}_0$ pertain to zero-frequency (static) information in the preceding expressions. When the response data come in the form of velocity or acceleration measurements, $\hat{B}_0$ and $\hat{c}_0$ have no meaning and should not be included in the model update analysis. Additionally, not all load cells used in to measure force in structural dynamics tests can measure static loads, which means that $\hat{A}_0$ may be meaningless as well. However, all of the zero-frequency

entries are included in the sine-dwell statistics analysis in case there is a DC offset introduced by the test equipment used to acquire the data.

5.3 Is Sine-Dwell Data Normally Distributed?

Preliminary Discussion

For the sum-of-squares error formulation presented in Chapter 3 to be valid, the errors on the data (composed of $\hat{c}$ vectors) must come from a multivariate normal distribution. If the errors do not, the formulation becomes non-optimal and generates parameter estimates with higher variances. Additionally, the introduction of bias error becomes possible, and parameter variance estimators become inaccurate.

The Central Limit Theorem

To address this issue, the central limit theorem [77] is used. It states that a linear combination (usually a sum) of random variables of *any* distribution will approach a normal distribution as the number of variables included in the combination increases. Normally, 30 or more random variables are required. This theorem can be used to demonstrate that the vectors $\hat{a}$ and $\hat{b}$ have normally distributed errors.

Since these two vectors are linear combinations of the excitation data vector e and the response data vector r, as shown in Eqs. (5.8) and (5.9), they can be treated as normally distributed data, even in cases where e and r contain errors that are *not* normally distributed. The vector $\hat{c}$, on the other hand, is a *non-linear* combination of the data vectors e and r (via vectors $\hat{a}$ and $\hat{b}$). For the vector $\hat{c}$ to be normally

distributed, the linearizations used in Eq. (5.17) and (5.19) must be valid. To test the validity of the linearization, a Monte Carlo study was performed.

The Monte Carlo Study

The purpose of the Monte Carlo study implemented here is to compare estimates of $\mathrm{Var}[\hat{c}]$ obtained using the multivariate delta method to measurements of $\mathrm{Var}[\hat{c}]$ obtained from Monte Carlo trials in which $\hat{c}$ vectors are generated. In each trial, Gaussian noise of a known amplitude is added to perfect data vectors $\boldsymbol{e}$ and $\boldsymbol{r}$. The vectors $\hat{\boldsymbol{a}}$ and $\hat{\boldsymbol{b}}$ are computed for each time-series data block using Eqs. (5.8) and (5.9), and the vector $\hat{c}$ is generated using (5.14).

In the example given here, both excitation and response signals have only a single frequency component with amplitude 1.0 and relative phase angle of 60°. A total of 64 time-series samples are taken at a rate of 16 samples per waveform. Figure 5.2 below shows Monte Carlo results for $\sigma_e = 0.1$ and $\sigma_r = 0.3$.

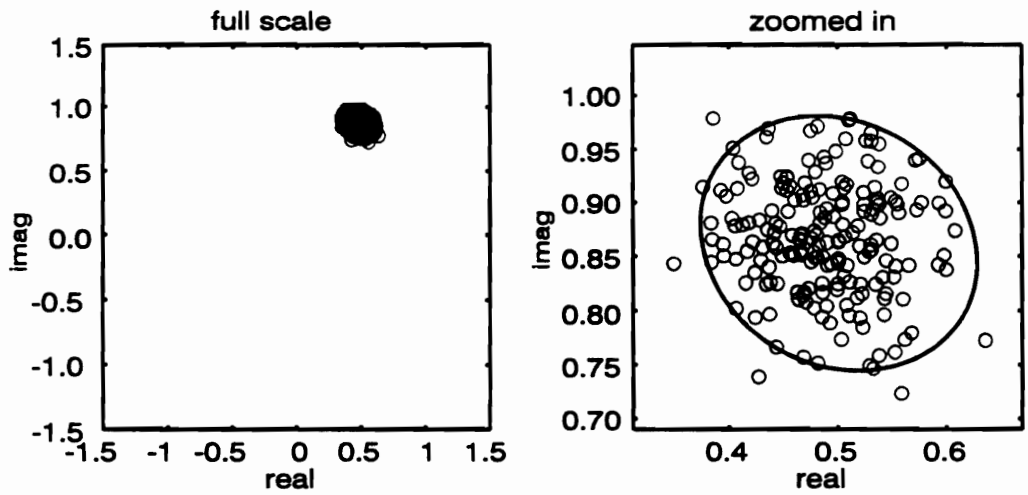

Figure 5.2: Monte Carlo Simulations, Set #1

It can be seen from Figure 5.2 that the ellipse predicted from Eq. (5.19) matches the scatter points generated in the Monte Carlo simulation well. Indeed, if a variance-covariance matrix $\mathrm{Var}[\hat{c}]$ is computed from the Monte Carlo trials, it can be seen from Eqs. (5.20) and (5.21) that the results match the predictions of Eq. (5.19) to almost five decimal places. Because the matrix $\mathrm{Var}[\hat{c}]$ can be predicted accurately, the data here is suitable for use in the Bayesian regression formulation.

$$\mathrm{Var}\begin{bmatrix} c_1 \\ c_2 \end{bmatrix}_{Monte\ Carlo} = \begin{bmatrix} +0.00306 & -0.00013 \\ -0.00013 & +0.00287 \end{bmatrix} \tag{5.20}$$

$$\mathrm{Var}\begin{bmatrix} c_1 \\ c_2 \end{bmatrix}_{Delta\ Method} = \begin{bmatrix} +0.00305 & -0.00013 \\ -0.00013 & +0.00289 \end{bmatrix} \tag{5.21}$$

However, if the excitation signal is very noisy ($\sigma_e = 0.6$), while the response signal is much less noisy ($\sigma_r = 0.01$), then the multivariate delta method approximation can be shown to break down. Figure 5.3 below shows that the predicted ellipse coming from Eq. (5.19) does *not* match the scatter points generated in the Monte Carlo simulations. There is some curvature present in the Monte Carlo results, which is a strong indication of non-normal errors in the estimates of $\hat{c}$.

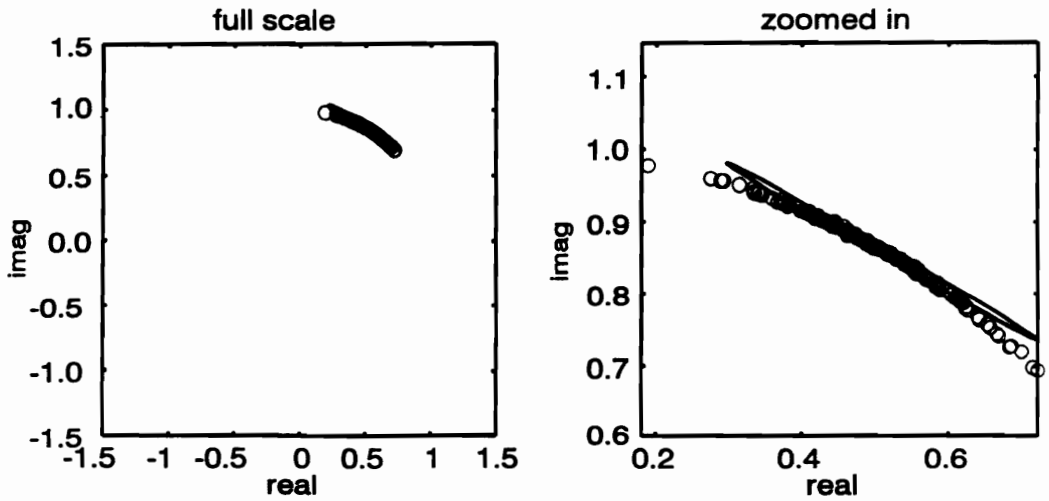

Figure 5.3: Monte Carlo Simulations, Set #2

If a variance-covariance matrix $\mathrm{Var}[\hat{c}]$ is computed from the Monte Carlo trials in this case [83], it can be seen from Eqs. (5.22) and (5.23) that the results match the predictions of Eq. (5.19) only to three decimal places. Because the matrix $\mathrm{Var}[\hat{c}]$ *cannot* be predicted accurately and because there is evidence of non-normality, the data here is *not* suitable for use in the Bayesian regression formulation of Chapter 3 and must be dropped from the analysis.

$$\mathrm{Var}\begin{bmatrix}\mathrm{Re} = c_1 \\ \mathrm{Im} = c_2\end{bmatrix}_{Monte\ Carlo} = \begin{bmatrix}+0.00832 & -0.00475 \\ -0.00475 & +0.00280\end{bmatrix} \tag{5.22}$$

$$\mathrm{Var}\begin{bmatrix}\mathrm{Re} = c_1 \\ \mathrm{Im} = c_2\end{bmatrix}_{Delta\ Method} = \begin{bmatrix}+0.00844 & -0.00487 \\ -0.00487 & +0.00282\end{bmatrix} \tag{5.23}$$

Data Acceptance Criteria

From the discussion in the previous section, it is apparent that some test data and statistical weights (some of the vectors $\hat{\boldsymbol{c}}$ and corresponding matrices $\boldsymbol{W} = \mathrm{Var}^{-1}[\hat{\boldsymbol{c}}]$) may not be suitable for use in a least-squares type formulation. To determine whether or not data from a particular point (data acquisition location/excitation location/ frequency set combination) is valid, the criteria of Eqs. (5.24) and (5.25) must be met. In these equations, the quantities $\hat{A}_l$ and $\hat{B}_l$ are the elements of the $\hat{\boldsymbol{A}}$ and $\hat{\boldsymbol{B}}$ vectors of Eqs. (5.8) and (5.9) corresponding to the lth harmonic. The corresponding variances are the lth diagonal entries of the two variance-covariance matrices given in Eq. (5.17).

$$\frac{\sqrt{\mathrm{Var}\left[\hat{A}_l\right]}}{\hat{A}_l} < 0.1 \tag{5.24}$$

$$2\left(\frac{\sqrt{\mathrm{Var}\left[\hat{A}_l\right]}}{\hat{A}_l}\right)^2 < \frac{\sqrt{\mathrm{Var}\left[\hat{B}_l\right]}}{\hat{B}_l} \tag{5.25}$$

The first rule, Eq. (5.24), is a limit that ensures that phase angle errors are not too large and do not cause too much curvature. The second rule, Eq. (5.25), ensures that curvature effects caused by errors in the excitation signal are small enough to be masked by effects caused by errors in the response signal. These criteria came from observations of many Monte Carlo studies in which different noise levels were tested on both the excitation and response data.

In practice, the easiest way to eliminate a point from the statistical analysis is to assign it a weight of zero. This corresponds to a variance of infinity and effectively removes the point from the Bayesian regression analysis.

5.4 Assembling Sine-Dwell Data

Assembling the Data Vector and Weighting Matrix

The preceding analysis describes how to analyze a block of time-series data representing excitation and response signals. This data would come from a *single* spatial location on the structure, using a *single* set of excitation frequencies at a *single* excitation location, and the analysis of the data will yield a *single* $\hat{c}$ vector and $\mathrm{Var}[\hat{c}]$ matrix. A full structural dynamics test, however, will often feature *multiple* data acquisition locations, *multiple* excitation locations, and *multiple* excitation frequency sets. The signal processing described in the previous section must be performed on *each* set of data coming from all combinations of data acquisition location, excitation location, and excitation frequency.

To gather all of the response data into a single place, it is necessary to concatenate all of the $\hat{c}$ vectors into a single y vector. It is important to note that these sine-dwell response coefficient *estimates* are treated as *data* in the larger-scale Bayesian regression formulation for updating models. Thus, the notation y is used instead of $\hat{y}$. Figure 5.4 below shows how the y vector is assembled. This vector will have a total number of elements $n_y = n_e n_f n_m n_h$.

$$y = \begin{bmatrix} \text{excit. loc \#1} \\ \text{excit. loc \#2} \\ \text{excit. loc \#3} \\ \vdots \\ \text{excit. loc \#n}_e \end{bmatrix} \begin{bmatrix} \text{base freq \#1} \\ \text{base freq \#2} \\ \text{base freq \#3} \\ \vdots \\ \text{base freq \#n}_f \end{bmatrix} \begin{bmatrix} \text{meas. loc \#1} \\ \text{meas. loc \#2} \\ \text{meas. loc \#3} \\ \vdots \\ \text{meas. loc \#n}_m \end{bmatrix} \begin{bmatrix} c_1 = \text{Re}_1 \\ c_2 = \text{Im}_1 \\ c_3 = \text{Re}_2 \\ c_4 = \text{Im}_2 \\ \vdots \\ c_{2n_h-1} = \text{Re}_{n_h} \\ c_{2n_h} = \text{Im}_{n_h} \end{bmatrix}$$

Figure 5.4: Sample y Vector from Sine-Dwell Data

Assembling the global weighting matrix W_y is accomplished in a similar fashion. The process is too large to show in a figure such as Figure 5.4, but sets of $\text{Var}^{-1}[\hat{c}]$ are placed on the diagonal of the main matrix, forming a very large block diagonal matrix, with each block having dimensions $(2n_h)\times(2n_h)$. It is almost essential that some form of sparse or banded matrix storage scheme be used here, as W_y has dimensions $n_y \times n_y$ and can be *very* large.

Assembling the Excitation Vector

Assembling the global excitation amplitude vector f is done differently than assembling the global response vector y. The reason this is done is that excitation amplitude should remain *constant* for a given excitation location/excitation frequency set combination. Response data can be acquired from a number of different measurement locations, but as long as the excitation location and excitation frequencies do not change, there is no reason to expect the excitation amplitudes to change during that portion of the test.

Therefore, instead of using an $\hat{A}$ vector from each excitation location/frequency set/data acquisition location combination, it is best to take an *average* of the $\hat{A}$ vectors corresponding to *all* data measurement locations for each excitation location/ frequency set combination.

A simple arithmetic average can be used here, but it is somewhat more robust to take a *weighted* average of the excitation amplitudes, particularly in resonance situations were force amplitudes are very low. The formulation for finding this weighted average is presented in Eqs. (5.26) and (5.27).

$$W_j = \mathrm{Var}^{-1}\left[\hat{A}_j\right] \tag{5.26}$$

$$\hat{A}_{avg} = \left(\sum_{j=1}^{n_m} W_j\right)^{-1}\left(\sum_{j=1}^{n_m} W_j \hat{A}_j\right) \tag{5.27}$$

As with the multiple $\hat{c}$ vectors that must be concatenated into a global y vector, the multiple $\hat{A}_{avg}$ vectors must be concatenated into a global f vector. This can be accomplished according to Figure 5.5. This vector will have a total number of elements $n_e n_f n_h$.

$$f = \begin{bmatrix} \text{excit. loc \#1} \\ \text{excit. loc \#2} \\ \text{excit. loc \#3} \\ \vdots \\ \text{excit. loc \#n}_e \end{bmatrix} \begin{bmatrix} \text{base freq \#1} \\ \text{base freq \#2} \\ \text{base freq \#3} \\ \vdots \\ \text{base freq \#n}_f \end{bmatrix} \begin{bmatrix} A_1 = \text{avg. excit. amp \#1} \\ A_2 = \text{avg. excit. amp \#2} \\ A_3 = \text{avg. excit. amp \#3} \\ \vdots \\ A_{n,h} = \text{avg. excit. amp \#n}_h \end{bmatrix}$$

Figure 5.5: Sample f Vector from Sine-Dwell Data

Chapter 6: Frequency Response Function Statistics

THE CORE EQUATIONS

data vector:

$$\hat{y} = \hat{y}(\hat{p}, f)$$

objective function:

$$SSE = (y - \hat{y})^{\mathrm{T}} W_y (y - \hat{y}) + (p_0 - \hat{p})^{\mathrm{T}} W_p (p_0 - \hat{p})$$

iteration for parameter estimation:

$$\Delta\hat{p} = \left(X^{\mathrm{T}} W_y X + W_p\right)^{-1} \left(X^{\mathrm{T}} W_y (y - \hat{y}) + W_p (p_0 - \hat{p})\right)$$

variance-covariance matrix for parameters:

$$\mathrm{Var}[\hat{p}] = \left(X^{\mathrm{T}} W_y X + W_p\right)^{-1}$$

Already derived:	$\hat{p}$	updated parameters estimates
	p_0	prior estimates of parameters
	W_p	weighting matrix for priors
To be derived here:	y	data vector for FRF data
	f	excitation vector for FRF data
	W_y	data weighting matrix for FRF data
Remaining to be derived:	$\hat{y}$	FE prediction of data vector
	X	sensitivity matrix of FE prediction vector

6.1 FRF TEST DATA

An alternative to discrete frequency sine-dwell testing is broad-band frequency response function (FRF) testing. This chapter discusses how signal processing

techniques and standard FRF estimators are used to compute elements of the FRF data vector $\hat{y}$ and how a statistical analysis of the FRF estimate is used to generate the associated weighting matrix W_y. The chapter concludes with a discussion of when the variance estimators for the FRF break down, along with the acceptance criterion used to determine whether or not a data point should be included in the Bayesian regression formulation for updating models.

Frequency Response Function Testing

The excitation used for broad-band FRF testing typically comes from a modal test hammer impact or burst-random excitation coming from an electromagnetic shaker. Standard FFT-based signal processing routines are used to generate a complex-valued FRF along with a coherence function that describes the quality of the FRF [81, 82]. As with the sine-dwell results, the FRF and measures of its quality become the data for the Bayesian regression formulation for updating models.

Basic FRF Signal Processing

When acquiring data for FFT-based signal processing, a number of blocks of time-series data $(n_a = 30+)$ are normally taken such that averages can be computed. Equations (6.1), (6.2), (6.3), and (6.4) show the relationships used to compute auto- and cross-spectra estimates, FRF estimates, and coherence estimates at frequency $f_j = (j-1)\Delta t / n_t$ (Δt = time sample interval, n_t = block size of FFT) [81].

X_k and F_k are results from the kth spectral line of FFT results obtained from the response data vector $\boldsymbol{r}$ and the excitation data vector $\boldsymbol{e}$, respectively. $G_{ff,k}$, $G_{xf,k}$,

$G_{fx,k}$, and $G_{xx,k}$ are auto- and cross-spectra estimates computed using the FFT results. The H_1 FRF estimator is intended for use with test data in which uncorrelated content is present only on the response signal, while the H_2 FRF estimator is intended for use with data in which uncorrelated content is present only on the force signal. The term γ^2 represents coherence, a correlation-based measure of quality of the FRF estimate that can have values between zero and one. Other FRF estimators include the H_v estimator [86], which is a weighted average of the H_1 and H_2 estimators, and the H_c estimator [87], which uses a third correlated signal to eliminate the need for computing potentially biased autospectra estimates.

$$\begin{aligned} F_k &= k^{\text{th}} \text{ spectral line of FFT}(\boldsymbol{e}) \text{ of } m^{\text{th}} \text{ time series block} \\ X_k &= k^{\text{th}} \text{ spectral line of FFT}(\boldsymbol{r}) \text{ of } m^{\text{th}} \text{ time series block} \end{aligned} \tag{6.1}$$

$$\begin{aligned} G_{ff,k} &= \sum_{m=1}^{n_a} \bar{F}_m F_k \qquad G_{xf,k} = \sum_{m=1}^{n_a} \bar{X}_m F_k \\ G_{fx,k} &= \sum_{m=1}^{n_a} \bar{F}_m X_k \qquad G_{xx,k} = \sum_{m=1}^{n_a} \bar{X}_m X_k \end{aligned} \tag{6.2}$$

$$H_{1,k} = \frac{G_{fx,k}}{G_{ff,k}} \qquad H_{2,k} = \frac{G_{xx,k}}{G_{xf,k}} \tag{6.3}$$

$$\gamma_k^2 = \frac{G_{fx,k} G_{xf,k}}{G_{ff,k} G_{xx,k}} = \frac{H_{1,k}}{H_{2,k}} \tag{6.4}$$

6.2 FRF Statistics

Magnitudes and Phase Angles

Of course, to use the Bayesian regression formulation, variances of the FRF estimates must be available as well. Bendat [72] and Yoshimura and Nagamatsu [67]

each discussed this problem in detail, but the answers they provide are different. Bendat obtained expressions based on a derivation that yielded the variance of the H_1 magnitude estimate *squared* as an intermediate result, i.e., $\mathrm{Var}\left[|H_{1,k}|^2\right]$. Equation (6.5) presents the final results of the derivation.

$$\mathrm{Var}\left[|H_{1,k}|\right] = \frac{\left(1-\gamma_k^2\right)|H_{1,k}|^2}{2\gamma^2 n_a} \qquad \mathrm{Var}\left[\phi_k\right] = \frac{\left(1-\gamma_k^2\right)}{2\gamma_k^2 n_a} \tag{6.5}$$

Yoshimura and Nagamatsu derived a different formulation based on the eigenvalue analysis used to compute the H_v, which yields the results presented in Eq. (6.6). These results were stated to be valid for the H_1 estimator also. The formulas differ from Bendat's by a factor of two in the denominator and the use of $(n_a - 1)$ instead of (n_a). The issue of phase angle variance estimates was not discussed.

$$\mathrm{Var}\left[|H_{v,k}|\right] = \frac{\left(1-\gamma_k^2\right)|H_{v,k}|^2}{\gamma_k^2(n_a-1)} \qquad \mathrm{Var}\left[|H_{1,k}|\right] = \frac{\left(1-\gamma_k^2\right)|H_{1,k}|^2}{\gamma_k^2(n_a-1)} \tag{6.6}$$

To determine which formula was correct, Monte Carlo simulations were performed. In these simulations, synthetic data was generated for a 512-frequency FRF on a two-mode system using $H_{true,k}$ given in Eq. (6.7). The force input into the system was assumed to be pseudo-random white noise.

$$H_{true,k} = \frac{1}{-\omega_k^2 + \mathrm{i}(0.15\cdot 170.7)\,\omega_k + (170.7)^2} + \frac{-1}{-\omega_k^2 + \mathrm{i}(0.05\cdot 341.3)\,\omega_k + (341.3)^2} \tag{6.7}$$

Gaussian noise was added to the excitation signal and/or the response signal. The FRF estimation formulas given in Section 6.1 were used to compute FRF estimates.

This was performed for 2000 trials, from which variance estimates of the FRF were determined [83].

The formula given by Yoshimura and Nagamatsu overestimated variances by a factor of 2, while the formulas given by Bendat slightly underestimated variances when fewer than 30 blocks of time-series data were used for averaging. Correct formulas for estimating FRF variances are given in Eq. (6.8). In these expressions, the denominator contains $2(n_a - 1)$ instead of just 2 or $(n_a - 1)$. They should be valid for both the H_1 and H_v FRF estimators.

$$\mathrm{Var}[|H_k|] = \frac{(1-\gamma_k^2)|H_k|^2}{2\gamma_k^2(n_a-1)} \qquad \mathrm{Var}[\phi_k] = \frac{(1-\gamma_k^2)}{2\gamma_k^2(n_a-1)} \tag{6.8}$$

Figure 6.1 below shows sample results from one of the Monte Carlo simulations. In this particular example, 30 time-series data blocks were used to generate each of the 2000 FFT averages computed, and Gaussian noise was only added to the response signal (in keeping with the H_1 assumption used by Bendat). The FRF plotted in Figure 6.1 contains an *average* of the 2000 averages, which makes it equivalent to an FFT generated using 60000 averages, which explains why the plot is so smooth. (Note: The small amount of bias error present in the lower right-hand portion of the magnitude plot is due to numerical discretization error, which effectively add noise to the excitation signal as well as the response signal, thus causing a minor violation of the H_1 assumption.)

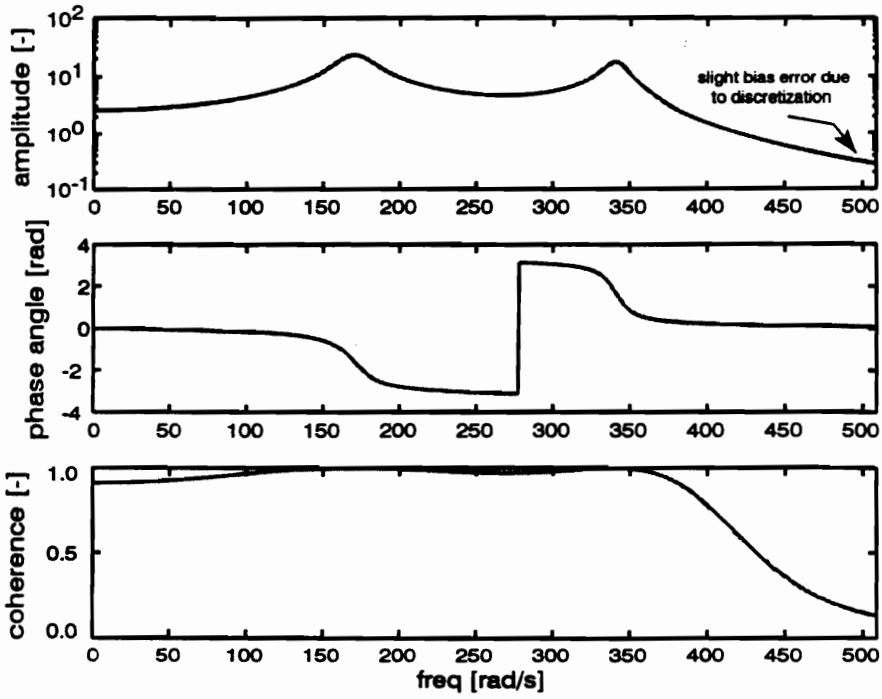

Figure 6.1: FRF Monte Carlo Results

The 2000 FFT averages were also used to determine "measured" variance estimates, which were compared to estimates computed using Eq. (6.8). As can be seen from Figure 6.2, the analytical estimates matches those generated from the Monte Carlo simulations quite closely.

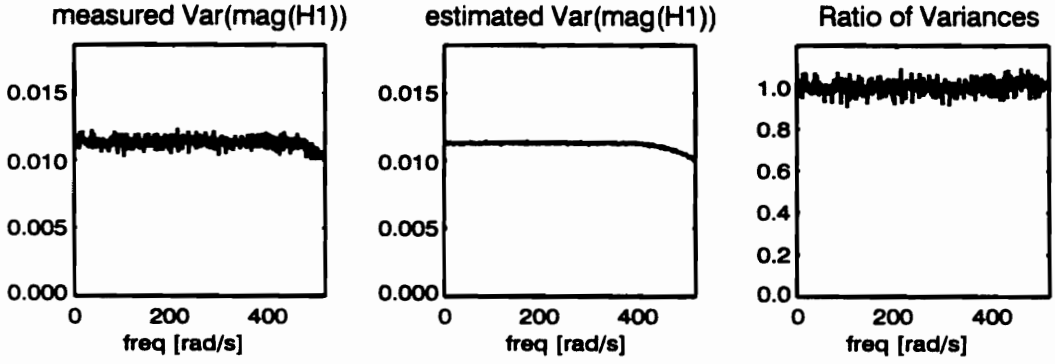

Figure 6.2: FRF Variance Comparison

The variance estimation formulas of Eq. (6.8) also worked well when synthetic data was generated with noise on excitation signal only (the H_2 assumption) or when noise was added to both signals. Even when an inappropriate FRF estimator was used and bias errors were present, variances were accurately estimated. Strictly speaking, however, the results of Bendat [72] and Yoshimura and Nagamatsu [67] were derived for only the H_1 and H_v estimators. There may be difficulties in using the variance estimator of Eq. (6.8) in H_2 estimator situations that were not revealed by this Monte Carlo study.

Real and Imaginary Components

If errors in the magnitude and phase angle estimates from Eq. (6.8) are assumed to be uncorrelated, it can be shown with an application of the multivariate delta method that these results imply the relationships of Eq. (6.11).

$$\Delta_{Re,Im,k} = \begin{bmatrix} \dfrac{|H_k|}{Re_k} & \dfrac{|H_k|}{Im_k} \\ -\dfrac{|H_k|^2}{Im_k} & \dfrac{|H_k|^2}{Re_k} \end{bmatrix} \tag{6.9}$$

$$\mathrm{Var}\begin{bmatrix} Re_k \\ Im_k \end{bmatrix} = \Delta^{\mathrm{T}}_{Re,Im,k} \begin{bmatrix} \mathrm{Var}[|H_k|] & 0 \\ 0 & \mathrm{Var}[\phi_k] \end{bmatrix} \Delta_{Re,Im,k} \tag{6.10}$$

$$\mathrm{Var}\begin{bmatrix} Re_k \\ Im_k \end{bmatrix} = \begin{bmatrix} \dfrac{(1-\gamma_k^2)|H_k|^2}{2\gamma_k^2(n_a-1)} & 0 \\ 0 & \dfrac{(1-\gamma_k^2)|H_k|^2}{2\gamma_k^2(n_a-1)} \end{bmatrix} \tag{6.11}$$

Bendat [81] shows that $\mathrm{Cov}\left[|G_{xx,k}|, \phi_k\right]$, $\mathrm{Cov}\left[|G_{fx,k}|, \phi_k\right]$, $\mathrm{Cov}\left[|G_{xf,k}|, \phi_k\right]$, $\mathrm{Cov}\left[|G_{ff,k}|, \phi_k\right]$ are all zero for $H_{1,k}$, with ϕ_k being the phase angle of H_k. Since $H_{1,k}$ is simply the cross-spectrum estimate $G_{fx,k}$ *rescaled* by the real-valued autospectrum estimate $G_{ff,k}$, the off-diagonal terms of the $\mathrm{Var}\left[|H_{1,k}|, \phi_k\right]$ matrix are zero. This happens because rescalings of uncorrelated random variables do not cause correlation between the variables. Thus, for the H_1 FRF estimator (and perhaps the H_v estimator), the $\mathrm{Cov}\left[|H_k|, \phi_k\right] = 0$ assumption that went into the multivariate delta analysis has been verified. However, the estimator $H_{2,k}$ is the autospectrum estimate $G_{xx,k}$ divided by the *complex-valued* cross-spectrum estimate $G_{xf,k}$. This is *not* a simple rescaling, and thus, the assumption of $\mathrm{Cov}\left[|H_k|, \phi_k\right] = 0$ is probably not true for the H_2 estimator.

These results are valid for information coming from a *single* spectral line of the FRF. It is also desirable to show that there are no correlations between results coming from *different* spectral lines. This is done by showing that the basic FFT algorithm is equivalent to a orthogonal least-squares fit of sine and cosine terms (see Appendix B), which in turn implies that errors in the FFT results are uncorrelated from one spectral line to the next.

It is important to note here that these FRF statistics are valid only for signal processing performed with a *rectangular window*. If other data windows (such as the Hanning) are used, it is likely that the statistics of the problem will be altered. Using pseudo-random or periodic chirp excitation would eliminate the need for windowing. The effects of leakage on FRF statistics are also unknown.

6.3 Is FRF Data Normally Distributed?

Preliminary Discussion

As with the sine-dwell data of Chapter 5, it is necessary to establish that errors in the elements of the data vector y come from a normal distribution. This is accomplished by examining Eqs. (6.1) through (6.3). If errors on the time-series data themselves are normally distributed, then X_k and F_k of Eq. (6.1) will have normally distributed errors, since the FFT operation is a linear operation. Linear operations performed on normal data preserve the normality.

Even if the errors on the time-series data are not normally distributed, the summation of Eq. (6.2) will cause errors on the auto- and cross-spectra estimates $G_{xx,k}$, $G_{xf,k}$, $G_{fx,k}$, and $G_{ff,k}$ to approach normality for 30 averages or more as predicted by the central limit theorem [77]. If errors on these auto- and cross-spectra terms are small enough, the non-linear division operation used to generate $H_{1,k}$ of Eq. (6.3) can effectively be linearized (via a Taylor series expansion). This means that errors on the FRF estimate will be normally distributed, as they are effectively linear combinations of the errors on the auto- and cross-spectra estimates.

Data Acceptance Criteria

Cobb [73] performed an extensive study of the statistics of FRF estimators, noting that the distribution of $|H_k|$ approaches the Rayleigh distribution (the distribution of $z = \sqrt{x_1^2 + x_2^2}$, where x_1 and x_2 are Gaussian random variables with mean zero and variance one) as variance levels increase on the real and imaginary parts of the FRF estimate. In high noise cases, this causes the FRF estimates to exhibit non-normality

and causes the approximations used in computing Eq. (6.5) to break down. The FRF data will not be properly suited for the Bayesian regression formulation of Chapter 3 and should not be included in the analysis.

To determine whether or not data from a particular data acquisition location/ excitation location/spectral line combination is valid, the criterion of Eq. (6.12) must be met. $\mathrm{Var}[|H_k|]$ should be estimated using Eq. (6.8). The acceptance criterion alternatively can be written as shown in Eq. (6.13), which can be derived by plugging Eq. (6.8) into Eq. (6.12). Thus, for $n_a = 30$, γ_k^2 would have to have a value of at least 0.63 for the results from the kth frequency bin to be included in the Bayesian regression formulation for updating FE models.

$$\frac{\sqrt{\mathrm{Var}[|H_k|]}}{|H_k|} < 0.1 \tag{6.12}$$

$$\gamma_k^2 > \frac{1}{(1 + 0.02(n_a - 1))} \tag{6.13}$$

6.4 Assembling FRF Data

Assembling the Data Vector and Weighting Matrix

As with the sine-dwell data, the FRF results obtained at different data acquisition locations using different excitation locations must be assembled into a single data vector y. Here, however, the basic unit of data comes in much larger pieces, as the FRF contains a real and imaginary part for each of n_f spectral lines. These subsets of data are assembled into a global y vector as shown in Figure 6.3.

$$y = \begin{bmatrix} \text{excit. loc \#1} \\ \text{excit. loc \#2} \\ \text{excit. loc \#3} \\ \vdots \\ \text{excit. loc \#n}_e \end{bmatrix} \begin{bmatrix} \text{meas. loc \#1} \\ \text{meas. loc \#2} \\ \text{meas. loc \#3} \\ \vdots \\ \text{meas. loc \#n}_m \end{bmatrix} \begin{bmatrix} \text{spectral line \#1} \\ \text{spectral line \#2} \\ \text{spectral line \#3} \\ \vdots \\ \text{spectral line \#n}_f \end{bmatrix} \begin{bmatrix} \text{real response} \\ \text{imag response} \end{bmatrix}$$

Figure 6.3: Sample y Vector from FRF data

With FRF estimates, assembling the data weighting matrix W_y is very straightforward. Since results in different frequencies bins have uncorrelated errors and since errors in the real and imaginary parts are also uncorrelated (at least for H_1), the matrix $\mathrm{Var}[y]$ becomes diagonal when the H_1 estimator is used. This in turn implies that $W_y = \mathrm{Var}^{-1}[y]$ is diagonal. The weights located on the diagonal come from the reciprocals of the variance estimates given in Eq. (6.11). The structure of this matrix makes it easy to use in a computer-based implementation of the Bayesian regression formulation.

Assembling the Excitation Vector

The excitation vector f that is assembled for FRF testing looks the same as it does for sine-dwell testing, with there being a single force amplitude for each excitation location/data acquisition location combination. However, since FRFs are *by definition* normalized, amplitudes are always one. Figure 6.4 shows how f is assembled for FRF data.

$$f = \begin{bmatrix} \text{excit. loc \#1} \\ \text{excit. loc \#2} \\ \text{excit. loc \#3} \\ \vdots \\ \text{excit. loc \#}n_e \end{bmatrix} \begin{bmatrix} \text{meas. loc \#1} \\ \text{meas. loc \#2} \\ \text{meas. loc \#3} \\ \vdots \\ \text{meas. loc \#}n_m \end{bmatrix} \begin{bmatrix} \text{spectral line \#1} \\ \text{spectral line \#2} \\ \text{spectral line \#3} \\ \vdots \\ \text{spectral line \#}n_f \end{bmatrix} \begin{bmatrix} 1.0 \end{bmatrix}$$

Figure 6.4: Sample f Vector from FRF data

Chapter 7: Finite Element Predictions

THE CORE EQUATIONS

data vector:

$$\hat{y} = \hat{y}(\hat{p}, f)$$

objective function:

$$SSE = (y - \hat{y})^{\mathrm{T}} W_y (y - \hat{y}) + (p_0 - \hat{p})^{\mathrm{T}} W_p (p_0 - \hat{p})$$

iteration for parameter estimation:

$$\Delta\hat{p} = \left(X^{\mathrm{T}} W_y X + W_p\right)^{-1} \left(X^{\mathrm{T}} W_y (y - \hat{y}) + W_p (p_0 - \hat{p})\right)$$

variance-covariance matrix for parameters:

$$\mathrm{Var}[\hat{p}] = \left(X^{\mathrm{T}} W_y X + W_p\right)^{-1}$$

Already derived:	$\hat{p}$	updated parameters estimates
	p_0	prior estimates of parameters
	W_p	weighting matrix for priors
	y	data vector
	f	excitation vector
	W_y	data weighting matrix
To be derived here:	$\hat{y}$	FE prediction of data vector
	X	sensitivity matrix of FE prediction vector
Remaining to be derived:	<none>	

7.1 FINITE ELEMENT MODELING

As stated in Chapter 1, the main purpose of the work presented in this dissertation is to update finite element (FE) models using frequency response data such that the

predictive capability of the model is improved. To this end, it is necessary to be able to compute a response *prediction vector* $\hat{y}$ (which is of the same form as the y vectors of Chapters 5 and 6) along with a *response sensitivity matrix* X. With linear FE models (composed of the mass, damping, and stiffness matrices M, C, and K), a direct dynamic stiffness approach can be used for this task.

Equations (7.1) below gives the fundamental equation of motion coming from a linear finite element model. If the system is excited harmonically at a single excitation frequency ω, the steady-state response of the system can be described in the frequency domain by modeling the FE force vector $F_0(t)$ as $Fe^{i\omega t}$ and the FE response vector $u_0(t)$ as $ue^{i\omega t}$. This results in the complex-valued frequency-domain formulation of Eq. (7.2). Many analysts include a structural damping coefficient γ in the frequency-domain formulation as well, as shown in Eq. (7.3). Structural damping is used to model energy losses that are proportional to displacement rather than velocity. The viscous damping matrix C alone cannot model these types of energy losses.

$$M\ddot{u}_0(t) + C\dot{u}_0(t) + Ku_0(t) = F_0(t) \tag{7.1}$$

$$(-\omega^2 M + i\omega C + K)u = F \tag{7.2}$$

$$(-\omega^2 M + i\omega C + (1 + i\gamma)K)u = F \tag{7.3}$$

To solve for u, a dynamic stiffness formulation is used. The dynamic stiffness matrix K_D is defined below in Eq. (7.4), which is then used to solve for u (assuming that F is given) as shown in Eq. (7.5).

$$K_D = (-\omega^2 M + i\omega C + (1 + i\gamma)K) \tag{7.4}$$

$$K_D u = F \qquad u = K_D^{-1} F \tag{7.5}$$

The dynamic response vector u is complex-valued, with the real part representing the portion of the response that is *in phase* with the excitation force and the imaginary part representing the portion that is *out of phase* with the force. Note that the vector u may provide several displacements (both translational and rotational) at a single nodal DOF. If velocity or acceleration predictions are required, u must be multiplied by $i\omega$ or $-\omega^2$, respectively.

7.2 Generating the Prediction Vector

In order to compare the predictions of the finite element model to the data collected in a structural dynamics test, a data prediction vector $\hat{y}$ must be computed from the model that corresponds *exactly* to the y vector that comes from the signal processing results described in Chapters 5 and 6 (see Figure 5.4 and Figure 6.3). Additionally, the *model* must be built according to the current values of the estimated modeling parameters $\hat{p}$.

If data was acquired from the structure at spatial locations corresponding to finite element nodal points, then construction of the prediction vector $\hat{y}$ is straightforward. First, a force amplitude A_{jkl} (corresponding to the jth excitation location and the lth harmonic of the kth excitation frequency set) must be extracted from the force vector f of Figure 5.5 or Figure 6.4. This amplitude must then be placed in the entry of the F vector of the FE model that corresponds to the excitation location.

For the given excitation frequency ω_k, a response vector u is computed using Eq. (7.5). The real and imaginary parts of this vector are then placed in the $\hat{y}$ vector according to Figure 5.4 or Figure 6.3 with *corrections being made for sensor orientation*. For example, the beam system shown below in Figure 7.1 has measurements taken with three transducers and is modeled using two finite elements. Degrees-of-freedom (DOF) 1, 3, and 5 are translational DOF, while DOF 2, 4, and 6 are rotational DOF.

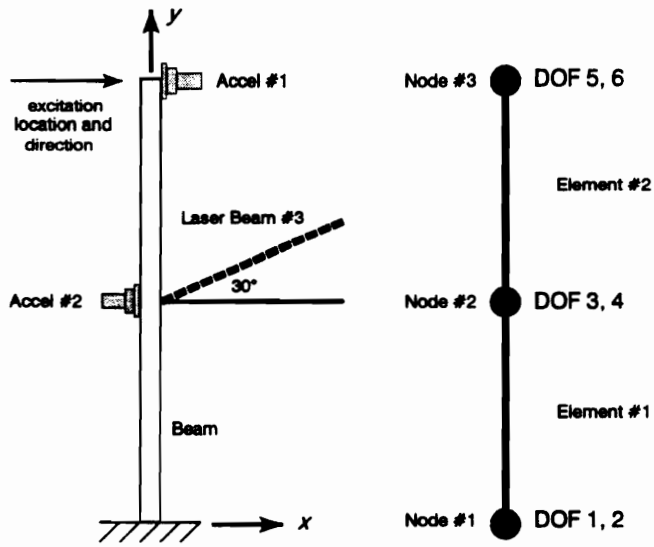

Figure 7.1: Sensor Orientation Example

Suppose that the beam has been excited at the top at a frequency of 10 rad/s with amplitude A_k. Accel #1 measures translational acceleration at node #3 while Accel #2 and Laser Beam #3 (coming from a laser Doppler vibrometer) measure a component of the translational acceleration and velocity, respectively, at node #2. After frequency response data is computed using the sine-dwell statistics of Chapter 5, the data vector y might appear as given in Eq. (7.6).

$$\text{subset}\{y\} = \begin{bmatrix} \text{Re from accel \#1} \\ \text{Im from accel \#1} \\ \text{Re from accel \#2} \\ \text{Im from accel \#2} \\ \text{Re from laser \#3} \\ \text{Im from laser \#3} \end{bmatrix} = \begin{bmatrix} -98\ \text{m/s}^2 \\ -9.7\ \text{m/s}^2 \\ 24\ \text{m/s}^2 \\ 2.3\ \text{m/s}^2 \\ 0.22\ \text{m/s} \\ -2.2\ \text{m/s} \end{bmatrix} \tag{7.6}$$

Accel #2 is mounted in the negative x direction and that the laser beam comes in at a direction of $\{\eta_x, \eta_y, \eta_z\} = \{-0.866, -0.500, 0.000\}$. This directional information must be taken into account when computing elements of the $\hat{y}$ vector. For example, suppose that for $\omega_k = 10$ rad/s (with excitation force applied at DOF #5) the response vector u_0 given below in Eq. (7.7) is obtained.

$$u = \begin{bmatrix} 0.000 + 0.000\,\text{i} \\ 0.000 + 0.000\,\text{i} \\ 0.250 + 0.025\,\text{i} \\ 0.050 + 0.005\,\text{i} \\ 1.000 + 0.100\,\text{i} \\ 0.100 + 0.010\,\text{i} \end{bmatrix} \tag{7.7}$$

The FE displacement vector u has a different form than the data vector y. Therefore, u must be rearranged to match it. The resulting prediction vector $\hat{y}$ is formulated using directional displacement information from the FE model as shown in Eq. (7.8), with terms such as $\hat{a}_{x,\#1}$ referring to a *prediction* of the x-direction acceleration at measurement location #1 (which happens to come from u_5, which is located at FE node #3). All of this information is compiled directly from the nodal displacements, as shown in Eq. (7.9), yielding a final estimate of the subset of y.

$$\text{subset}\{\hat{y}\} = \begin{bmatrix} (\hat{a}_{x,\#1})_{Re} \\ (\hat{a}_{x,\#1})_{Im} \\ (-\hat{a}_{x,\#2})_{Re} \\ (-\hat{a}_{x,\#2})_{Im} \\ (-0.866\hat{v}_{x,\#3} - 0.500\hat{v}_{y,\#3})_{Re} \\ (-0.866\hat{v}_{x,\#3} - 0.500\hat{v}_{y,\#3})_{Im} \end{bmatrix} \tag{7.8}$$

$$\text{subset}\{\hat{y}\} = \begin{bmatrix} \mathrm{Re}\left((-\omega^2 u_5)\right) \\ \mathrm{Im}\left((-\omega^2 u_5)\right) \\ \mathrm{Re}\left(-(-\omega^2 u_3)\right) \\ \mathrm{Re}\left(-(-\omega^2 u_3)\right) \\ \mathrm{Re}\left(-0.866(\mathrm{i}\omega u_3) - 0.500(0) + 0\right) \\ \mathrm{Im}\left(-0.866(\mathrm{i}\omega u_3) - 0.500(0) + 0\right) \end{bmatrix} = \begin{bmatrix} -100 \\ -10 \\ 25 \\ 2.5 \\ 0.2165 \\ -2.165 \end{bmatrix} \tag{7.9}$$

If data were acquired at non-nodal points on the structure, the finite element interpolation functions would have to be used to find $\{u_x, u_y, u_z\}$ at each measurement location. This would moderately increase the complexity of the problem, but it was not necessary in this work since all data was acquired at the locations of the finite element nodes.

This $\hat{y}$-subset assembly procedure would have to be repeated for each frequency (or harmonic) in the frequency set, yielding a larger subset of the $\hat{y}$ matrix. The larger $\hat{y}$-subset assembly procedure would then be repeated for *all* excitation location/frequency set combinations, yielding a global prediction vector $\hat{y}$.

7.3 Generating The Sensitivity Matrix

In addition to the $\hat{y}$ matrix, it is necessary to compute a sensitivity matrix X, which has entries $x_{ij} = (\partial \hat{y}_i / \partial \hat{p}_j)$. One method of computing this matrix is to use the finite difference method. Equation (7.10) below shows how this matrix would be assembled. The term $\hat{y}_{low,i}$ refers to a $\hat{y}$ vector computed for a $\hat{p}_{low,i}$ parameter vector, where $\hat{p}_i$ is replaced with $(\hat{p}_i - \Delta\hat{p}_i)$. The term $\hat{y}_{high,i}$ would be computed similarly, except with $(\hat{p}_i + \Delta\hat{p}_i)$ in place of $\hat{p}_i$.

$$X = \left[\left(\frac{\hat{y}_{high,1} - \hat{y}_{low,1}}{2\Delta\hat{p}_1} \right) \left(\frac{\hat{y}_{high,2} - \hat{y}_{low,2}}{2\Delta\hat{p}_2} \right) \cdots \left(\frac{\hat{y}_{high,n_p} - \hat{y}_{low,n_p}}{2\Delta\hat{p}_{n_p}} \right) \right] \tag{7.10}$$

The finite difference method is simple and robust. The only input required by the analyst is the selection of the finite difference steps $\Delta\hat{p}_i$. Unfortunately, the finite difference method is also expensive computationally, making it worthwhile to seek an alternative for computing X.

This other alternative is to compute *analytical* derivatives. The basic theory for this analysis comes directly from Eq. (7.3). If this equation is differentiated with respect to $\hat{p}_i$, the expression of Eq. (7.11), or alternatively, Eq. (7.12), results. Simply premultiplying Eq. (7.12) by K_D yields the desired expression of $(\partial \boldsymbol{u} / \partial \hat{p}_i)$ found in Eq. (7.13). Note: $(\partial \boldsymbol{F} / \partial \hat{p}_i)$ is usually zero.

$$\left(-\omega^2 \frac{\partial \boldsymbol{M}}{\partial \hat{p}_i} + i\omega \frac{\partial \boldsymbol{C}}{\partial \hat{p}_i} + (1 + i\gamma) \frac{\partial \boldsymbol{K}}{\partial \hat{p}_i} \right) \boldsymbol{u} + \left(-\omega^2 \boldsymbol{M} + i\omega \boldsymbol{C} + (1 + i\gamma) \boldsymbol{K} \right) \frac{\partial \boldsymbol{u}}{\partial \hat{p}_i} = \frac{\partial \boldsymbol{F}}{\partial \hat{p}_i} \tag{7.11}$$

$$\frac{\partial \boldsymbol{K}_D}{\partial \hat{p}_i} \boldsymbol{u} + \boldsymbol{K}_D \frac{\partial \boldsymbol{u}}{\partial \hat{p}_i} = \frac{\partial \boldsymbol{F}}{\partial \hat{p}_i} \tag{7.12}$$

$$\frac{\partial \boldsymbol{u}}{\partial \hat{p}_i} = \boldsymbol{K}_D^{-1}\left(-\frac{\partial \boldsymbol{K}_D}{\partial \hat{p}_i}\boldsymbol{u} + \frac{\partial \boldsymbol{F}}{\partial \hat{p}_i}\right) \tag{7.13}$$

Of course, the expression $(\partial \boldsymbol{u}/\partial \hat{p}_i)$ is not precisely what is needed to generate the $\boldsymbol{X}$ matrix; rather, $(\partial \hat{\boldsymbol{y}}/\partial \hat{p}_i)$ is required. Therefore, it is necessary to use the entries of each $(\partial \boldsymbol{u}/\partial \hat{p}_i)$ vector to compose $(\partial \hat{\boldsymbol{y}}/\partial \hat{p}_i)$, just as the entries of $\boldsymbol{u}$ were used to compose $\hat{\boldsymbol{y}}$. This includes selecting the appropriate DOF and making corrections for sensor orientation, just as was shown in Eqs. (7.7), (7.8), and (7.9).

Finding expressions such as $(\partial \boldsymbol{K}/\partial \hat{p}_i)$ is highly dependent on how the problem is formulated. For certain systems, the FE system matrices can be factored into "elementary" matrices. For example, if $\boldsymbol{K}$ can be expressed as a sum of the matrices K_0, K_1, and K_2, as shown in Eq. (7.14), then matrix partial derivatives can be found quite easily as demonstrated in Eq. (7.15).

$$\boldsymbol{K} = \frac{Ebh^3}{12}\mathrm{K}_0 + k_1\mathrm{K}_1 + k_2\mathrm{K}_2 \tag{7.14}$$

$$\frac{\partial \boldsymbol{K}}{\partial b} = \frac{Eh^3}{12}\mathrm{K}_0 \qquad \frac{\partial \boldsymbol{K}}{\partial h} = \frac{Ebh^2}{4}\mathrm{K}_0 \qquad \frac{\partial \boldsymbol{K}}{\partial k_1} = \mathrm{K}_1 \qquad \frac{\partial \boldsymbol{K}}{\partial k_2} = \mathrm{K}_2 \tag{7.15}$$

This type of FE matrix formulation allows the FE matrices $\boldsymbol{K}$ and $\boldsymbol{M}$ (and derivatives of these matrices) to be calculated easily and quickly. However, if the formulation of the FE system matrices is more complex, it may be necessary to perform the differentiation at the matrix entry level. This can be substantially more expensive computationally, at which point the finite difference method may become the more attractive alternative.

7.4 Concluding Remarks

With the completion of this discussion on $\hat{y}$ and X, all parts of the Bayesian regression formulation have been defined, and the basic theory of the model update is complete. This work included the Bayesian statistical theory used to formulate the regression problem, the sources of prior information used in the analysis, the signal processing necessary to generate statistically qualified frequency response data, and the use of a dynamic stiffness formulation to quickly and effectively generate finite element predictions of the data.

In the next part of the dissertation, Part III, a number of "quality control" issues are discussed, including computational issues, update verification statistics, and visualization statistics.

PART III:

"Quality Control" Issues

Chapter 8: Computational Issues

THE CORE EQUATIONS

data vector:

$$\hat{y} = \hat{y}(\hat{p}, f)$$

objective function:

$$SSE = (y - \hat{y})^{\mathrm{T}} W_y (y - \hat{y}) + (p_0 - \hat{p})^{\mathrm{T}} W_p (p_0 - \hat{p})$$

iteration for parameter estimation:

$$\Delta\hat{p} = \left(X^{\mathrm{T}} W_y X + W_p\right)^{-1} \left(X^{\mathrm{T}} W_y (y - \hat{y}) + W_p (p_0 - \hat{p})\right)$$

variance-covariance matrix for parameters:

$$\mathrm{Var}[\hat{p}] = \left(X^{\mathrm{T}} W_y X + W_p\right)^{-1}$$

Already derived:

$\hat{p}$	updated parameters estimates
p_0	prior estimates of parameters
W_p	weighting matrix for priors
y	data vector
f	excitation vector
W_y	data weighting matrix
$\hat{y}$	FE prediction of data vector
X	sensitivity matrix of FE prediction vector

INTRODUCTION

In Part I of this dissertation, a complete Bayesian regression formulation for updating finite element models was presented. If infinite precision arithmetic were available on the computer used to implement the formulation, the formulation would

be complete. However, with only finite precision arithmetic available, several computational issues must be addressed. These issues include proper use of modern matrix decompositions, parameter rescaling, reformulation of the problem to use matrix decompositions, step size determination, and convergence testing. The chapter concludes with a discussion of computation times.

8.1 Matrix Decompositions

There are two modern matrix decompositions that are used in implementing the Bayesian regression formulation of Chapter 3. The first is the Cholesky decomposition. With this decomposition, a symmetric positive-definite matrix $W_{n \times n}$ is represented with an upper triangular matrix $C_{n \times n}$, where $W = C^{\mathrm{T}} C$. This decomposition is often used in solving certain systems of simultaneous linear equations (such as linear FE statics problems) and has applications in statistics as well. This will be discussed in more detail in Section 8.3.

The second decomposition is the QR decomposition. Here, the rectangular matrix $X_{m \times n}$ (with $n < m$) is represented by the orthogonal matrix $Q_{m \times n}$ and the upper triangular matrix $R_{n \times n}$, where $X = QR$. Since Q is orthogonal, $Q^{\mathrm{T}} Q = I_{n \times n}$. Equations (8.1), (8.2), and (8.3) show how QR decomposition is used to solve an ordinary least-squares regression problem.

$$\Delta \hat{p} = (X^{\mathrm{T}} X)^{-1} X^{\mathrm{T}} (y - \hat{y}) = (R^{\mathrm{T}} Q^{\mathrm{T}} Q R)^{-1} R^{\mathrm{T}} Q^{\mathrm{T}} (y - \hat{y}) \tag{8.1}$$

$$\Delta \hat{p} = (R^{\mathrm{T}} R)^{-1} R^{\mathrm{T}} Q^{\mathrm{T}} (y - \hat{y}) = R^{-1} R^{-T} R^{\mathrm{T}} Q^{\mathrm{T}} (y - \hat{y}) \tag{8.2}$$

$$\Delta \hat{p} = R^{-1} Q^{\mathrm{T}} (y - \hat{y}) \tag{8.3}$$

Performing the regression using the QR decomposition provides several numerical benefits. First and foremost is the fact that $\boldsymbol{R}$ can be inverted instead of $(\boldsymbol{X}^{\mathrm{T}}\boldsymbol{X})$. $\boldsymbol{R}$ is considerably better conditioned than $(\boldsymbol{X}^{\mathrm{T}}\boldsymbol{X})$. Indeed, it can be shown that the condition numbers of $\boldsymbol{R}$ and $(\boldsymbol{X}^{\mathrm{T}}\boldsymbol{X})$ are related by the expression $\mathrm{Cond}(\boldsymbol{R}) = \sqrt{\mathrm{Cond}(\boldsymbol{X}^{\mathrm{T}}\boldsymbol{X})}$. This reduces the number of significant digits required for matrix computations by half. Additionally, $\boldsymbol{R}$ is an upper triangular matrix, which means that a simple back-substitution algorithm can be used to solve for $\Delta\boldsymbol{p}$ instead of using a more complex algorithm for solving linear systems.

An added benefit of using QR decomposition is reduced computation time in cases where multiple regression problems are to be solved using the same $\boldsymbol{X}$ matrix. In this situation, the QR decomposition can be computed and stored ahead of time, to be used with all regression problems having the same $\boldsymbol{X}$ matrix. The sine-dwell statistics of Chapter 5 were implemented with LAPACK [88] using this strategy. The QR decomposition is also used in the reformulation of the Bayesian regression procedure discussed in Section 8.3.

8.2 Parameter Rescaling

A second computational issue which must be addressed is parameter rescaling. When working with parameters that represent engineering quantities, large variations in scale sometimes result. For example, in Chapter 12, the density parameter ρ has a value of 7.85×10^{-9} Mg/mm^3 while the rotational joint stiffness parameter $k_{r,x}$ has a value of 2.53×10^{8} N·mm. These values differ in scale by more than 16 orders of magnitude. Variations such as this cause extreme ill-conditioning in the $\boldsymbol{X}$ matrix.

Even a QR decomposition-based regression algorithm may fail due to numerical difficulties in this case. An algorithm based on the inversion of $(X^{\mathrm{T}}X)$ will almost certainly fail.

To deal with this problem, the parameters must be rescaled. One possible rescaling would consist of dividing all of the parameters by their nominal values (the prior values of Chapter 4), which would be $\hat{p}_i^* = \frac{\hat{p}_i}{p_{0,i}}$. The scaled parameters $\hat{\boldsymbol{p}}^*$ would then represent the fraction change in the parameters $\hat{\boldsymbol{p}}$.

An alternative rescaling is to use parameters $\hat{\boldsymbol{p}}^*$ that represent the number of standard deviations the parameters is away from its nominal value. This rescaling was used in the computer implementation of the Bayesian regression algorithm. Eq. (8.4) gives the formal definition of the parameter rescaling. A more general formulation is given in Eq. (8.5), where $\boldsymbol{C}_p$ is the Cholesky decomposition of the inverse of the prior variance-covariance matrix, i.e., $\boldsymbol{C}_p^{\mathrm{T}}\boldsymbol{C}_p = \boldsymbol{W}_p = \mathrm{Var}^{-1}[\boldsymbol{p}_0]$. Equation (8.5) is only necessary if there is correlation between prior estimates, which normally is not the case. When $\mathrm{Var}^{-1}[\boldsymbol{p}_0]$ is a diagonal matrix, the two expressions yield identical results.

$$\hat{p}_i^* = \frac{(\hat{p}_i - p_{0,i})}{\sigma_{p_i}} \tag{8.4}$$

$$\hat{\boldsymbol{p}}^* = \boldsymbol{C}_p(\hat{\boldsymbol{p}} - \boldsymbol{p}_0) \tag{8.5}$$

With this rescaling, the vector of normalized prior estimates $\boldsymbol{p}_0^*$ (corresponding to prior estimate vector $\boldsymbol{p}_0$) becomes zero. The matrix $\mathrm{Var}^{-1}[\boldsymbol{p}_0^*]$ becomes an identity matrix, as shown in Eq. (8.6).

$$\mathrm{Var}[\hat{p}^*] = C_p \mathrm{Var}[\hat{p}] C_p^{\mathrm{T}} = C_p C_p^{-1} C_p^{-\mathrm{T}} C_p^{\mathrm{T}} = I_{n_p \times n_p} \tag{8.6}$$

8.3 Bayesian Regression Reformulation

One problem with using QR decomposition to solve regression problems is that it was not designed to include weighting matrices or prior information. To use QR decomposition with *all* aspects of the Bayesian regression formulation of Chapter 3. Specifically, the problem must be reformulated such that an ordinary least-squares algorithm based on QR decomposition can be used. To this end, a new X^* and y^* are defined as given in Eqs. (8.7) and (8.8). C_y is the Cholesky decomposition of the data weighting matrix W_y, i.e., $C_y^{\mathrm{T}} C_y = W_y = \mathrm{Var}^{-1}[y]$, and C_p is again the Cholesky decomposition of the prior weighting matrix W_p, i.e., $C_p^{\mathrm{T}} C_p = W_p = \mathrm{Var}^{-1}[p_0]$.

$$X^* = \begin{bmatrix} C_y X C_p^{-1} \\ C_p C_p^{-1} \end{bmatrix} = \begin{bmatrix} C_y X C_p^{-1} \\ I_{n_p \times n_p} \end{bmatrix} \tag{8.7}$$

$$y^* = \begin{bmatrix} C_y y \\ C_p C_p^{-1} p_0^* \end{bmatrix} = \begin{bmatrix} C_y y \\ p_0^* \end{bmatrix} = \begin{bmatrix} C_y y \\ 0 \end{bmatrix} \qquad \hat{y}^* = \begin{bmatrix} C_y \hat{y} \\ C_p C_p^{-1} \hat{p}^* \end{bmatrix} = \begin{bmatrix} C_y \hat{y} \\ \hat{p}^* \end{bmatrix} \tag{8.8}$$

If these expressions are plugged into the standard ordinary least-squares iteration shown in Eq. (8.9), it can be shown the process is mathematically equivalent to the Bayesian regression iteration shown in Eq. (3.18) of Chapter 3. This is demonstrated in Eqs. (8.10) through (8.14). The expansion $I = C_p^{-\mathrm{T}} C_p^{\mathrm{T}} C_p C_p^{-1}$ is used as a part of this derivation.

$$\Delta \hat{p}^* = (X^{*\mathrm{T}} X^*)^{-1} X^{*\mathrm{T}} (y^* - \hat{y}^*) \tag{8.9}$$

$$C_p \Delta \hat{p} = \left(C_p^{-\mathrm{T}} X^{\mathrm{T}} C_y^{\mathrm{T}} C_y X C_p^{-1} + I\right)^{-1} \left(C_p^{-\mathrm{T}} X^{\mathrm{T}} C_y^{\mathrm{T}} C_y (y - \hat{y}) + C_p (p_0 - \hat{p})\right) \tag{8.10}$$

$$\begin{aligned} C_p \Delta \hat{p} = &\left(C_p^{-\mathrm{T}} X^{\mathrm{T}} C_y^{\mathrm{T}} C_y X C_p^{-1} + \left(C_p^{-\mathrm{T}} C_p^{\mathrm{T}} C_p C_p^{-1}\right)\right)^{-1} \\ &\cdot \left(C_p^{-\mathrm{T}} X^{\mathrm{T}} C_y^{\mathrm{T}} C_y (y - \hat{y}) + \left(C_p^{-\mathrm{T}} C_p^{\mathrm{T}} C_p C_p^{-1}\right) C_p (p_0 - \hat{p})\right) \end{aligned} \tag{8.11}$$

$$\begin{aligned} C_p \Delta \hat{p} = &\left[C_p^{-\mathrm{T}} \left(X^{\mathrm{T}} C_y^{\mathrm{T}} C_y X + C_p^{\mathrm{T}} C_p\right) C_p^{-1}\right]^{-1} \\ &\cdot C_p^{-\mathrm{T}} \left(X^{\mathrm{T}} C_y^{\mathrm{T}} C_y (y - \hat{y}) + C_p^{\mathrm{T}} C_p (p_0 - \hat{p})\right) \end{aligned} \tag{8.12}$$

$$C_p \Delta \hat{p} = C_p \left(X^{\mathrm{T}} W_y X + W_p\right)^{-1} C_p^{\mathrm{T}} C_p^{-\mathrm{T}} \left(X^{\mathrm{T}} W_y (y - \hat{y}) + W_p (p_0 - \hat{p})\right) \tag{8.13}$$

$$\Delta \hat{p} = \left(X^{\mathrm{T}} W_y X + W_p\right)^{-1} \left(X^{\mathrm{T}} W_y (y - \hat{y}) + W_p (p_0 - \hat{p})\right) \tag{8.14}$$

Note that the final result, shown in Eq. (8.14), is exactly the same as the standard Bayesian regression iteration given in Eq. (3.18) and in the core equations, which is the desired result. The reformulated X^* and y^* should be used with QR decomposition to obtain $Q^* R^* = X^*$. The iteration $\Delta \hat{p}^* = R^{*-1} Q^{*\mathrm{T}} (y^* - \hat{y}^*)$ can then be used to obtain parameter estimate vector $\hat{p}^*$ and an estimated variance-covariance matrix $\mathrm{Var}[\hat{p}^*] = (R^{*\mathrm{T}} R^*)$. In addition, the effects of numerical ill-conditioning will have been greatly reduced.

At the end of the parameter estimation process, it is necessary to transform back to the original parameters $\hat{p}$. Expressions for $\hat{p}$ and its variance-covariance matrix are given below in Eqs. (8.15) and (8.16).

$$\hat{p} = C_p^{-1} \hat{p}^* + p_0 \tag{8.15}$$

$$\mathrm{Var}[\hat{p}] = C_p^{-1} \mathrm{Var}[\hat{p}^*] C_p^{-\mathrm{T}} \tag{8.16}$$

8.4 Step Size Determination

The final computational issue that must be addressed is that of iteration convergence. If the matrix X^* is constant (not a function of $\hat{p}^*$), then the iteration of Eq. (8.10) converges in a *single* step to the value of $\hat{p}^*$ that minimizes *SSE*. However, if X^* is *not* constant (meaning that the regression problem is nonlinear), multiple steps will be required to reach the minimum. If the non-linearity is extreme enough, the $\hat{p}^*$ vectors generated by the iteration $\Delta\hat{p}^* = R^{*-1}Q^{*T}(y^* - \hat{y}^*)$ may not reduce the *SSE* value *at all*, in which case the iteration will fail to converge. It should be noted that the model update formulation of Part II of the dissertation is *nonlinear* despite the fact that the finite element model is assumed to be linear. This is caused by use of the *inverse* of the dynamic stiffness matrix K_D of Chapter 7.

To ensure convergence, one must first note the fact that the step defined by Eq. (8.10) *always* points in a direction (in normalized parameter space) that reduces *SSE*, in other words, it is a descent direction. However, this direction is only guaranteed to be a descent direction *at the* $\hat{p}^*$ *at which* X^* *is computed*. If X^* changes enough over the course of the step, the *SSE* values may rise instead.

Therefore, when a step is generated that increases the *SSE* value, the step size should be reduced, as shown in Eq. (8.17). This expression is the same as found in Eq. (8.10), except that a step size modifier β, which always has a value less than one, has been included. Similar results are given for the QR decomposition based iteration from Eq. (8.18).

$$\Delta\hat{p}^* = \beta(X^{*T}X^*)^{-1}X^{*T}(y^* - \hat{y}^*) \tag{8.17}$$

$$\Delta \hat{p}^* = \beta R^{*-1} Q^{*T} (y^* - \hat{y}^*) \tag{8.18}$$

A number of different schemes exist for determining the optimal β [89]. However, it is sufficient to repeatedly halve β until the *SSE* value obtained has been decreased. Additionally, it is sometimes desirable to limit the initial step size *before* checking to see if the new $\hat{p}^*$ yields a reduced *SSE* value. This is particularly true in systems where the X^* matrix is ill-conditioned, which can potentially generate large parameter changes. The expression given in Eq. (8.19) provides a restriction on the initial size of the step, effectively limiting the average change (in an RMS sense) in a parameter to one standard deviation.

$$\text{if } (\Delta \hat{p}^{*T} \Delta \hat{p}^*) > n_p, \text{ then } \beta_0 = \sqrt{\frac{n_p}{\Delta \hat{p}^{*T} \Delta \hat{p}^*}}, \text{ else } \beta_0 = 1 \tag{8.19}$$

8.5 Convergence Testing

When using any iterative least-squares procedure, the analyst should run the procedure multiple times with different initial parameter estimates (which is not the same as different *prior* estimates, as described in Chapter 4). If all of the initial estimates converge to the same final parameter estimate, the analyst can be confident that the unique *SSE*-minimizing estimate has been obtained. *Unique* in this context means unique for the Bayesian regression formulation with a particular set of data and set of prior information. It does not mean that *all* other model update formulations and data sets would give identical answers.

If the different initial estimates converge to two or three *different* final parameter estimates, the analyst may be having difficulties with *local minima*, which are points in parameter space that appear to be error-minimizing solutions, but are not. The analyst can choose the best of the different parameter estimates simply by picking the one that provides the lowest SSE value, as given in Eq. (3.17).

If the regression iteration never converges to a final parameter estimate, or converges to a different estimate every time, then there is a problem with either the model update formulation (typically poor parameter choices) or a defect in the Bayesian regression implementation or the FE model. In this case, the analyst must re-examine *everything* carefully.

8.6 Computation Time

One disadvantage to using a Bayesian statistics formulation over some other model update formulations (e.g., direct matrix update methods) is a greatly increased need for computing power. In these iterative approaches, the finite element is rebuilt and resolved *repeatedly*, sometimes hundreds of times. This is particularly true when the dynamic response of a structure is computed at multiple frequencies, as described in Chapters 5 and 6. Indeed, a dynamic response must be computed for *each* frequency. This can represent a significant amount of computational work, particularly when FRF data is used.

Of course, it is possible to significantly reduce computation times with strategic use of matrix decompositions [80]. A modal summation approach for FRF predictions might also be worth considering. In this approach, an eigensolution would be com-

puted for the finite element model, providing natural frequencies and mode shapes. This is expensive to compute, but once it is finished, standard modal summation can then be used to quickly predict FRF values at as many frequencies as desired [82]. However, there are three difficulties with this approach: (1) modal truncation becomes an issue; (2) computation of FRF sensitivities becomes more complex; and (3) the types of damping models that can be used in the finite element model are restricted. None of these difficulties is intractable, but all represent disadvantages over the direct computation of frequency response. In cases in which sine-dwell data excitation is used, it is probably not cost effective to use modal summation.

8.7 Concluding Remarks on Numerical Issues

Clearly, there were a number of numerical concerns in the Bayesian statistics formulation that were addressed in the course of performing this research. However, *all* of these steps were necessary to ensure rapid and reliable convergence of the Bayesian regression iteration. The parameter rescaling and step size determination in particular were very important. The use of the QR and Cholesky decompositions with the reformulated X^* and y^* further increased stability and computation speed.

The issue of frequency response prediction computation times was not handled as well in this work. All of the examples presented in this dissertation were implemented in MATLAB [90], which is a high-level programming environment that provides many routines for use with general matrices. However, MATLAB does not provide routines for optimal use of matrix decompositions (especially routines that take advantage of certain matrix properties, such as symmetry, bandedness, or positive

definiteness). An implementation that used a modern matrix computation library such as LAPACK [88] would run faster and provide more accurate results. However, the amount of programming and debugging required would be greatly increased as well.

Chapter 9: Model Update Verification

Once the model update has been accomplished, it is desirable to perform a number of tests to ensure that the updated model is *representative* of the behavior of the structure. There are four different categories of tests available: (1) data stationarity testing; (2) lack-of-fit testing and compensation; (3) parameter consistency testing; and (4) cross-validation testing. These tests increase confidence that data was acquired correctly, that the model fits the data, that the updated model parameters make sense, and that the model is capable of predicting *other* data sets besides the specific set used to update the model.

9.1 Time-Invariance Testing

There are two implicit assumptions that are made whenever a model update is performed with experimental data: (1) the data is acquired correctly; and (2) the dynamic properties of the structure/test apparatus do not change over the course of testing. Ensuring that data is obtained correctly is best accomplished by using proper experimental technique. If the structure does not change over the course of testing, the data should be *time-invariant*, which means that the statistical properties of the data do not change over time. An autocorrelation test can be performed as a test of this characteristic [77].

Specifically, if data is acquired in a sequential fashion during a discrete-frequency test (usually a scanning LDV test), a large amount of force data can be obtained. Clearly, the amplitude of this force signal should remain constant for the entire duration of the test. If it does not, the structure or test equipment has probably experienced some change, often due to changes in the ambient temperatures surrounding the system [91].

The Durbin-Watson Statistic

During the course of a laser-Doppler vibrometer test, a block of excitation data is acquired with *each* block of response data. This means that if a block of velocity measurements is taken at each of 45 data acquisition locations, 45 blocks of force data will be available as well. 45 estimates of force amplitude $\hat{A}_i$ (each corresponding to data acquisition location i) can be computed according to Eq. (5.12).

These 45 $\hat{A}_i$ vectors should all be the same (if the system is time-invariant), plus or minus some small error caused by noise on the excitation time-series data. Additionally, the errors in the estimates should be *uncorrelated*, since the errors present in one time-series data block should be completely unrelated to errors present in another time-series data block.

To estimate the errors in the 45 force amplitude vectors $\hat{A}_i$, the average force amplitude vector $\hat{A}_{avg}$ is computed, as described in Eq. (5.27), and then subtracted from each of the $\hat{A}_i$ vectors. If the true force amplitude is not constant, there will be a trend to the residuals. The top plot of Figure 9.1 shows uncorrelated errors (with no

trend present), while the bottom plot shows positively correlated errors (with a downward trend present).

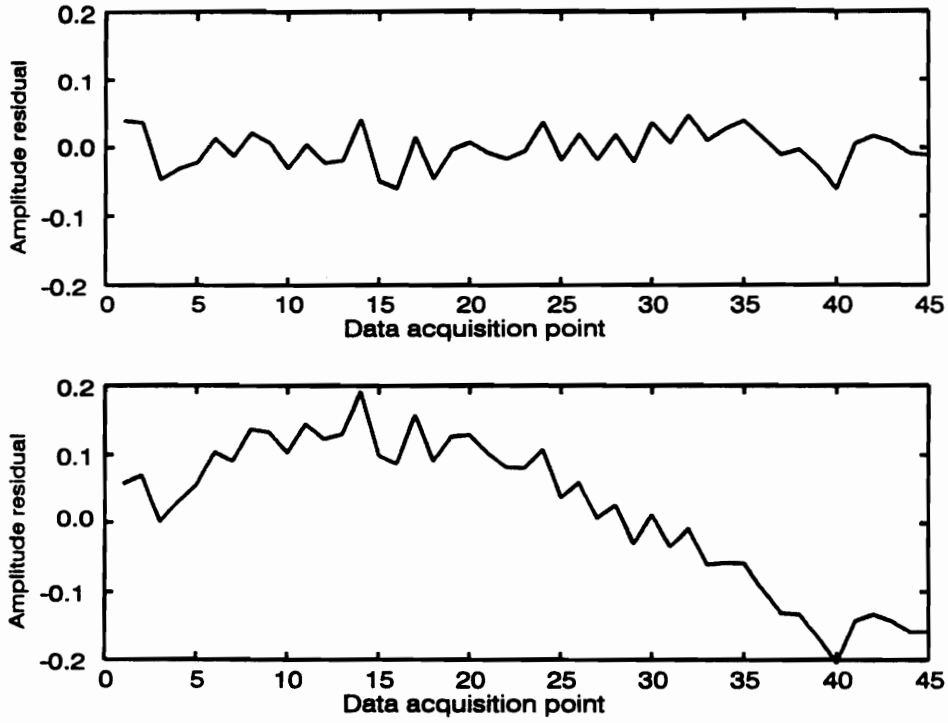

Figure 9.1: Force Amplitude Residuals

Equation (9.1) below gives the definition of the Durbin-Watson statistic [78] used to test for positive correlation between residuals. It is designed for use with scalar residuals (in this case, $e_i = A_i - A_{avg}$ from single frequency-excitation results). The statistic d will have a value of approximately 2 when the residuals are normally distributed and uncorrelated.

$$d = \left(\frac{n_m - 1}{n_m - 2} \right) \frac{\sum_{i=2}^{n_m} (e_i - e_{i-1})^2}{\sum_{i=1}^{n_m} (e_i)^2} \tag{9.1}$$

Table 9.1 below shows some critical values for the Durbin-Watson statistic for different numbers of data acquisition locations. If $d < d_L$, then the analyst can firmly conclude that autocorrelation exists. If $d > d_U$, then the analyst can firmly conclude that autocorrelation does *not* exist. If $d_L \leq d \leq d_U$, then the results are inconclusive.

Table 9.1: Durbin-Watson Critical Values

n_m	d_L	d_U
30	1.26	1.61
60	1.47	1.66
100	1.61	1.71

The Durbin-Watson statistic, when used on the 45 data points shown in Figure 9.1, generates a value of 1.854 for the top plot (clearly indicating that autocorrelation is *not* present) and 0.129 for the bottom plot (clearly indicating that autocorrelation *is* present).

The Modified Durbin-Watson Statistic

If more than one excitation frequency is being used (or multiple harmonics of the main excitation frequency are being fitted), then a more generalized form of the test can be used, as given in Eq. (9.2), where the vector $\boldsymbol{e}_i = \left(\hat{\boldsymbol{A}}_i - \hat{\boldsymbol{A}}_{avg}\right)$ is computed instead of a scalar. The lth element of the modified Durbin-Watson statistic vector $\boldsymbol{d}$ (corresponding to the harmonic excitation frequency ω_l) is computed using Eq. (9.2) and would be tested using Table 9.1 just as the statistic d of Eq. (9.1) was tested.

$$d_l = \left(\frac{n_m - 1}{n_m - 2} \right) \frac{\sum_{i=2}^{n_m} \left(e_{i,l} - e_{i-1,l} \right)^2}{\sum_{i=1}^{n_m} \left(e_{i,l} \right)^2} \tag{9.2}$$

A similar test can be performed on the driving point response (if it is available), except that $\hat{c}$ vectors are used in place of the $\hat{A}$ vectors. The real *and* imaginary components of the frequency response should exhibit time-invariance, which is equivalent to requiring that magnitude *and* phase angle exhibit time-invariance.

Other Comments on Time-Invariance

Performing these tests to ensure that the structure has not changed during the course of data acquisition is relatively easy. However, it is more difficult to ensure that the structure does not change *between* tests. The only way to statistically test for changes of this sort is to repeat at least a portion of *all* previous tests (same excitation frequency, force levels, and response measurement locations) and compare statistically. Both the force and response signals should be the same for repeated portions of the tests. Unfortunately, this significantly increases the amount of work required and was not done in this research.

9.2 LACK-OF-FIT TESTING

Once it has been established that data was taken properly and that the structure did not change during the course of testing, the model update can be performed. After the model update, a *lack-of-fit* (LOF) test can be performed. This test determines whether

or not the updated model fits the data as well as possible. This test can only be performed in the context of a weighted least-squares formulation in which *estimated* weighting matrices (like those of Chapters 5 and 6) are used.

The lack-of-fit statistic is the *SSE* term of Eq. (3.17). With proper weights, the *SSE* term becomes equivalent to a sum of independent z^2 statistics, where z is a Gaussian random variable with zero mean and unit variance [77]. A z^2 is equivalent to a chi-squares statistic with one degree of freedom, i.e., χ_1^2. If n of these χ_1^2 statistics are added together, a chi-squares statistic with n degrees of freedom results, i.e., χ_n^2 [77]. When a degree-of-freedom for each fitted parameter is subtracted off, the relationship of Eq. (9.3) results, which means that the *SSE* term comes from a $\chi_{n_y}^2$ distribution. Because of this, the relationships of Eq. (9.4) also apply.

$$\begin{aligned}\chi_{LOF}^2 = SSE = (\boldsymbol{y} - \hat{\boldsymbol{y}})^{\mathrm{T}} \boldsymbol{W}_y (\boldsymbol{y} - \hat{\boldsymbol{y}}) + (\boldsymbol{p}_0 - \hat{\boldsymbol{p}})^{\mathrm{T}} \boldsymbol{W}_p (\boldsymbol{p}_0 - \hat{\boldsymbol{p}}) \\ \sim \chi_{n_y + n_p - n_p}^2 \sim \chi_{n_y}^2\end{aligned} \tag{9.3}$$

$$\mathrm{E}[SSE] = n_y \qquad \mathrm{Var}[SSE] = 2n_y \tag{9.4}$$

For a large number of data points ($n_y > 30$), the distribution of the *SSE/LOF* statistic approach normality, as predicted by the central limit theorem [77]. Knowing this, the statistic can be normalized into a z-score, as shown in Eq. (9.5).

$$z_{LOF} = \frac{(SSE - n_y)}{\sqrt{2n_y}} \tag{9.5}$$

If z_{LOF} has a value in excess of some critical z_0 value (1.96 for 97.5% confidence), the model can be said to exhibit *lack-of-fit*. This means that the model is not

fitting the data as well as could be expected, and that the *SSE* value has been artificially inflated. This lack-of-fit can be the result of model form errors, data acquisition errors unaccounted for by the signal processing statistics, or poor/incomplete parameter selection. Examples of modeling form errors include bad boundary condition models and discretization errors, while data acquisition errors might be caused by misplaced or miscalibrated transducers, FRF leakage, or over-filtering of time-series data.

If $z_{LOF} < z_0$, there is no statistical evidence for lack-of-fit and no statistical reason to expect that *any* model could fit the data *any* better. Unfortunately, the power [77] of the LOF test becomes *very* great for a large n_y, which means that even the *slightest* lack of agreement between the model and data will cause a z_{LOF} greater than 1.96 to be generated. Only if the FE model, data acquisition procedure, and signal processing technique are all *perfect* will lack-of-fit not be detected by the test. Thus, instead of insisting that a model pass the lack-of-fit test (which is virtually impossible), it is better to *compensate* for lack-of-fit.

When lack-of-fit occurs, the quantity $SSE_y = (\boldsymbol{y} - \hat{\boldsymbol{y}})^{\mathrm{T}} \boldsymbol{W}_y (\boldsymbol{y} - \hat{\boldsymbol{y}})$ is artificially inflated relative to the priors, "drowning out" $SSE_p = (\boldsymbol{p} - \hat{\boldsymbol{p}})^{\mathrm{T}} \boldsymbol{W}_p (\boldsymbol{p} - \hat{\boldsymbol{p}})$. This keeps the priors from influencing the analysis as much as they should. To compensate for this *SSE* inflation, the data residuals can be downweighted, restoring the effect of residuals from the priors. Equations (9.6), (9.7), and (9.8) show how the sum-of-squares error, the Gauss-Newton step, and the estimated parameter variance-covariance matrix are

reformulated with the downweighted data. The lack-of-fit compensation coefficient α has value less than one.

$$SSE = \alpha^2(y - \hat{y})^{\mathrm{T}} W_y (y - \hat{y}) + (p_0 - \hat{p})^{\mathrm{T}} W_p (p_0 - \hat{p}) \tag{9.6}$$

$$\Delta p = \left(\alpha^2 X^{\mathrm{T}} W_y X + W_p\right)^{-1} \left(\alpha^2 X^{\mathrm{T}} W_y (y - \hat{y}) + W_p (p_0 - \hat{p})\right) \tag{9.7}$$

$$\mathrm{Var}[\hat{p}] = \left(\alpha^2 X^{\mathrm{T}} W_y X + W_b\right)^{-1} \tag{9.8}$$

Two reasonable schemes for computing α exist, each developed with a slightly different objective in mind. The first coefficient, given in Eq. (9.9), eliminates the artificial *SSE* inflation by appropriately scaling down the data residuals. Koh and See [64] used a similar downweighting scheme in a Kalman filtering context. The second coefficient, given in Eq. (9.10), keeps confidence intervals from becoming arbitrarily small (even in the presence of *infinite* data) by downweighting the data more strongly as more data is included. Both of the lack-of-fit compensation coefficients were tried in the case studies of Chapters 12 and 13.

$$\alpha_1 = \sqrt{\frac{n_y}{SSE}} \tag{9.9}$$

$$\alpha_2 = \sqrt{\frac{z_0^2 + 1}{z_{LOF}^2 + 1}} \tag{9.10}$$

9.3 Parameter Consistency Testing

As mentioned above, using Bayesian statistics is supposed to generate a parameter estimate that is consistent with both data *and* prior information. This statement can be

tested with the statistical tests given in Eqs. (9.11) and (9.12), with n_p being the number of parameters and $\chi^2_{n_p,1-\alpha}$ being a critical chi-squared value. (Note: Strictly speaking, an F-test should be used when comparing to data-based parameter estimates. However, the chi-squared test becomes an increasingly good approximation as the number of data points used in the regression increases [78]. Typically, at least 30 data points must be used for the approximation to be valid. Thousands of data points are often used in model update problems.)

$$\text{if } (\hat{p}_{bayes} - \hat{p}_{data})^{\mathrm{T}} W_{data} (\hat{p}_{bayes} - \hat{p}_{data}) > \chi^2_{n_p,1-\alpha}, \quad \text{then declare inconsistent with data} \tag{9.11}$$

$$\text{if } (\hat{p}_{bayes} - p_0)^{\mathrm{T}} W_p (\hat{p}_{bayes} - p_0) > \chi^2_{n_p,1-\alpha}, \quad \text{then declare inconsistent with prior} \tag{9.12}$$

The quantity $\hat{p}_{data}$ refers to a parameter estimate obtained *without* using any prior information (computed using the weighted least-squares iteration of Eq. (3.9)), while $\hat{p}_{bayes}$ refers to the normal Bayesian regression parameter estimate. The data weighting matrix W_{data} is equal to $(X^{\mathrm{T}} W_y X)^{-1}$, and the prior weighting matrix is again $W_p = \mathrm{Var}^{-1}[p_0]$, as described in Chapter 4. Table 9.2 below provides critical values for $\chi^2_{n_p,1-\alpha}$ for different values of n_p at the 95% significance level [77].

Table 9.2: Critical Chi-Squared Values

n_p	$\chi^2_{n_p, 0.05}$	n_p	$\chi^2_{n_p, 0.05}$
1	3.841	7	14.067
2	5.991	8	15.507
3	7.815	9	16.919
4	9.488	10	18.307
5	11.070	11	19.675
6	12.592	12	21.026

Of course, it was mentioned in Chapter 3 that using Bayesian statistics provides a parameter estimate that is consistent with both data and prior information. The only situation in which the Bayesian estimate does *not* provide consistent estimates is when confidence regions from the data and confidence regions from prior information do not overlap *at all*. The Bayesian formulation will nevertheless come up with an average estimate located between the two, but it will be located in a region of extremely low probability and will thus register as inconsistent.

9.4 CROSS-VALIDATION TESTING

A final model verification technique that can be used is the cross-validation test. The premise of the test here is very simple but very powerful. In a cross-validation test, a portion of test data (usually half or more) is used to update the model. The updated model is then used to *predict* the portion of the data *not* included in the model update. If the new predictions fit the unused data as well as the model fit the original data, the model has passed a *cross-validation test*. Once the test is passed, it is reasonable to repeat the model update using *all* of the test data. If the cross-validation

test is not passed, there is probably a model form error or an important parameter has been left out of the analysis.

An acceptance criterion for determining if an updated model (based on fitted data subset #1) effectively predicts a different set of data (unfitted data subset #2) is given in Eq. (9.13). The selected critical value of 2.0 provides a small allowance for variations in relative noise levels in the data sets. The ideal result of Eq. (9.13) is 1.0, while results much larger than 2.0 mean that the model is *incapable* of predicting data beyond the specific set used to update the model.

$$\left(\frac{n_{y,\,subset\ \#1}}{SSE_{subset\ \#1}}\right)\left(\frac{SSE_{subset\ \#2}}{n_{y,\,subset\ \#2}}\right) < 2 \qquad \textbf{(9.13)}$$

Chapter 10: Visualization Statistics

The model update procedure described in Part II of this dissertation is complete. The only statistical quantity strictly required for interpreting the results is the sum-of-squares error term of Eq. (3.17). However, it is helpful to have a number of test-analysis *visualization* statistics available. These statistics allow the analyst to better understand the results of the model update. They can also be used as tools to locate problems with the model and/or data, either in terms of spatial location or excitation frequency.

Three visualization schemes are presented in this chapter. The first two are intended for use with sine-dwell test data, while the third is intended for use with broad-band FRF data.

10.1 Sine-Dwell Visualization Statistics

The Correlation Coefficient

In order to better determine how well an updated model predicts sine-dwell test data, two visualization statistics were developed. The first is a correlation coefficient r_k^2. Here, a subset of the data measurements, y_k, is compared to a prediction of the same subset, $\hat{y}_k$, using the correlation function given in Eq. (10.1). Values for r_k^2 can fall between zero and one.

$$r_k^2 = \frac{\left(y_k^{\mathrm{T}} W_{y,k} \hat{y}_k\right)^2}{\left(y_k^{\mathrm{T}} W_{y,k} y_k\right)\left(\hat{y}_k^{\mathrm{T}} W_{y,k} \hat{y}_k\right)} \tag{10.1}$$

A variety of subset definitions can be used, but the most useful way to break down the data is by *frequency*. Thus, y_k would correspond to the subset of the data that was generated with the excitation frequency ω_k. The purpose of the test would then be to compare response *shapes*, independent of scaling. If the results of test and analysis match perfectly, r_k^2 will have a value of 1.0. Values less than one indicate response shape discrepancies at the excitation frequency ω_k.

Using the r_k^2 statistic in this manner makes it very similar to the modal assurance criterion (MAC) [2] commonly used in modal testing to compare mode shapes. With the MAC, results are often compared between *different* frequencies as well, since mode shapes corresponding to different natural frequencies are expected to be orthogonal. However, there is no point in computing these off-diagonal terms in a dynamic response setting, since there is no reason for any given pair of response shapes to exhibit orthogonality. When used in this context, the term r_k^2 is called the frequency response assurance criterion (FRAC) [41].

The Scaling Factor

A second comparison that can be made is one between measured and predicted *response amplitudes*. Again, this can be done with any subset of the data, but it is most useful to have y_k and $\hat{y}_k$ correspond to the data and predictions generated using excitation frequency ω_k. The statistic that is computed here is the scaling factor c_k given in Eq. (10.2), which effectively gives the constant by which the actual data y_k would have to be multiplied to have amplitudes comparable to the predicted data $\hat{y}_k$.

$$c_k = \frac{y_k^T W_{y,k} \hat{y}_k}{y_k^T W_{y,k} y_k} \tag{10.2}$$

As with the correlation coefficient, c_k will have a value of 1.0 if the model matches the data perfectly. Values other than one indicate a response amplitude discrepancy. It should be noted that there is no restriction on the possible values for c_k, as there are with the correlation coefficient r_k^2. Any value can potentially be obtained. This type of comparison is normally not done with mode shapes, since they are usually rescaled according to some normalization criterion, but it can be a valuable statistic to use with dynamic response shapes.

10.2 FRF Visualization Statistics

It is possible to compute r_k^2 and c_k statistics for FRF data, but a much simpler means of visually comparing test and analysis is to plot FRFs from both test and analysis on the same chart. This can be done with real and imaginary components of the FRF, but it is usually more intuitive to look at magnitude and phase angle, since the positive-valued magnitudes can be plotted on a semi-logarithmic chart.

PART IV:

Case Studies

Chapter 11: The Simulated Beam

11.1 Simulation Overview

This study of a simulated beam was performed for the purpose of testing the Bayesian regression formulation presented in Chapter 3. The objective of the study was to study the stability of the model update process and to verify confidence interval estimates coming from the variance-covariance matrix of Eq. (3.19).

The Beam

Figure 11.1 below shows a schematic of the beam model used in the confidence interval verification study. Ten Euler-Bernoulli beam elements (with consistent mass matrices) were used to model the beam. All material properties and beam dimensions were held fixed and thus not included as parameters in the study. Also, the beam was assumed to have a 0.1% structural damping.

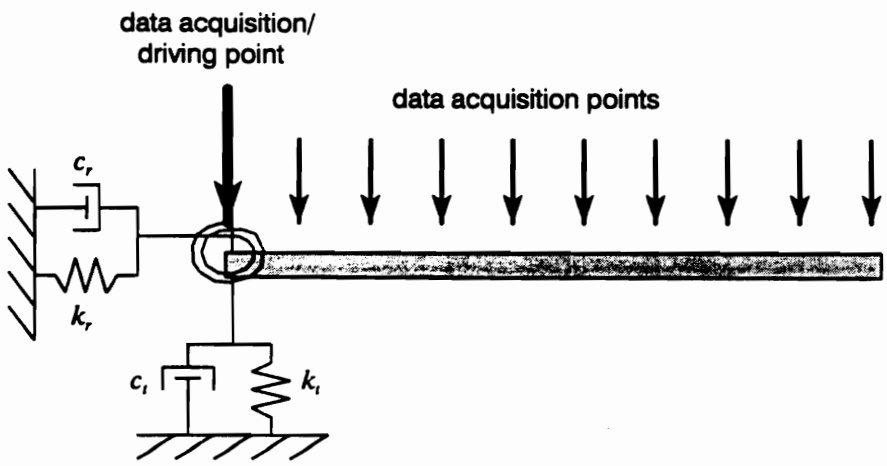

Figure 11.1: Analytical Beam Model

The four unknowns in the problem consisted of the springs and dampers shown in Figure 11.1, which might represent an elastic shock cord suspending the beam and a metallic stinger connecting a shaker to the top of the beam. The four parameters c_r, c_t, k_r, and k_t are estimated using the Bayesian regression formulation of Chapter 3.

Obtaining "Experimental" Data

In order to obtain "experimental" data, it was necessary to first choose "true" values for the four update parameters. The values shown in Table 11.1 below were selected. The stiffness values were based on previous research [92] concerning the particular beam and suspension system under test, while damping values were arbitrarily picked such that damping effects were noticeable (but not dominant) in a driving point FRF.

Table 11.1: Update Parameter Target Values

Translational stiffness,	k_t = 87.56 N/m	(0.50 lbf/in)
Translational damping,	c_t = 3.503 N·s/m	(0.020 lbf·sec/in)
Rotational stiffness,	k_r = 0.339 N·m/rad	(3.0 lbf·in/rad)
Rotational damping,	c_r = 0.0 N·m·s/rad	(0.0 lbf·in·sec/rad)

"Experimental data" was generated analytically by computing the dynamic response of the system at eight different excitation frequencies using Eq. (7.5), and then adding a *known* level of Gaussian noise to the response shapes obtained. The excitation frequencies of Table 11.2 were used.

Table 11.2: Excitation Frequencies

near mode 1 [Hz]		near mode 2 [Hz]		near mode 3 [Hz]		near mode 4 [Hz]	
17.30	17.35	47.55	48.52	93.20	95.09	154.07	157.18

Specifically, the "experimental" data was generated by adding Gaussian noise to each of the 11 displacement DOF coming from FE dynamic response predictions (both on the real and imaginary parts). The RMS amplitude of the noise was 4% of the RMS amplitude of the noise-free analytical response, meaning that the effective signal-to-noise ratio of the data was approximately 25-to-1. It should be noted that simulating the data in this manner bypassed the sine-dwell analysis of Chapter 5. The data described here are equivalent to what would be produced by that analysis. The rotational DOF of the FE model were excluded from the data set, since rotation data are normally not available in a structural dynamics test.

Selections of priors

Since the model update algorithm is based on Bayesian statistics, prior information is needed. Normally, these estimates would come from independent measurements, engineering judgement, etc., but the priors of Table 11.3 were specifically chosen for illustrative purposes. Variances are given in 95% confidence interval form, i.e., $\mu \pm 1.96\,\sigma$ for normally distributed parameters [77]. A comparison between Table 11.1 and Table 11.3 reveals that the prior estimates are not correct. However, this is the situation that will most likely occur in real-world situations.

Table 11.3: Prior Knowledge about Parameters

k_t = 70.05 ± 35.0 N/m	(0.40 ± 0.20 lbf/in)
c_t = 1.751 ± 0.175 N·s/m	(0.010 ± 0.001 lbf·sec/in)
k_r = 0.4518 ± 0.113 N·m/rad	(4.0 ± 1.0 lbf·in/rad)
c_r = 0.0000 ± 0.0123 N·m·s/rad	(0.00±0.10 lbf·in·sec/rad)

11.2 Simulation Results

Table 11.4 presents results for a single data set in which all eight response shapes (with noise added) were fitted simultaneously. The Bayesian regression formulation was used first *without* including the prior information of Table 11.3, and then it was used a second time *with* the prior information. The confidence interval estimates were extracted from the diagonal elements of $\mathrm{Var}[\hat{p}]$, as described in Chapter 3.

Table 11.4: Simulated Model Update Results

param.	units	target	prior	95% C.I.	data-only	95% C.I.	Bayesian	95% C.I.
k_t	N/m	87.56	70.05	±35.0	87.42	±15.8	91.24	±5.57
c_t	N·s/m	3.503	1.751	±0.175	3.534	±0.0665	3.320	±0.0583
k_r	N·m/rad	0.3390	0.4518	±0.113	0.8035	±1.21	0.4560	±0.112
c_r	N·m·s/rad	0.0	0.0	±0.0113	-1.82e-3	±2.44e-3	3.88e-3	±2.30e-3

A Monte Carlo study was performed to verify the confidence interval estimates of Table 11.4. In this study, 500 trials were run in which random noise was added to the true response shapes. The model update algorithm was used in each trial (on all eight noisy shapes simultaneously) to obtain updated parameter estimates. A "measured" $\mathrm{Var}[\hat{p}]$ was determined from the Monte Carlo trials [83]. Again, studies were run both with and without the use of prior information, and in both cases the measured variance-covariance matrix $\mathrm{Var}[\hat{p}]$ matched the estimate coming from Eq. (3.19) to three significant figures.

It should be noted that the confidence interval sizes coming from the Bayesian analysis were the smallest for *all* parameters. The use of prior information prevented a meaningless k_r estimate from being generated, as happened in the data-only case.

Also, the Bayesian regression iteration of Eq. (3.18) was *extremely* stable for this problem. Even if initial parameter guesses were as far as five standard deviations away from the prior estimates, the iteration of (3.18) always converged to same answer in less than 20 iterations, requiring less than a minute of CPU time on a Hewlett-Packard 9000/715 workstation.

Visualization Statistics

As described in Chapter 10, it is possible to compute a correlation coefficient (FRAC diagonal) r_k^2 and a scaling factor c_k for each excitation frequency ω_k. Figure 11.2 below shows these statistics for the results of Table 11.4 *before* the model update, where the FE model was assembled using prior information alone. It is apparent from Figure 11.2 that the model breaks down the most at low frequencies. This happened because the incorrectly modeled end conditions influence the low frequency behavior of the beam more than the high frequency behavior.

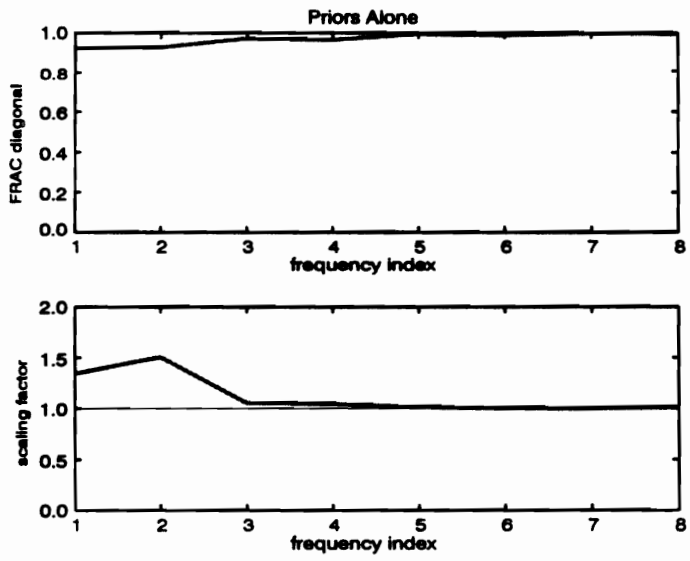

Figure 11.2: Visualization Statistics before Update

These same statistics were computed after the model update as well, as shown in Figure 11.3. Clearly, better results were obtained. In the top plot of Figure 11.3, the line representing r_k^2 is so close to 1.0 that it cannot be distinguished from the top border of the plot.

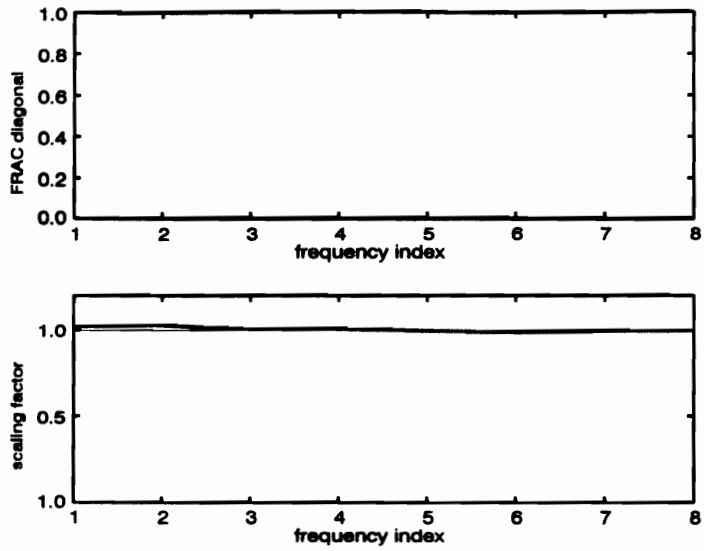

Figure 11.3: Visualization Statistics after Update

Model Update Verification Results

Since the data used here was entirely computer generated, there was no need to perform time-invariance testing or lack-of-fit testing. However, it was possible to perform a parameter consistency check. The result of the two consistency checks are given below in Eqs. (11.1) and (11.2).

$$\chi^2_{data} = (\hat{p}_{bayes} - \hat{p}_{data})^T W_{data} (\hat{p}_{bayes} - \hat{p}_{data}) = 39.87 \tag{11.1}$$

$$\chi^2_{prior} = (\hat{p}_{bayes} - p_0)^T W_p (\hat{p}_{bayes} - p_0) = 310.14 \tag{11.2}$$

Clearly, both of these results exceed the critical chi-squared value $\chi^2_{4,0.05} = 9.488$ coming from Table 9.2, which means that the parameter consistency test was failed. As described in Chapter 9, this indicates some sort of problem in the model update. In this case, at least on one of four things has gone wrong: (1) the model is incorrect (too few elements, neglected mass, bad boundary condition model, etc.) and is causing errors in the parameter estimates; (2) the data is defective (miscalibrated or mislocated) and is causing errors; (3) an important parameter has been left out of the analysis; or (4) the prior information provided by the analyst is wrong.

Because this study is based on simulated data, options (1), (2), and (3) can be ruled out. However, a careful comparison of Table 11.1 and Table 11.3 reveals that the prior estimate for c_t is grossly incorrect, and that the prior estimate for k_r is of marginal quality. This bad prior information has skewed the results of the entire analysis. Indeed, computation of a third chi-squared statistic, given in Eq. (11.3), shows that the final Bayesian estimates are inconsistent with the true target parameter values. Note: This third parameter consistency test can be performed only with simulated data. It cannot be done in the "real world."

$$\chi^2_{target} = (\hat{p}_{bayes} - p_{target})^{\mathrm{T}} W_{bayes} (\hat{p}_{bayes} - p_{target}) = 46.52 \qquad \textbf{(11.3)}$$

If better prior information is used, as given in Table 11.5, the results improve considerably, as shown in Table 11.6. New chi-squared statistics are shown in Eqs. (11.4), (11.5), and (11.6). All are well below the critical chi-squared value of 9.488. This means that the parameter estimates obtained using Bayesian regression are

consistent with the data, with prior information, and most importantly, with the true values. Indeed, this is the entire point of the exercise.

Table 11.5: Improved Prior Knowledge

k_t = 70.05 ± 35.0 N/m	(0.40 ± 0.20 lbf/in)
c_t = 3.590 ± 0.175 N·s/m	(0.0205 ± 0.0010 lbf·sec/in)
k_r = 0.3953 ± 0.113 N·m/rad	(3.5 ± 1.0 lbf·in/rad)
c_r = 0.0000 ± 0.0123 N·m·s/rad	(0.00±0.10 lbf·in·sec/rad)

Table 11.6: Update Results from Improved Priors

param.	units	target	prior	95% C.I.	data-only	95% C.I.	Bayesian	95% C.I.
k_t	N/m	87.56	70.05	±35.0	87.42	±15.8	91.24	±5.57
c_t	N·s/m	3.503	3.590	±0.175	3.534	±0.0665	3.320	±0.0583
k_r	N·m/rad	0.3390	0.3953	±0.113	0.8035	±1.21	0.4560	±0.112
c_r	N·m·s/rad	0.0	0.0	±0.0113	-1.82e-3	±2.44e-3	3.88e-3	±2.30e-3

$$\chi^2_{data,new} = (\hat{p}_{bayes,new} - \hat{p}_{data})^T W_{data} (\hat{p}_{bayes,new} - \hat{p}_{data}) = 0.49 \tag{11.4}$$

$$\chi^2_{prior,new} = (\hat{p}_{bayes,new} - p_0)^T W_p (\hat{p}_{bayes,new} - p_0) = 1.93 \tag{11.5}$$

$$\chi^2_{target,new} = (\hat{p}_{bayes,new} - p_{target})^T W_{bayes} (\hat{p}_{bayes,new} - p_{target}) = 6.79 \tag{11.6}$$

These results support the hypothesis of Chapter 1, which states that the use of Bayesian statistics is an effective framework for performing updates of finite element models. In this simulated study, the inclusion of prior information considerably improved the quality of the parameter estimates obtained. Additionally, the statistical tools of Chapter 9 were used to detect a problem with the model update, which was eliminated when improved prior information was used.

Chapter 12: The Sandia Test Frame

This chapter contains the results of *two* model updates performed on a single finite element model of a test frame used in research at Sandia National Laboratories [44]. The first update was performed with sine-dwell data taken from the structure, and the second was performed with FRF data taken from the structure. Issues relating to both update problems are discussed initially, with sine-dwell and FRF results following. The chapter concludes with a comparison of the two sets of update results.

12.1 Preliminary Issues

The Test Structure

The Sandia test frame was a frame built specifically for the purpose of developing joint models in structures made of tubular steel. A schematic of the test frame is shown in Figure 12.1. The frame was approximately one meter tall and weighed approximately 20 kg.

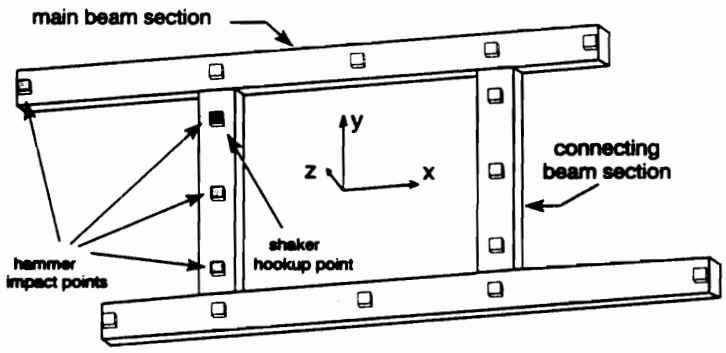

Figure 12.1: Sandia Test Frame

Test Configuration

To acquire dynamic response data, sixteen sets of triaxial accelerometers (for a total of 48) were mounted on the frame as shown in Figure 12.1 and Figure 12.2. Two dynamic response tests were performed. The first utilized harmonic excitation delivered through an electromagnetic shaker, generating data appropriate for the sine-dwell statistical analysis of Chapter 5. The second utilized broad-band excitation delivered through the impact of a modal test hammer, generating data appropriate for the FRF statistical analysis of Chapter 6. All excitation was delivered from the rear the frame in the positive z direction. Details on data acquisition are presented in the individual sections concerning the sine-dwell results and the FRF results.

Also, the weight of test frame was measured twice (once each on two different scales), generating two additional pieces of data to be used according to Eq. (3.23). The measurements were 20.06 ± 0.11 kg and 20.18 ± 0.11 kg.

The Finite Element Model

A finite element model of the frame was built in NASTRAN using beam elements. Figure 12.2 shows the node and element locations (units are in mm). Also shown are the four *double node* locations at which four sets of six springs (three translational and three rotational) were inserted *between* the beam elements. These springs represent the effective joint stiffness of the welds. The elements between the double nodes and main beam sections were assigned zero mass, since the connecting beams do not reach to the neutral axes of the main beam sections. To account for the effect of the accelerometers being offset from the neutral axes of the beams, rigid elements

were used in the finite element model to generate an additional node at the center of *each* accelerometer, for a total of 624 degrees-of-freedom. Point masses corresponding to the accelerometers were added at each additional node.

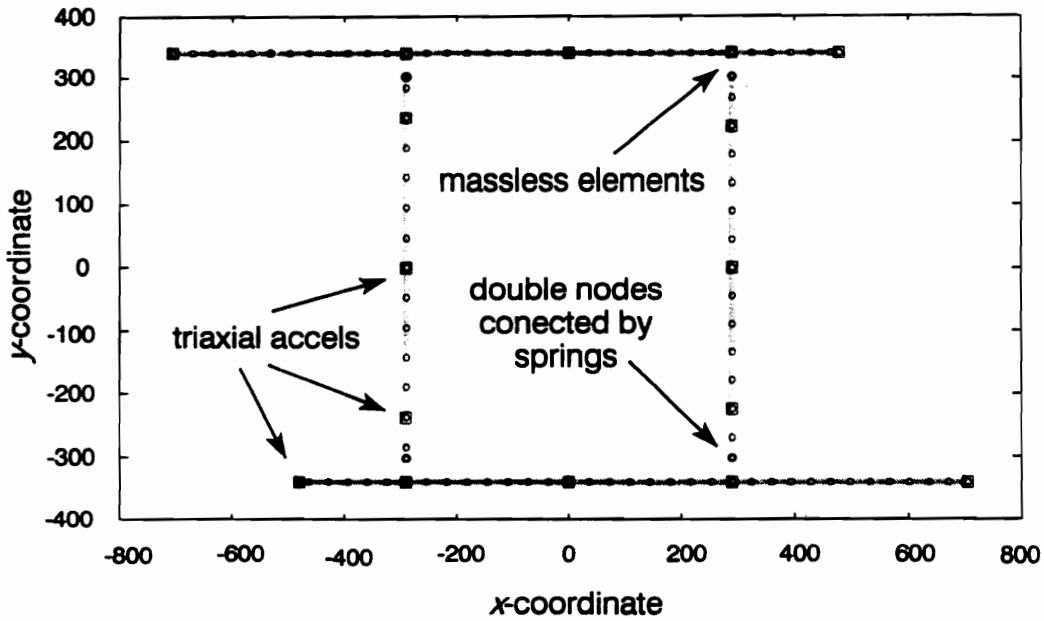

Figure 12.2: NASTRAN Model of Frame

Parameter selection

In order to update the model of the frame, modeling parameters affecting the behavior of the structure had to be selected. Additionally, the parameters had to be chosen such that the NASTRAN beam model could be modified based on changes in the parameters. As discussed in Chapter 4, it is best to have estimates of mean and variance for each parameter. This information is required to assemble the prior estimate vector p_0 and weighting matrix W_p, as discussed in Chapter 4.

The 16 parameters listed in Table 12.1 were selected as possible parameters to be used in the model update process. These parameters can be broken up into five groups: joint stiffness parameters, cross-section property parameters, material property parameters, damping parameters, and a force miscalibration adjustment parameter. Also listed with the parameters are the nominal values and confidence intervals (estimated means and variances) that define the prior for each parameter. All four joints were assumed to be the same, thus requiring only 6 parameters for joint modeling instead of 24. Parameters such as I_1 and I_2 were used instead of thickness and width parameters because the NASTRAN system matrices were linear with respect to I_1 and I_2. This made interfacing with NASTRAN and computing sensitivity matrices significantly easier. Also, these were the same parameters as used in prior research [44] concerning the test frame.

Table 12.1: Sandia Test Frame Update Parameters

$k_{t,x}$: translational joint stiffness	6.01e6 N/mm (±20000%)
$k_{t,y}$: translational joint stiffness	6.01e6 N/mm (±20000%)
$k_{t,z}$: translational joint stiffness	6.01e6 N/mm (±20000%)
$k_{r,x}$: rotational joint stiffness	2.53e8 N.mm (±20000%)
$k_{r,y}$: rotational joint stiffness	1.96e8 N.mm (±20000%)
$k_{r,z}$: rotational joint stiffness	4.80e8 N.mm (±20000%)
A: cross-section area	737 mm^2 (±3%)
I_1: major area moment of inertia	3.11e5 mm^4 (±6%)
I_2: minor area moment of inertia	5.89e5 mm^4 (±6%)
J: torsional moment of inertia	6.15e5 mm^4 (±15%)
E: modulus of rigidity	2.07e5 N/mm^2 (±5%)
ρ: density	7.85 Mg/mm^2 (±5%)
α_K: damping proportional to K	0.00 (±0.002)
α_M: damping proportional to M	0.00 (±20)
γ: structural damping ratio	0.00 (±0.2)
c: force miscalibration factor	1.00 (±0.05)

The α_K and α_M parameters are used to form a proportional viscous damping matrix $C = \alpha_K K + \alpha_M M$, while γ is used to form a complex stiffness matrix $(1 + i\gamma)K$ for structural damping. The force miscalibration correction factor is included to account for a possible miscalibration of the force transducer. If miscalibrated force signals are used, bias errors in all other parameters could result. Ideally, a calibration parameter would be included for every transducer used in the test, but this would result in far too many parameters (and extreme ill-conditioning) when 48 accelerometers are used.

If the parameters of Table 12.1 are considered carefully, it becomes evident that changes in certain parameters may have nearly (or even exactly) the same effects that changes in other parameters have. This would be manifested in the X matrix of Chapter 7 as a linear dependency which will cause the Bayesian regression formulation to fail. Because of this, it is probably not possible to *realistically* update the model by changing all 16 parameters. Indeed, in preliminary testing, all 16 parameters were used and completely unrealistic updates were obtained, even though the data was fitted well. Thus, the set of parameters was *restricted*, as explained below.

Since the effects of material property changes were highly correlated with the effects of beam cross-section property changes, the material property parameters were excluded from the study. Similarly, α_K and α_M have effects highly correlated with γ effects and were also left out. Finally, the force miscalibration correction factor c was excluded because it was likely to be *highly* correlated with many of the parameters. After these parameters were dropped, the six joint stiffnesses, four cross-

section properties, and one structural damping ratio remained, leaving a total of 11 parameters to be updated.

12.2 SINE-DWELL STUDY

The NASTRAN model of the frame was first updated using sine-dwell test data. The sine-dwell statistics developed in Chapter 5 were used to provide statistically qualified data (estimates $\hat{y}$ and weights W_y) for the model update algorithm. A summary of the test and the analysis follow.

Data Acquisition

There are basically two "categories" of excitation frequency for sine-dwell excitation. The first is near-resonance, where a small force generates a large response. The response at near-resonant frequencies is very sensitive to most structural parameters, including damping and any parameters that might shift natural frequencies. The second category is off-resonance, where a large force generates a small response. The response at off-resonance frequencies is less sensitive to most structural parameters. In particular, damping has almost no effect on off-resonance behavior. Table 12.2 below lists the 13 excitation frequencies used in the test, along with the category into which each frequency fits.

Table 12.2: Excitation Frequencies

1.	70 Hz	off-resonance
2.	94 Hz	near-resonance (slightly low)
3.	99 Hz	near-resonance (slightly high)
4.	140 Hz	off-resonance
5.	190 Hz	off-resonance
6.	245 Hz	near-resonance (slightly low)
7.	275 Hz	near-resonance (slightly high)
8.	425 Hz	off-resonance
9.	493 Hz	near-resonance (slightly low)
10.	503 Hz	near-resonance (slightly high)
11.	900 Hz	off-resonance
12.	940 Hz	near-resonance (slightly low)
13.	950 Hz	near-resonance (slightly high)

The frame was excited with an electromagnetic shaker at the locations shown in Figure 12.1. Time-series data were acquired from the force gauge and 47 of the accelerometers simultaneously. For each excitation frequency, 256 time samples per channel were acquired at a rate of 4096 samples per second. The 48th accelerometer was not used because the data acquisition equipment was limited to 48 channels total (47 accels and 1 force gauge). This process was repeated for each of the 13 excitation frequencies of Table 12.2.

The data were processed using the sine-dwell statistics of Chapter 5. Data points were accepted or rejected on the basis of Eqs. (5.24) and (5.25). All 1196 data points were accepted. The resulting data can be viewed as 13 complex-valued operating shapes, each with 47 spatial degrees-of-freedom. The task of the model updating process effectively becomes that of simultaneously fitting the 13 response shapes.

For illustrative purposes, a histogram of response data variances (the diagonal elements of $\mathrm{Var}[y]$) is shown in Figure 12.3. The bars toward the left end of the

histogram represent the number of data points with little "noise" or uncertainty, while bars on the right represent the number of data points with greater noise or uncertainty. This plot is not required for any type of numerical data analysis, but it does show why a *weighted* least-squares analysis is required for experimentally-acquired frequency response data. If weights were not used, the high variance data would completely dominate the regression analysis.

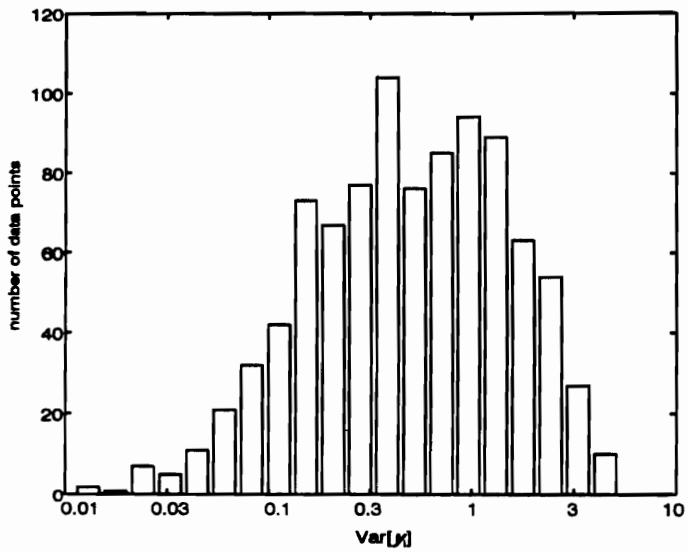

Figure 12.3: Variances of Sine-Dwell Data

The ratio of highest variance to lowest is approximately 470-to-1, with the bulk of the variances covering a two order-of-magnitude span. This is comparable to the 100-to-1 variance ratio presented in the example of Chapter 3. These variance ratios, combined with the fact that $n_t = 256$ data points were used to compute each variance estimate, means that estimated weights *should* be here, according to the criteria established by Deaton *et al* [74].

It should be noted that variance matrix $\mathrm{Var}[y]$ computed here is approximate, since the signal processing of Chapter 5 was developed for a single-input/single-output (SISO) system instead of a single-input/multi-output (SIMO) system. Correlations arise *between data points* in a SIMO system when there is noise on the force signal. This is not accounted for in the SISO signal processing, making the resulting statistical analysis approximate. The lack-of-fit compensation procedure of Chapter 9 helps compensate for this approximation. It should also be noted that the time-invariance testing of Chapter 9 was not performed because of the simultaneous nature of the data acquisition.

Updating Results with Visualization Statistics

Figure 12.4 below show visualization statistics (from Chapter 10) from the initial model. It is quite apparent that the model does not fit the data well. Correlations are poor, and amplitudes predictions are even worse. Also, the initial model predicted a structural weight of 20.69 kg, which is a statistically significant 3% heavier than the measured 20.13 kg.

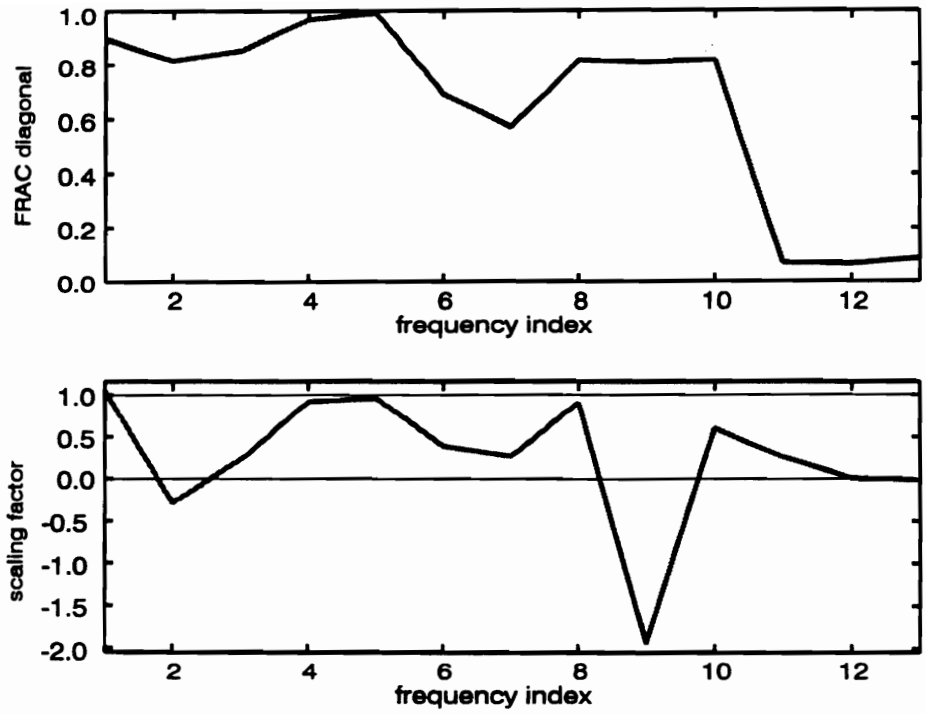

Figure 12.4: Visualization Statistics from Initial Model

As a first trial on updating the model, all 13 response shapes were used to update all 11 parameters. Unfortunately, this worked poorly; the high frequency response shapes predicted by the model were completely inaccurate. The reformulated Bayesian regression iteration of Chapter 8 effectively "got lost," becoming trapped in a local minimum in parameter space that yielded unrealistic parameter estimates.

To deal with this difficulty, a subset of the parameters was updated using only low frequency data. Specifically, only the cross-section property parameters and structural damping ratio were updated using only the 70 and 94 Hz response measurements. As shown in Figure 12.5, results were improved considerably. The *SSE* value was reduced from 1.50×10^9 to 1.66×10^8 (a factor of 9). It also reduced the subset *SSE* (for 70 and 94 Hz only) from 5.47×10^7 to 3.71×10^5 (a factor of 150). (Note: In

Chapter 9, data down-weighting schemes to compensate for lack-of-fit were discussed. The lack-of-fit compensation coefficient α_1 from Eq. (9.9) was used. Using α_2 from Eq. (9.10) downweighted the data to the point where they had no effect. As a result, the prior information almost *completely* dominated the analysis, leaving the model essentially unchanged.)

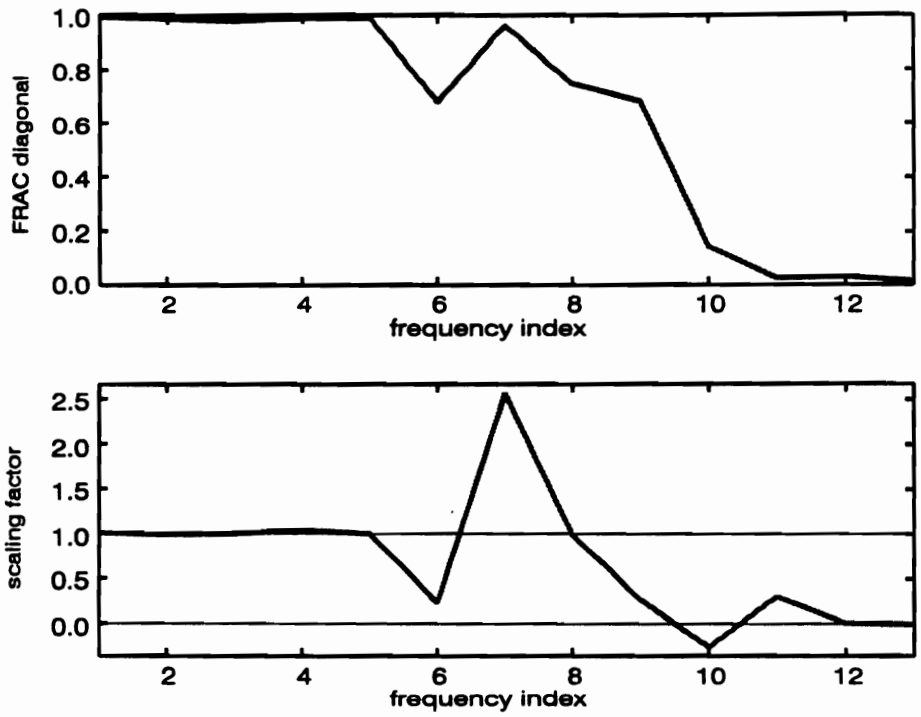

Figure 12.5: Visualization Statistics after Preliminary Update

The results from this preliminary analysis were used as the starting point for a second analysis which included more frequencies. This was done repeatedly until the first ten frequencies were relatively well fitted. Attempts were made to include the last three frequencies, but the model became inaccurate at such high frequencies, probably due to discretization error. Nevertheless, the results for the first ten

frequencies were good, as Figure 12.6 shows. *SSE* values were reduced from 1.50×10^9 to 1.77×10^7 (a factor 85) over the frequencies used.

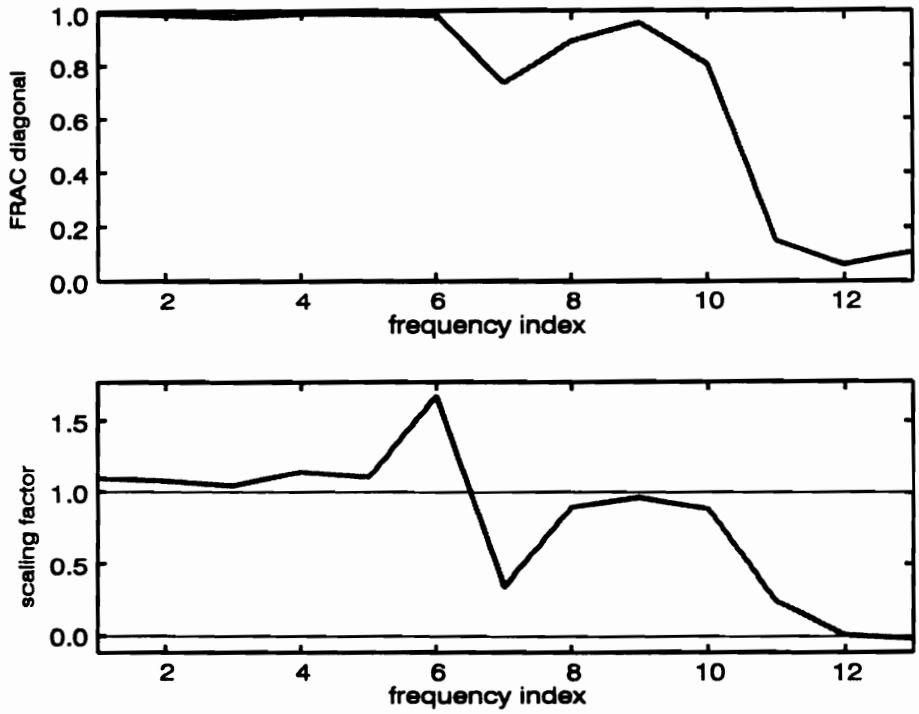

Figure 12.6: Visualization Statistics after Intermediate Update

The parameter estimates from this reduced parameter analysis were then used as the starting point for an analysis that included all 11 parameters and the first 10 frequencies. Results improved further as shown in Figure 12.7, although it remained impossible to obtain a good fit on the final three frequencies. The *SSE* value was reduced from 1.50×10^9 to 4.77×10^6 (a factor of 320). It should be noted that the structural weight predicted by the updated model was 20.22 kg, a statistically insignificant 0.45% away from the measured 20.13 kg. Total CPU time for the model update process (including all stages of adding frequencies and parameters) was approximately 20 hours. 200 iterations were typically required for each Bayesian regression solution.

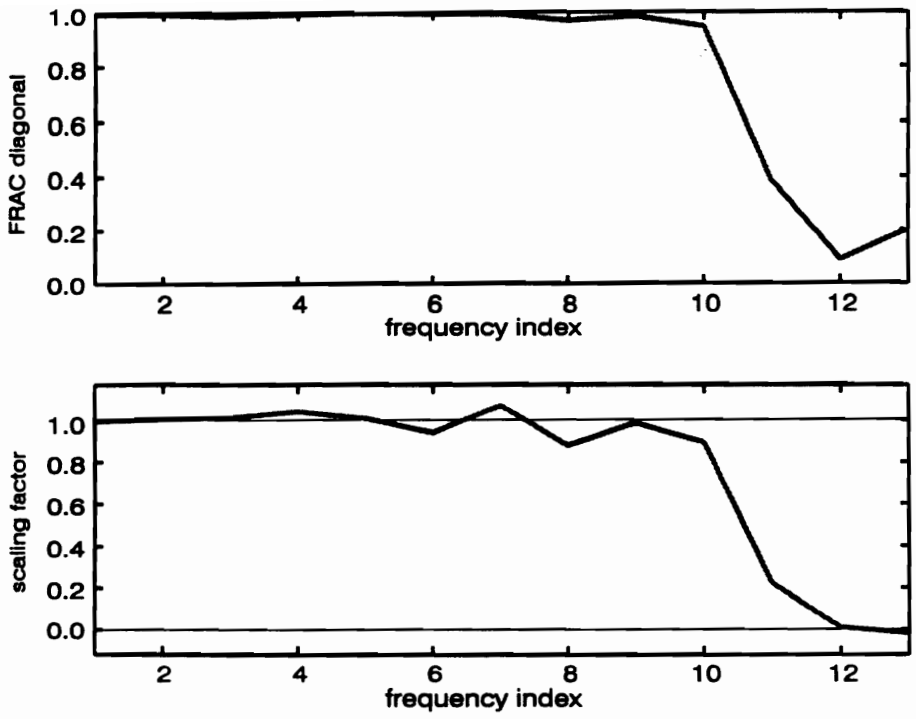

Figure 12.7: Visualization Statistics after Final Update

Sine-dwell Parameter Estimates

Table 12.3 contains a final list of updated parameter estimates. In the case of the translational stiffness parameters, the sizes of the confidence interval were significantly larger than the parameter estimates themselves. This occurs because the response of the structure was very insensitive to changes in those parameters. Since meaningless estimates were obtained for the k_t parameters, they were arbitrarily reset to their original values. Indeed, this was done when the plot of Figure 12.7 was generated. No meaningful difference in the *SSE* quantity was obtained.

Table 12.3: Parameter Estimates from Sine-Dwell Test

Parameter		prior	95% C.I.	data-only	95% C.I.	Bayesian	95% C.I.
$k_{t,x}$	10^6 N/mm	6.01	±1176.00	219.51	±8530.07	4.31	±1175.88
$k_{t,y}$	10^6 N/mm	6.01	±1176.00	0.01	±2761.38	1.79	±675.21
$k_{t,z}$	10^6 N/mm	6.01	±1176.00	299.52	±4690.60	22.71	±1175.55
$k_{r,x}$	10^8 N·mm/rad	2.53	±588.00	0.93	±0.05	0.90	±0.03
$k_{r,y}$	10^8 N·mm/rad	1.96	±392.00	20.84	±2.42	9.87	±0.91
$k_{r,z}$	10^8 N·mm/rad	4.80	±980.00	1.06	±1.02	1.06	±0.09
A	mm^2	737	±20	693	±13	720	±10
I_1	10^5 mm^4	3.11	±0.20	2.80	±0.05	2.94	±0.04
I_2	10^5 mm^4	5.89	±0.39	7.62	±0.75	6.29	±0.34
J	10^5 mm^4	6.15	±0.98	5.76	±0.31	7.50	±0.14
γ	--	0.00%	±20%	0.27%	±0.08%	0.61%	±0.06%

As mentioned earlier, the confidence intervals given in Table 12.3 were computed using lack-of-fit compensation coefficient α_1 from Eq. (9.9). The alternative downweighting coefficient α_2 was tried as well, but it downweighted the data to the point where the priors *completely* dominated the analysis.

A careful examination of the results of Table 12.3 reveals that the rotational joint stiffnesses were important to the analysis and were estimated accurately, while the translational joint stiffnesses were not. Slight improvements were made to the beam cross-section property estimates, which improved the weight estimate of the beam in addition to improving the predictive capability of the model. Also, a reasonable estimate of structural damping was obtained.

If the insignificant parameters (those dominated by the Bayesian priors) are dropped from the analysis, the same results are obtained. Table 12.4 summarizes these results.

Table 12.4: Reduced Parameter Results: Sine-Dwell

Parameter		prior	95% C.I.	data-only	95% C.I.	Bayesian	95% C.I.
$k_{r,x}$	10^8 N·mm/rad	2.53	±588.00	0.93	±0.05	0.90	±0.03
$k_{r,y}$	10^8 N·mm/rad	1.96	±392.00	20.84	±2.42	9.87	±0.91
$k_{r,z}$	10^8 N·mm/rad	4.80	±980.00	1.06	±1.02	1.06	±0.09
A	mm^2	737	±20	693	±13	720	±10
I_1	10^5 mm^4	3.11	±0.20	2.80	±0.05	2.94	±0.04
I_2	10^5 mm^4	5.89	±0.39	7.62	±0.75	6.29	±0.34
J	10^5 mm^4	6.15	±0.98	5.76	±0.31	7.50	±0.14
γ	--	0.00%	±20%	0.27%	±0.08%	0.61%	±0.06%

Model Update Verification

Parameter consistency checks were performed to ensure that the parameter estimates provided by the Bayesian statistics parameter update methodology were consistent with both data and prior information. Equations (9.11) and (9.12) were used to compute parameter consistency statistics of 17.052 and 4.036, respectively, which were below the critical chi-squared value of $\chi^2_{11,0.05} = 19.675$ from Table 9.2. This meant that the parameter consistency checks were passed and that realistic parameters had been obtained from the model update.

A cross-validation test was also performed to ensure that the model's predictive capability went beyond that of the data used in the model update. In this test, parameter estimate $\hat{\boldsymbol{p}}_{1\text{-}9}$ (obtained using only the first *nine* excitation frequencies of Table 12.2) was used to compute a response shape for the 10th frequency. The cross-validation ratio $\left(\frac{SSE_{10}}{n_{y,10}}\right)\left(\frac{n_{y,1\text{-}9}}{SSE_{1\text{-}9}}\right)$ from Eq. (9.13) came out at 1.43, which was below the critical value of 2.0, indicating a successful cross-validation test.

A second cross-validation test was performed in which $\hat{p}_{1\text{-}10}$ (the same as given in Table 12.3) was used to compute response shapes for the 11th, 12th, and 13th frequencies (900, 940, and 950 Hz). In this case, the cross-validation ratio $\left(\frac{SSE_{11\text{-}13}}{n_{y,11\text{-}13}}\right)\left(\frac{n_{y,1\text{-}10}}{SSE_{1\text{-}10}}\right)$ came out at 280, failing the test. These results imply that the predictive capability of the model is valid up to 500 Hz, but does not go much beyond that. A finer FE mesh or improved joint model would probably be required for accurate higher frequency predictions.

12.3 FRF Study

A second test was conducted on the Sandia test frame with impact excitation (from a modal test hammer) being used instead of harmonic excitation. Statistically-qualified FRF data (coming from the H_1 signal processing discussed in Chapter 6) was acquired from the same 48 accelerometers. The same 11 parameters were updated.

Data acquisition

A modal test hammer was used at four points on the structure, as shown in Figure 12.1 and Figure 12.2. Thirty averages were taken at each point. With each impact, 9192 time samples were taken on each channel at a rate of 4096 samples per second. This allowed for FFT computation of H_1 FRF estimates with 0.5 Hz resolution up to 2048 Hz. Due to time considerations, however, only a subset of the frequency lines was used. Specifically, one out of every 32 lines (every 16 Hz) was used up to 500 Hz, with the upper frequency limit being based on the results of the sine-dwell study of Section 12.2. However, there is no fundamental theoretical reason

that *all* of the spectral lines up to 500 Hz could not be used. Better data handling techniques and FRF prediction algorithms would have helped in this regard by reducing computation times.

With this data, the task of the Bayesian regression problem effectively became that of fitting (4 impact sites) * (48 accels) = 192 FRFs, each with 32 frequency lines. The FRF data and coherence estimates were generated by the data acquisition software (I-DEAS Masters' Series) used to collect the time-series data. Data points were accepted or rejected on the basis of the criterion given in Eq. (6.12), and a total of 2216 out of 12288 data points were thrown out due to excessive variance levels. Variances for the real and imaginary components of the FRF were computed using Eq. (6.11), as described in Chapter 6.

Again, it is possible to show the range of variances obtained using a histogram, as shown in Figure 12.8. Here, the ratio of maximum variance to minimum variance was 2400-to-1. However, most of the variances lay within a two order-of-magnitude span, which again was comparable to the span of the example given in Chapter 3. The range of variances seen in the FRF data is primarily due to the variability of the magnitude of the FRF. For a given coherence γ_k^2, the variance of the FRF magnitude H_k is proportional to the *square* of the FRF magnitude, as indicated by Eq. (6.11). Since 30 averages were used in computing the FRF estimates, statistical weights should be used with this data according to the guidelines established by Deaton *et al* [74].

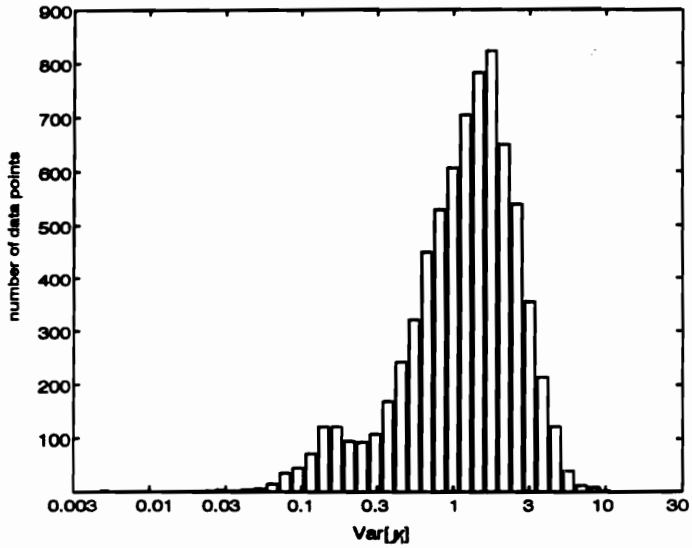

Figure 12.8: Variances of FRF Data

It should be noted that an exponential window was applied to the data to reduce the effects of leakage. Unfortunately, this probably affected the statistics of the FRF obtained from the data, but it is reasonable to expect that errors in the variance estimates were relatively small, especially when compared to the 100-to-1 variances ratios seen in Figure 12.8. As a source of *relative* weightings, the variance estimates served well, although they were no longer statistically optimal (in terms of minimizing parameter estimate variances). Confidence interval estimation might have also been affected, but the lack-of-fit compensation coefficient α_1 of Eq. (9.9) helped compensate for the use of these approximate weights.

FRF Results

The updating of the model using FRF data was performed in a manner similar to that used in the sine-dwell study. Initially, a subset of the update parameters (the same

subset as with the sine-dwell data) was used with only low frequency test data. The amount of frequency data included in each successive stage was increased, with parameter estimates from one solution being used as the starting point for the next. This was repeated three times until a reasonable frequency range was spanned (in this case, from zero to 500 Hz), and then all 11 parameters were included in the model update. Total CPU time was approximately 50 hours, with approximately 200 iterations being required per Bayesian regression solution.

Figure 12.9 and Figure 12.10 show two FRFs (out of 192 total) predicted using the initial model plotted with the FRFs *measured* from the frame. It is apparent that the initial model does not predict the data well, particularly at higher frequencies.

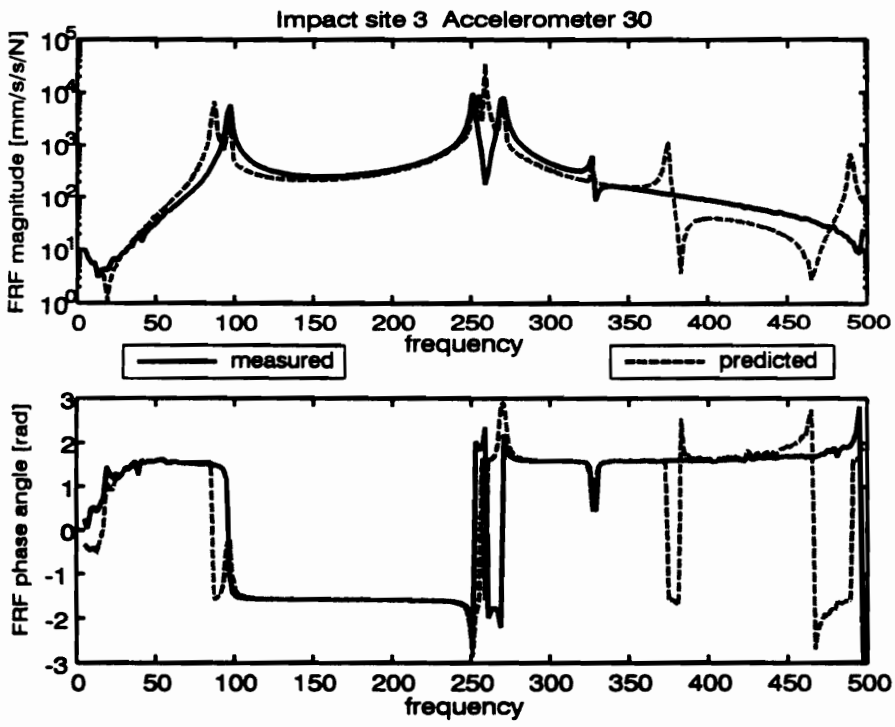

Figure 12.9: Initial Model FRF Comparison

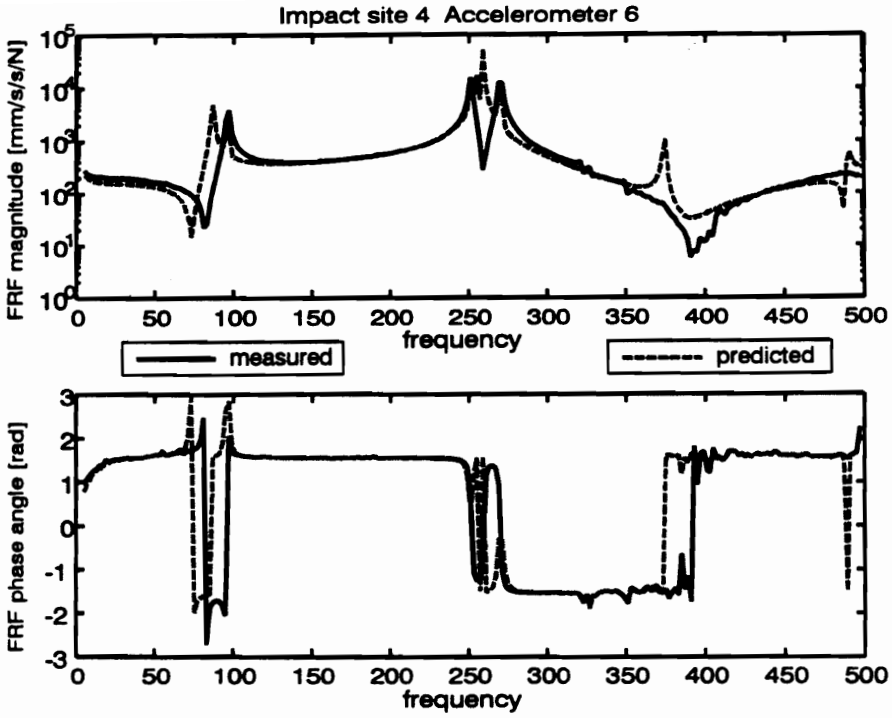

Figure 12.10: Additional Initial Model FRF Comparison

After the model updating was completed, the predicted frequency response functions became considerably more accurate, as the *SSE* of Eq. (3.17) was reduced from 1.64×10^9 to 2.47×10^7 (a factor of 67). The frequency response functions plots are shown again in Figure 12.11 and Figure 12.12 using updated parameter estimates. The estimated weight dropped to 20.08 kg, a statistically insignificant 0.27% away from the measured 20.13 kg.

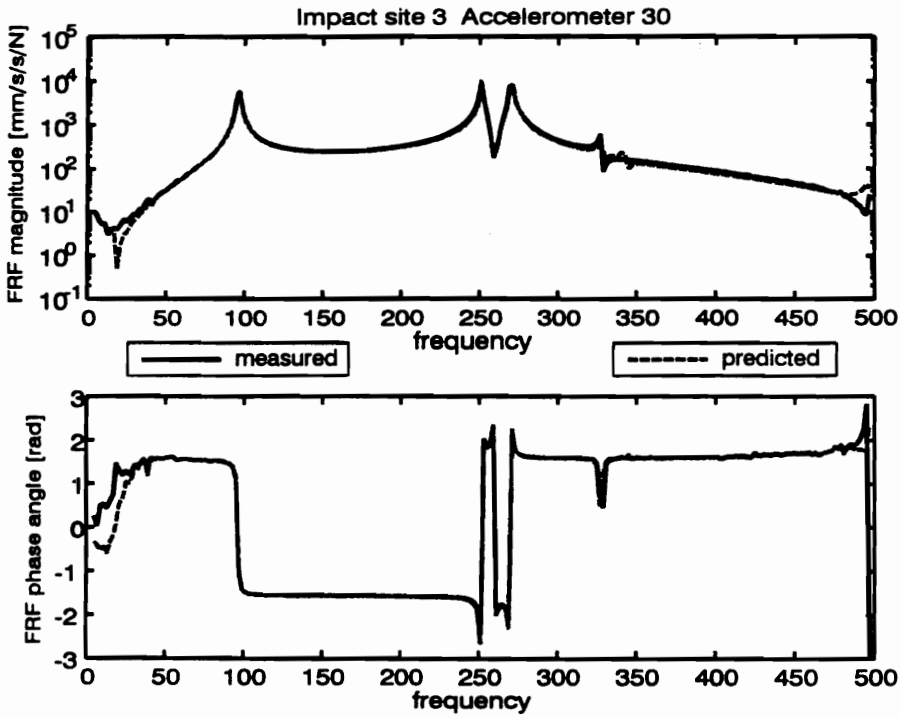

Figure 12.11: Final Model FRF Comparison

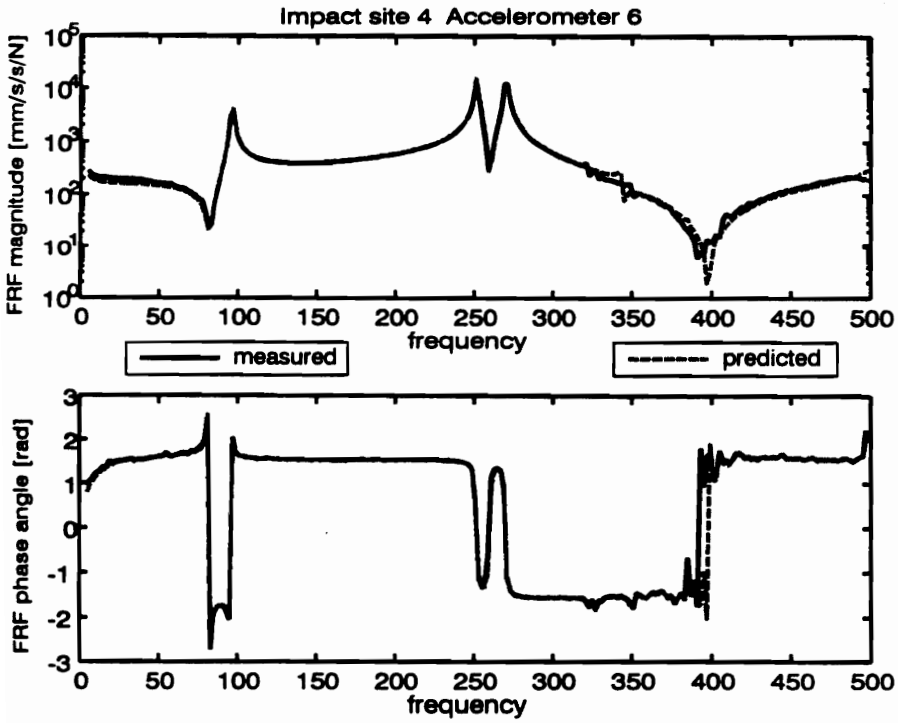

Figure 12.12: Additional Final Model FRF Comparison

Table 12.5 below shows the updated parameters obtained from the FRF fit. Again, parameters with confidence interval sizes larger than the parameter estimate itself were arbitrarily reset to their initial values, as was done in generating the FRF plots of Figure 12.11 and Figure 12.12.

Table 12.5: Parameter Estimates from FRF Test

Parameter		prior	95% C.I.	data-only	95% C.I.	Bayesian	95% C.I.
$k_{t,1}$	10^6 N/mm	6.01	±1176.00	12.54	±4641.12	2.42	±1172.17
$k_{t,2}$	10^6 N/mm	6.01	±1176.00	0.03	±1356.82	2.34	±273.91
$k_{t,3}$	10^6 N/mm	6.01	±1176.00	76.15	±2671.64	17.91	±1165.12
$k_{r,1}$	10^8 N·mm/rad	2.53	±588.00	0.909	±0.013	0.906	±0.012
$k_{r,2}$	10^8 N·mm/rad	1.96	±392.00	9.33	±0.12	9.38	±0.11
$k_{r,3}$	10^8 N·mm/rad	4.80	±980.00	1.03	±0.05	1.03	±0.05
A	mm^2	737	±20	713	±4	715	±3
I_1	10^5 mm^4	3.11	±0.20	2.80	±0.01	2.92	±0.01
I_2	10^5 mm^4	5.89	±0.39	7.62	±0.19	6.25	±0.17
J	10^5 mm^4	6.15	±0.98	5.76	±0.04	7.38	±0.04
γ	--	0.00%	±20%	-0.50%	±0.01%	-0.31%	±0.01%

As with the sine-dwell results of Section 12.2, using FRF data in the Bayesian regression formulation of Chapter 3 yielded accurate estimates of the rotational joint stiffnesses used to model the welded joints in the test frame, as seen in Table 12.5. The translational joint stiffness parameters could not be estimated accurately, as the response of the system was almost completely insensitive to these parameters. Improvements were again made to the beam cross-section property estimates, which again improved the estimate of the weight of the beam. The confidence intervals for

the rotational joint stiffnesses and cross-section properties overlapped the intervals of Table 12.3 coming from the sine-dwell test.

However, the confidence intervals for structural damping did not overlap. A negative structural damping coefficient was obtained with FRF data, which is not a meaningful result. The application of an exponential window to the data or leakage effects may have caused this, but the true source of the negative damping coefficient estimate remains unknown.

If the insignificant parameters (those dominated by the Bayesian priors) are dropped from the analysis, nearly identical results are obtained. Table 12.6 summarizes this second set of results.

Table 12.6: Reduced Parameter Results: FRF

Parameter		prior	95% C.I.	data-only	95% C.I.	Bayesian	95% C.I.
$k_{r,1}$	10^8 N·mm/rad	2.53	±588.00	0.909	±0.012	0.906	±0.011
$k_{r,2}$	10^8 N·mm/rad	1.96	±392.00	9.33	±0.05	9.38	±0.04
$k_{r,3}$	10^8 N·mm/rad	4.80	±980.00	1.03	±0.01	1.03	±0.01
A	mm^2	737	±20	713	±4	715	±3
I_1	10^5 mm^4	3.11	±0.20	2.80	±0.01	2.92	±0.01
I_2	10^5 mm^4	5.89	±0.39	7.62	±0.15	6.25	±0.13
J	10^5 mm^4	6.15	±0.98	5.76	±0.02	7.37	±0.02
γ	--	0.00%	±20%	-0.50%	±0.01%	-0.31%	±0.01%

Model Update Verification

As with the sine-dwell results, parameter consistency checks were performed on the $\hat{p}$ vector obtained using the FRF data. Equations (9.11) and (9.12) were again used to compute the chi-squared statistics 17.771 and 2.086, respectively, which were

less than the critical chi-squared value of $\chi^2_{11,0.05} = 19.675$ from Table 9.2. Thus, the Bayesian parameter estimates passed the parameter consistency check.

Since only a subset of the FRF data was used in the model update, performing a cross-validation test here was even easier. The original data came from frequency set #1, which consisted of the frequencies {5 Hz, 17 Hz, 29 Hz, ···, 497 Hz}. The results from this set were used to predict FRF values at frequency set #2, which consisted of the frequencies {7 Hz, 19 Hz, 31 Hz, ···, 499 Hz}. The cross-validation ratio $\left(\frac{SSE_{\#2}}{n_{y,\#2}}\right)\left(\frac{n_{y,\#1}}{SSE_{\#1}}\right)$ of Eq. (9.13) came out at 1.002, which is a nearly ideal result that easily passes the cross-validation test. For frequency interpolation purposes, this updated model is almost ideal.

12.4 Concluding Remarks on Sandia Test Frame

If the results from Table 12.5 are compared to those of Table 12.3, it will be noticed that the confidence intervals obtained from the FRF data are smaller than those obtained from the sine-dwell data. The smaller size of the confidence intervals is due primarily to the increased amount of data available for the update (10072 points vs. 974 points). As pointed out in Chapter 9, however, ever-increasing amounts of data will cause confidence intervals to become arbitrarily small, possibly around the *wrong answer* if there is a significant lack-of-fit problem with the model. The lack-of-fit compensation factor α_2 was developed to deal with this problem, but the compensation it provided was too strong, effectively eliminating the data from the analysis. Therefore, only α_1 was used, possibly resulting in Table 12.5 having smaller confidence intervals than it should.

Fortunately, even if the sizes of intervals are off somewhat due to lack-of-fit, they are still correct *relative* to each other. This helps the analyst determine which variables are most important to the model update analysis and which are not. Fortunately, the confidence intervals from both studies overlapped (except for the structural damping coefficient γ) in this study, which adds credibility to the results.

Chapter 13: The Cantilever Beam

INTRODUCTION

This chapter contains the results of finite element model update performed on a cantilever beam. The purpose of the study was to investigate how closely the clamping apparatus (used to hold the beam) approximated *fixed* boundary conditions at the end of the beam. It is more complete than the Chapter 92 study of the Sandia test frame, as all of the data verification tests of Chapter 9 were used.

13.1 PRELIMINARY ISSUES

The Test Beam

Figure 13.1 below shows a schematic of the beam used. The beam had dimensions 0.00635 m × 0.0381 m × 0.6096 m (0.25 in × 1.50 in × 24.00 in) and was made of steel. The beam was bolted vertically into a clamping bracket such that 400 mm was exposed. Two transducers (a force gauge and accelerometer) were attached to the beam 6.5 mm from the top. An electromagnetic shaker was attached to the force gauge with a thin metallic stinger.

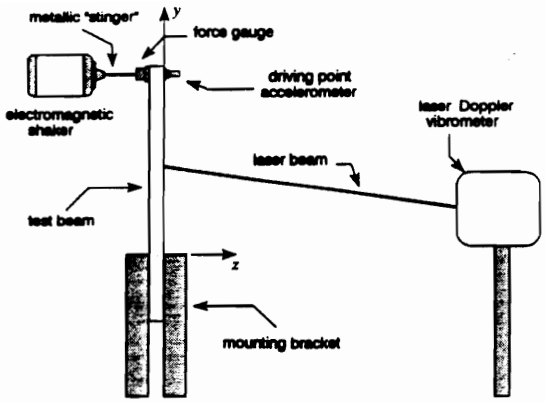

Figure 13.1: Cantilever Beam Setup

Figure 13.2 below shows a more detailed schematic of the clamping brackets used to hold the beam, since they were the focus of the study. Each bracket was composed of 10 mm steel plates welded together. The beam was positioned between the two brackets, which were then clamped together using four 10 mm bolts. The entire assembly was then bolted to a large concrete block.

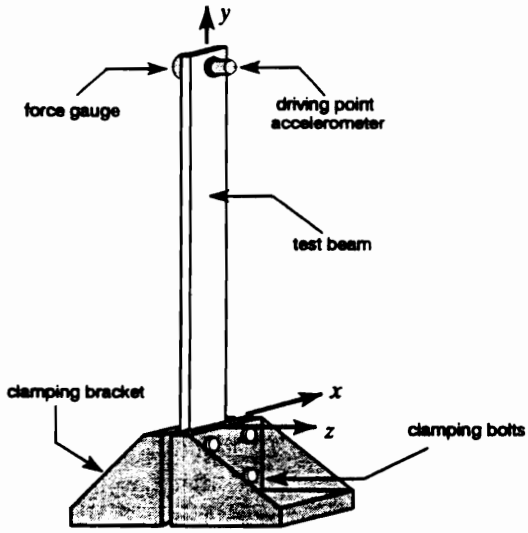

Figure 13.2: Clamp Schematic

The Finite Element Model

The beam was modeled using 65 Euler-Bernoulli beam elements (each with two nodes and four degrees-of-freedom). Consistent mass matrices were used. When assembled, the resulting FE model had 66 nodes and 132 degrees-of-freedom, as shown in Figure 13.3 below. Note: the nodes were assembled essentially as if there were 64 elements in the model. An extra element and node were inserted 6.5 mm from the top of the beam at the location where the two transducers were located. Because the shaker was attached to the force gauge, this also was the location of the driving point. The entire model was implemented using MATLAB m-files, with beam element definitions coming from Przemieniecki [84].

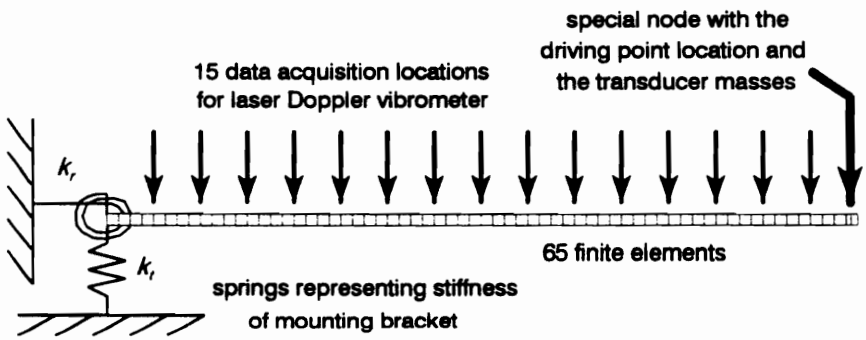

Figure 13.3: FE Model of Cantilever Beam

The two springs in Figure 13.3 represent the effective stiffness of the clamping brackets used to hold the beam. Obtaining good estimates for k_r and k_t was the objective of this study. A lumped mass and rotatory inertia, 0.01385 kg and 4.248×10^{-6} kg·m^2 respectively, were placed at the extra node to represent the mass

loading effects caused by the force gauge and accelerometer. The sources of the estimates for these numbers are given in Appendix E.

Since data was to be acquired at frequencies near the natural frequencies of the first three modes, it was decided that the finite element model must be converged up to at least the fourth mode. A number of different mesh densities were tried, and 65 elements were sufficient to converge the 4th natural frequency to within 0.01 Hz.

Parameter selection

In building this model, ten parameters were used to construct the finite element model, as listed in Table 13.1. These can be broken up into five groups: effective clamp stiffness parameters, material property parameters, beam cross-section property parameters, and lumped mass/stiffness parameters. Also listed with the parameters are their priors, which are estimates of mean and variance summarizing the quality of the initial estimates. The material property numbers came from a materials reference [93], while the other priors came from careful measurements of the system as described in Appendix E.

Table 13.1: Cantilever Beam Update Parameters

k_r: translational clamp stiffness	6.00e7 N·m/rad (±1000%)
k_t: rotational clamp stiffness	3.00e5 N/m (±1000%)
E: modulus of rigidity	2.00e11 N/m^2 (±5%)
ρ: density	7860 kg/m^2 (±5%)
γ: structural damping ratio	0.0003 (±100%)
t: thickness	0.00640 m (±0.31%)
w: width	0.03810 m (±0.53%)
m_t: effective transducer mass	0.01385 kg (±20%)
I_t: effective transducer rotatory inertia	4.24e-6 kg·m^2 (±20%)
k_s: stinger rotational stiffness	0.328 N·m/rad (±20%)

Data Acquisition

As with the Sandia test frame of Chapter 12, two categories of excitation frequency were used for sine-dwell excitation. The first was near-resonant, where a small force generates a large response, while the second was off-resonant, where a large force generates a small response. Table 13.2 below lists the 12 excitation frequencies used in the test, along with the category into which each frequency fits.

Table 13.2: Excitation Frequencies

1.	15 Hz	off-resonance
2.	26.25 Hz	near-resonance (slightly low)
3.	28.25 Hz	near-resonance (slightly high)
4.	50 Hz	off-resonance
5.	90 Hz	off-resonance
6.	170 Hz	near-resonance (slightly low)
7.	180 Hz	near-resonance (slightly high)
8.	250 Hz	off-resonance
9.	400 Hz	off-resonance
10.	450 Hz	near-resonance (slightly low)
11.	470 Hz	near-resonance (slightly high)
12.	530 Hz	off-resonance

Blocks of time-series data were acquired from the force gauge, the accelerometer, and the scanning laser Doppler vibrometer (SLDV) for each of the 45 data acquisition points, as shown in Figure 13.4. The y-axis values were picked such that data was acquired at FE nodes $\{\#5, \#9, \#13, \cdots, \#61\}$ (one in every four FE nodes), while x-axis values were arbitrarily set at $\{-12.7\text{ mm}, 0.0\text{ mm}, 12.7\text{ mm}\}$. Appendix D describes how the SLDV was registered in space relative to the beam and how scanning angles were computed to hit the desired points. For each excitation frequency, 250 time samples were acquired at a rate of 2000 samples per second.

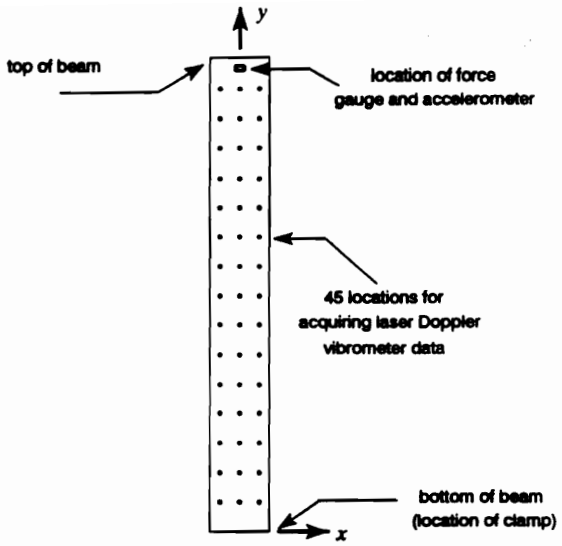

Figure 13.4: Data Acquisition Pattern

The data was processed using an LAPACK-based [88] implementation of the sine-dwell statistics of Chapter 5. Three additional harmonics were fitted along with each fundamental excitation frequency for the purpose of detecting harmonic distortion. Harmonic distortion was detected in the 26.25 Hz and 28.25 Hz results, probably due to distortion in the amplifier system used to drive the electromagnetic shaker rather than nonlinear behavior in the beam. The extra information coming from the additional harmonics was *not* included in the model update process, since it failed the variance requirements of Eqs. (5.24) and (5.25).

For informational purposes, a histogram of data variances (the diagonal elements of $\mathrm{Var}[y]$) is shown below in Figure 13.5. As in Chapter 12, this plot is unnecessary for the data analysis, but it does show why a *weighted* least-squares analysis is required for experimentally acquired frequency response data.

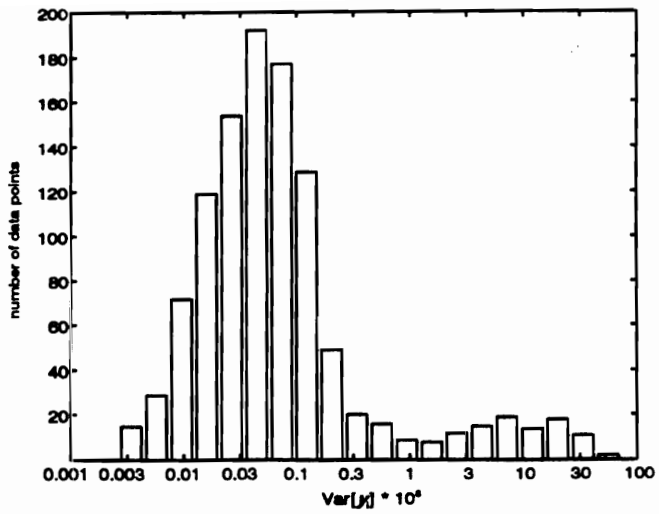

Figure 13.5: Variances of Data from Cantilevered Beam

Specifically, the ratio of the highest variance to the lowest is approximately 27000-to-1, with the bulk of the variances covering a four order-of-magnitude span. This is much larger than the 100-to-1 ratio of the example presented in Chapter 3. These ratios, combined with the fact that 250 points were used to compute each variance estimate, means that a weighted least-squares formulation should be used with this data according to the guidelines established by Deaton *et al* [74].

The reason that the histogram of Figure 13.5 is "tail-heavy" is because of a phenomenon known as "drop-outs" in the laser-Doppler vibrometer data. Drop-outs occur when the laser beam strikes an optically rough point on the surface of the structure, reducing the strength of the reflected laser beam. If the reflected beam becomes too weak, the demodulator in the laser system is unable to produce a meaningful velocity signal and spikes are produced in the time-series data. This increases the variance associated with a least-squares fit of the time-series data. Fortunately, drop-outs happened at only a few points on the structure.

Ensuring Data Quality

In order to ensure that the frequency response data generated using the signal processing of Chapter 5 were valid, variance testing was performed. Data points from the SLDV, consisting of real and imaginary response components from each data acquisition location/excitation frequency combination were accepted or rejected on the basis of Eqs. (5.24) and (5.25). Sixteen of the 990 total data points were rejected and thus excluded from the Bayesian regression analysis.

Tine-invariance testing was also performed on force amplitudes and driving point response components for each of the 12 excitation frequencies using the modified Durbin-Watson test described in Chapter 9. Table 13.3 below show the modified d_l values computed for the fundamental excitation frequency using Eq. (5.17).

Table 13.3: Time-Invariance Testing Results

frequency [Hz]	d_l for force ampl.	d_l for real(accel)	d_l for imag(accel)	comments
15	1.49	1.41	2.09	inconclusive
26.25	2.07	1.96	2.45	inconclusive
28.25	1.67	1.51	1.86	inconclusive
50	2.01	2.59	1.79	passed
90	2.34	2.07	1.37	inconclusive
170	2.47	2.26	1.93	passed
180	1.77	1.53	1.99	inconclusive
250	2.20	2.19	2.66	passed
400	1.72	2.60	2.33	passed
450	**0.12**	**0.03**	2.53	**failed strongly**
470	1.38	1.64	1.74	inconclusive
530	2.10	1.75	1.99	passed

Only 6 of the 12 sets of dynamic response data completely passed the test. Careful examination of the 5 inconclusive sets revealed no perceptible pattern to the residuals. The set corresponding to 450 Hz excitation, however, failed strongly. Figure 13.6 below shows the force amplitudes and driving point response components from this particular set. Clearly, there is a trend to the data, which is probably due to a change in the settings of the charge amplifiers used to power the force gauge and accelerometer. Insufficient time was allowed for the units to settle. As a result of this analysis, the data set corresponding to 450 Hz was discarded from the analysis.

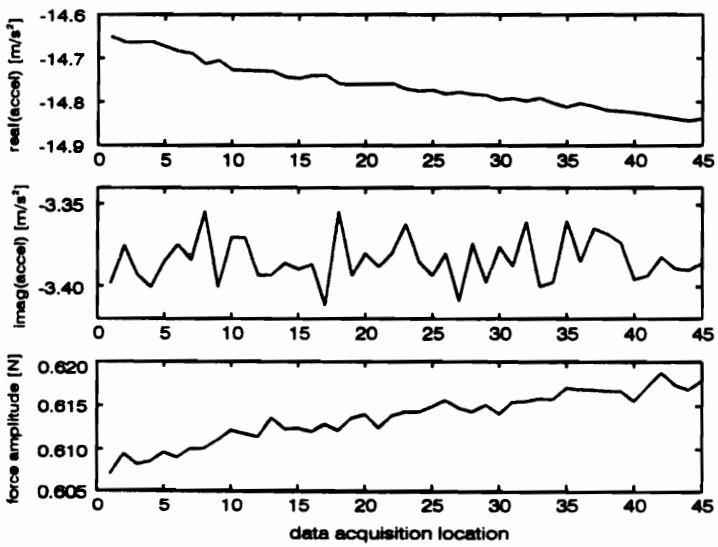

Figure 13.6: Evidence of Time-Variation in 450 Hz Data

Additionally, the data set corresponding to 470 Hz was thrown out since the beam was exhibiting torsional behavior at that frequency, an effect for which the beam elements of the FE model could not account. Thus, after the signal processing was complete and data points/sets thrown out, 10 complex-valued response shapes were available, each with 45 spatial degrees-of-freedom (minus the few DOF excluded due

to variance considerations). The task of model updating effectively became that of simultaneously fitting the 10 response shapes.

Data acquired from the accelerometer was also included in the model update process. Instead of using multiple accelerometer-based $\hat{c}$ vectors, an average response vector was computed for each excitation frequency using Eq. (5.27), where accelerometer-based $\hat{c}$ vectors were used instead of $\hat{a}$ vectors). A measurement of the weight of the beam, 1158.5 ± 0.3 g, was also included.

13.2 Model Updating Results

The procedure that was used to estimate parameters for the Sandia test frame was used again with the cantilevered beam. Initially, only a subset of the frequency response data was used with a subset of the parameters; in this case, it was the first five excitation frequencies with parameters k_r, k_t, E, and ρ. More frequencies were added until all 10 shapes had been fitted, and then all 10 parameters were included. The *SSE* term of Eq. (3.17) was reduced from 4.57×10^9 to 5.20×10^6 (a factor of 880).

Total computing time required was on the order of 3 hours. A small convergence study was performed by plugging different numbers (up to five standard deviations away from the priors for all parameters except clamp stiffnesses) in at the beginning of the process. This was performed 10 times, and the results converged to the same result all 10 times, although the number of iterations required for convergence differed in each case.

The results of the model update are given in Table 13.4. Unfortunately, the problem was so poorly conditioned *without* the priors that it was impossible to obtain data-only results as was done for comparison purposes back in Chapters 11 and 12. To quantify this ill-conditioning, the condition number of the correlation matrix $\mathrm{Corr}[\hat{p}]$ of Eqs. (3.5) and (3.6) was computed for the parameter estimates of Table 13.4. A condition number of 1.73×10^4 was obtained, which is a reasonable number for a ten parameter problem. If the correlation matrix is also computed for an estimate of $\mathrm{Var}[\hat{p}]$ *without* using W_p, then a condition number of 1.82×10^{16} is obtained, which effectively means that the system is singular, having a linear dependency present.

Table 13.4: Parameter Estimates from Cantilever Beam

Parameter		prior only	95% C.I.	Bayesian	95% C.I.
k_t	10^8 N/m	1.35	±135.00	0.052	±0.005
k_r	10^4 N·m/rad	2.80	±280.00	0.458	±0.008
E	10^9 N/m^2	200	±10	201.3	±2.8
ρ	kg/m^3	7860	±393	7794	±46
γ	--	0.030%	±0.030%	0.020%	±0.030%
t	mm	6.40	±0.02	6.40	±0.02
w	mm	38.1	±0.2	38.1	±0.2
m_0	g	13.85	±2.50	13.26	±0.88
I_0	10^{-6} kg·m^2	4.25	±0.85	3.92	±0.84
k_s	N·m/rad	0.328	±0.066	0.323	±0.065

As with the Sandia test frame model update, the lack-of-fit compensation coefficient α_1 from Eq. (9.9) was used to downweight the data and to adjust the confidence intervals sizes. It is quite apparent from the results of Table 13.4 that prior informa-

tion dominated several of the parameter estimates. The five parameters t, w, γ, I_0, and k_s were influenced by the priors the most, having confidence interval sizes little or no smaller than the original confidence interval sizes. If these five parameters are held fixed at their original values and left out of the analysis entirely, an identical reduction of the *SSE* term is obtained. The results for the reduced parameter analysis (in which parameters t, w, γ, I_0, and k_s were dropped) are given in Table 13.5. Confidence interval sizes dropped since some of the parameters that were eliminated had effects that were correlated with the effects of the parameters left in the analysis.

Table 13.5: Reduced Parameter Results: Cantilever Beam

Parameter		prior only	95% C.I.	Bayesian	95% C.I.
k_t	10^8 N/m	1.35	±135.00	0.052	±0.003
k_r	10^4 N·m/rad	2.80	±280.00	0.458	±0.006
E	10^9 N/m^2	200	±10	201.4	±1.0
ρ	kg/m^3	7860	±393	7794	±1.3
m_0	g	13.85	±2.50	13.23	±0.50

In both analyses, the estimates for E and m_0 did not change significantly, but the confidence interval sizes did drop. This indicates that confidence in the E and m_0 estimates has been increased. The parameter ρ was changed significantly, improving the estimate of the weight of the beam. Finally, new estimates for the parameters k_t and k_r were obtained, which was the main purpose in performing the model update. These estimates are a considerable improvement over the crude estimates of Appendix E and represent a success of the Bayesian regression formulation for updating FE models.

Visualization Statistics

As with the study of the Sandia test frame of Chapter 12, visualization statistics can be used to provide insight into how model predictions compare to the test data. Correlation coefficients and scaling factors, from Eqs. (10.1) and (10.2) respectively, are shown for the initial model in Figure 13.7.

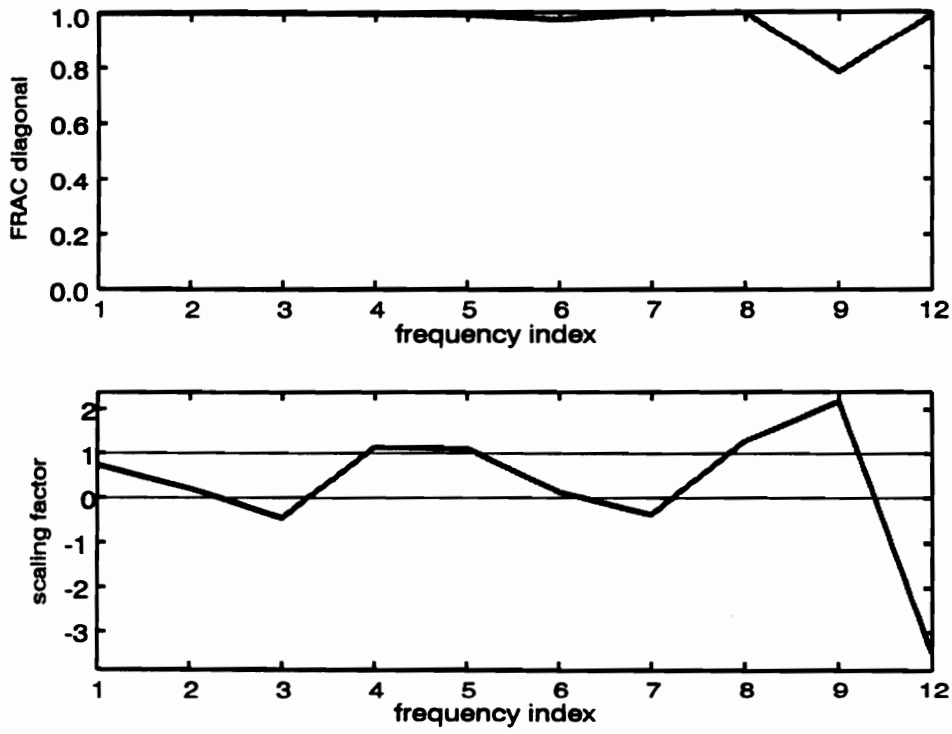

Figure 13.7: Visualization Statistics from Initial Model

From Figure 13.7, it is apparent that the *shapes* of the dynamic response predicted by the model are closely matched, but the relative amplitudes are not. Additionally, the predicted weight of the beam was 1168.3 g, a statistically significant 0.88% higher than the measured 1158.5 g.

Visualization statistics from the improved model are shown below in Figure 13.8. The measured response shapes again were again matched well, and the response amplitudes became much more accurate. The predicted weight of the beam dropped to 1158.4 g, a statistically insignificant 0.008% lower than the measured 1158.5 g.

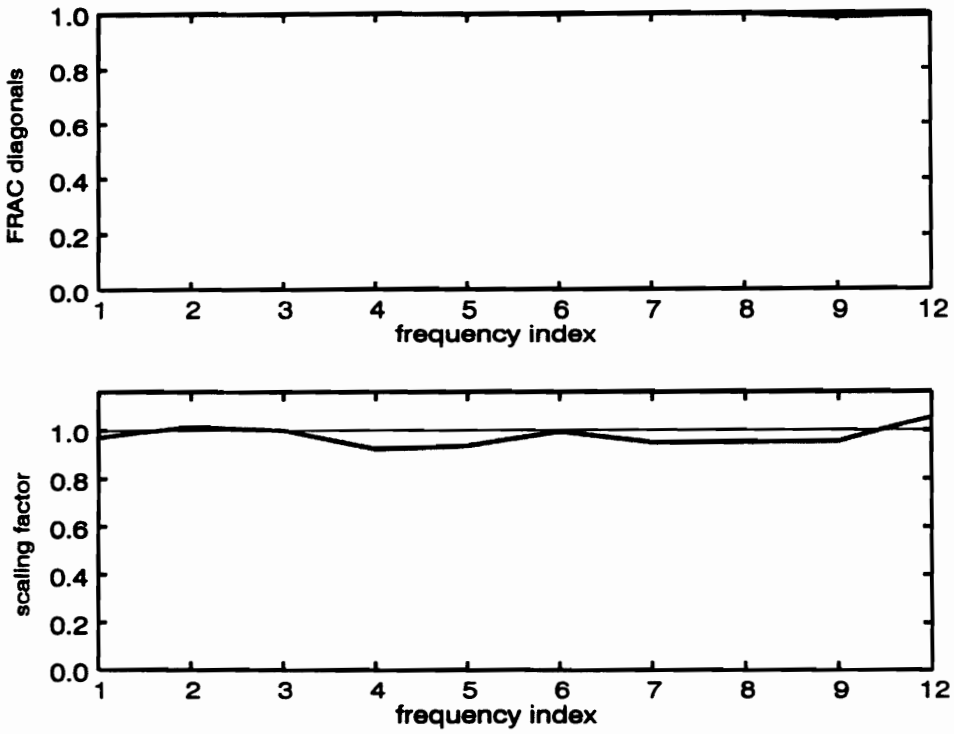

Figure 13.8: Visualization Statistics after Final Update

A second method by which the results can visually examined is the generation of response shape plots. This was impossible with the Sandia test frame of Chapter 12 due to the limited spatial resolution of the data and the complexity of the structure. However, response shape plots are quite easy to generate with the cantilever beam. Figure 13.9 and Figure 13.10 below show measured and predicted response shapes at both low and high excitation frequencies.

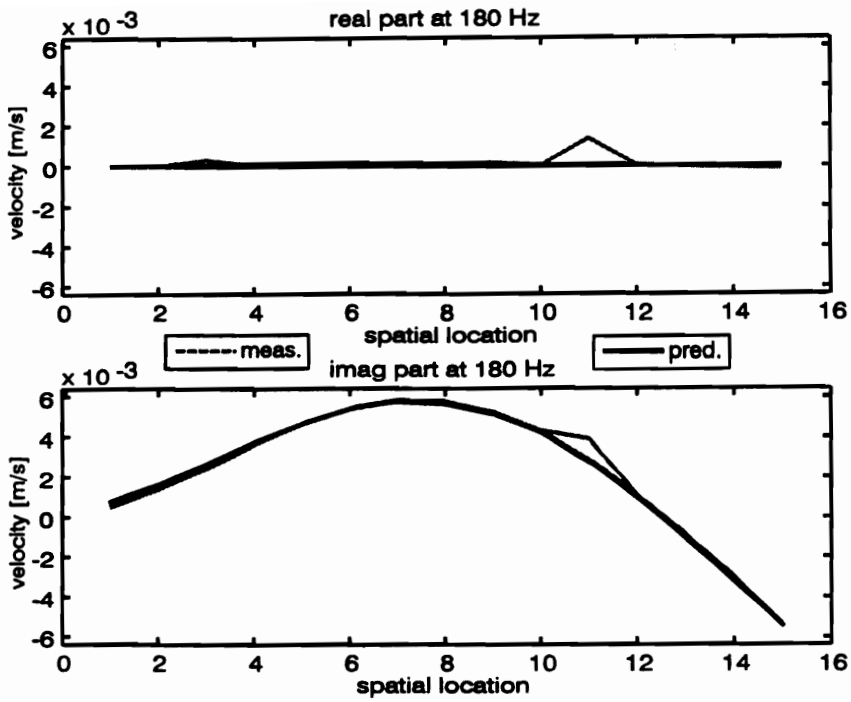

Figure 13.9: Low Frequency Response Shape

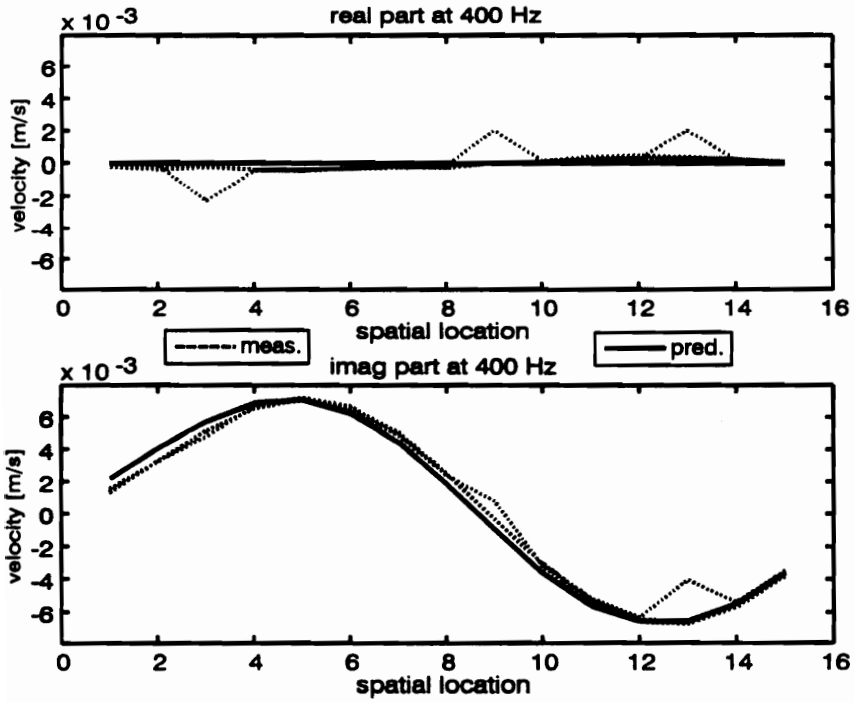

Figure 13.10: High Frequency Response Shape

It is clear from the low frequency plot of Figure 13.9 that the updated FE model is capable of predicting the behavior of the beam quite well at low frequencies. However, at the highest excitation frequency, there is a slight difference between the measured and predicted mode shapes. In particular, the model predicts more motion at the clamped end of the beam than was actually measured. This reason for this discrepancy is unknown, but it is probably due to the clamp exhibiting wave-like behavior of its own at the higher frequencies. When this happens, the simple translational and rotational spring system used to model the effect of the clamp on the beam becomes insufficient. Additionally, it is possible that a defect or irregularity in the beam caused the assumption of *uniform* beam properties to be invalid.

Model Verification

Parameter consistency checks were performed on the Bayesian parameter estimates to ensure that the results were consistent with the prior information. As mentioned earlier, results could not be obtained for the data-only case because of extreme ill-conditioning present in the problem. The chi-squared statistic of Eq. (9.12) came out at 5.50, which is well below the critical value of $\chi^2_{10,0.05} = 18.307$ for a 10 parameter analysis. This means that the updated parameter estimates are reasonable and realistic, making sense in light of the prior information.

A cross-validation test was perform in the same manner that the cross-validation test was performed for the sine-dwell results of Chapter 12. Here, the first nine frequencies were used to predict the response shape of the 12th excitation frequency. The cross-validation ratio $\left(\frac{SSE_{12}}{n_{y,12}}\right)\left(\frac{n_{y,1\text{-}9}}{SSE_{1\text{-}9}}\right)$ came out at 1.37, indicating a moderately

successful cross-validation test. This means that the model can be trusted to generate accurate dynamic response predictions at least up to 400 Hz. No further statements can be made about the predictive capability of the model without additional data.

Fortunately, there was additional data available on the cantilever beam. Early in the lab setup process, an HP FFT analyzer was used to roughly measure the first four natural frequencies of the beam. These results were compared to those computed using the updated modeling parameters. These results are given in Table 13.6. For verification purposes, natural frequency results were also computed using BEAM VI [94], an analysis package that can solve beam problems using both Euler-Bernoulli beam theory and shear deformation beam theory. The results between the FE model and the BEAM VI Euler-Bernoulli results match quite closely, as would be expected. In inclusion of shear deformation effects did not have a significant effect on the natural frequency estimates. The differences are quite small compared to the changes caused by the model update.

Table 13.6: Cantilever Beam Natural Frequencies

mode	from beam [Hz]	before update [Hz]	after update [Hz]		
	measured	FE model	FE model	BEAM VI Euler-Bernoulli	BEAM VI shear deformation
1	27.20 ± 0.25	30.64	27.20	27.20	27.20
2	174.50 ± 0.50	192.83	174.08	174.08	173.99
3	476.00 ± 1.00	540.64	483.64	483.64	483.08
4	956.00 ± 1.00	1058.25	915.58	915.57	913.86

From Table 13.6, it is apparent that the updated model predicted the natural frequencies of the first two modes much more accurately that the original model did. However, the updated model does *not* predict the natural frequencies of the third and fourth modes very accurately. Curiously, it *overpredicted* the third natural frequency and *underpredicted* the fourth natural frequency. As with the response shape plots, the reason for the inaccurate frequency predictions is not known, but they are probably due to wave-like behavior in the clamp or irregularities in the beam. It should be noted that the response shape plot of Figure 13.10 comes from an excitation frequency that is above the third natural frequency, which is a high enough frequency for the model to begin breaking down. The resulting difference between test and analysis can be seen in this plot.

13.3 Concluding Remarks on Test Beam

The use of the Bayesian regression model update formulation appeared to work quite well for the cantilevered beam. Accurate estimates for unknown parameters k_t and k_r were obtained, which was the primary purpose of the exercise. Additionally, estimates for E, ρ, and m_0 were either improved or verified. The data provided little information on the parameters γ, t, w, I_0, and k_s, but the use of prior information prevented the Bayesian regression formulation from generating meaningless estimates for these parameters. Indeed, leaving these parameters out of the analysis did not change the results, except to drop confidence interval sizes somewhat.

Time-invariance tests were used to determine whether or not the data were suitable for use in the model update. Parameter consistency checks were used to

ensure that the parameter estimates obtained were reasonable and realistic. The cross-validation test was used to confirm that the model did more than just predict the specific data set used in the model update.

The net conclusion of these tests was that the model could be used to predict the behavior of the cantilever beam up to 400 Hz. However, a study of the first four natural frequencies of the beam revealed that the model broke down at higher frequencies. The reason for this breakdown is unknown, but it is probably due to wave-like behavior in the clamp or irregularities in the beam. Nevertheless, for low frequencies, the predictive capability of the beam model was substantially *improved*.

PART V:

Conclusions and Recommendations

Chapter 14: Conclusions and Recommendations

14.1 Conclusions

Comments on Model Updating

This dissertation presented a Bayesian regression formulation for updating the modeling parameters used to build a finite element (FE) model. The model update procedure yields a model with substantially improved predictive capability along with statistically-qualified estimates of the updated modeling parameters.

With this information available, the analyst can determine whether or not the updated model is sufficiently correct for the modeling task at hand. If it is sufficiently correct, the analyst will have an improved basis on which to perform structural modification or optimization. If it is not sufficiently correct, the analyst knows that more modeling work or experimental work will be required to obtain a sufficiently correct model.

Summary of Dissertation

In Part I of this dissertation, the Bayesian regression formulation for model updating was introduced and placed in context with other model update formulations. In Part II, the complete Bayesian regression formulation was presented, covering the basic Bayesian regression theory, the signal processing techniques used to generate statistically-qualified frequency response data (both sine-dwell and FRF), and the

modeling techniques used to make finite element predictions of the data. Part III presented the numerical and statistical issues that must be addressed to develop a robust computer implementation of the model update process and to ensure that a valid model update is obtained.

Part IV of the dissertation provided three case studies involving implementations of the Bayesian regression formulation. The first study, which involved the successful update of a beam model using simulated data, was performed to verify confidence interval estimation procedures. In the second study, joint stiffness and beam cross-section parameters in a finite element model of a steel frame were updated to improve its predictive capability. Good results were obtained with both sine-dwell and FRF data. In the third study, stiffness parameters representing a clamp holding a cantilever steel beam were updated, as were other modeling parameters used to build the beam model. Significant improvements were made to several of the parameters, while the Bayesian regression formulation prevented the regression procedure from generating meaningless estimates for the non-significant parameters.

Contributions to the Field

Advancements made in this work include: (1) the formulation of a true Bayesian statistics analysis; (2) the use of experimentally-derived statistical weights; (3) the development of lack-of-fit compensation procedures; (4) the matrix-decomposition based reformulation of the Bayesian regression problem to improve numeric conditioning; and (5) the development of time-invariance tests and cross-validation tests.

Final Comments

To summarize, most of the goals of this research were met. The primary goal of updating finite element models with frequency response was accomplished successfully. Key to this goal were the sine-dwell and FRF statistics of Chapters 5 and 6, and with the Bayesian regression reformulation of Chapter 8. Without these parts of the research, none of the results of Chapters 11 through 13 would have been possible. The visualization and model verification statistics also worked well, although the performance of the lack-of-fit compensation coefficients of Chapter 9 was not entirely satisfactory.

It was discovered in the course of this research that parameter selection is *extremely* important to the task of model updating. Poor parameter selection can cause numerous difficulties when estimating parameters. It is also helpful to having accurate prior information.

14.2 Recommendations for Future Work

Expand Sine-Dwell Statistics

The sine-dwell statistics presented here were formulated for unscaled real and imaginary components of the single frequency response. A different formulation would use an amplitude/phase angle representation instead of the complex number representation. This formulation would work better in the resonance situations where the complex number formulation fails (see Chapter 5). However, dealing with phase angle wraparound becomes an issue, and the task of computing response sensitivities become more difficult. *Scaled* sine-dwell statistics (in which the response is divided

by the force amplitude) would also be worth investigating, as would multi-input multi-output (MIMO) formulations. These formulations would enable the analyst to use data many different form in additional to providing for more accurate data acquisition.

Expand FRF Statistics

A second area of investigation concerns statistics of the FRF. Bendat [72] and Yoshimura and Nagamatsu [67] addressed this issue in considerable detail, but the effects of leakage and data windowing techniques on variance estimates were not addressed. These considerations would allow proper weighting matrices to be used in the Bayesian regression formulation, instead of the approximate weighting matrices used in the FRF study of Chapter 12.

Lack-of-Fit Compensation

Another potential area of investigation would be techniques used to compensate for lack-of-fit. Two data rescaling coefficients were presented in this dissertation (see Chapter 9). Coefficient α_1 clearly worked better than α_2 in the case studies presented in Chapters 12 and 13, but coefficient α_2 has more "philosophical appeal." Resolving this difficulty might require alternative approaches to adjusting the data weighting matrix or even alternative approaches to computing confidence intervals.

Incorporate Robust Regression Techniques

The use of robust regression techniques [71] to fit time-series data coming from a sine-dwell test would also be worth investigating. The ordinary least-squares fit described in Chapter 5 works quite well for data having errors that are approximately

Gaussian. However, the scanning laser Doppler vibrometer (SLDV) can sometimes generate dropouts, which are brief duration spikes in the data having variances levels *much* greater than that found in the rest of the data. The use of robust regression techniques would increase the quality of the fit and reduce parameter variance estimates, allowing the data to contribute more to the Bayesian regression formulation.

Incorporate Spatial Error

Before a scanning LDV can be used to acquire test data from a structure, it must be *registered* in space relative to the structure. Specifically, this means determining the position and orientation (three translations and three rotations) of the SLDV assembly in structural coordinates. Earlier works by Zeng *et al* [95] and Montgomery and West [96] used a direct solution technique in which estimated ranges play in key role in solving this problem. Later works by Zeng [97] and Lindholm [98] use non-linear regression to estimate six laser locations parameters (three translations and three rotations). Because there are errors in the data used to estimate the position and orientation of the SLDV, estimates of *where* the laser beam measures velocities and the *direction* at which is measures can also have errors. A more complete model update algorithm would account for these potential sources of error.

Use Non-Gaussian Priors

In this dissertation, all prior information was assumed to come from Gaussian distributions. However, for parameters such as damping coefficients, more realistic

distributions such as the chi-squared or Weibull [77] might be useful, as they restrict allowable parameter values to positive numbers.

The primary disadvantage of using non-Gaussian priors is increased complexity in the Bayesian regression implementation. The *SSE* term of Eq. (3.17) would gain terms significantly more complicated than the squared/weighted residuals, and the *SSE* minimization would require a constrained optimization algorithm substantially more sophisticated than the simple parameter iteration of Eq. (3.18).

Final Comments

Of the recommendations for future work, incorporating spatial error is probably the most important. Spatial error is the most significant source of uncertainty *not* addressed in the research presented in this dissertation. The use of non-Gaussian priors and improved lack-of-fit compensation would also be a substantial improvements. The other recommendations are minor modifications to the Bayesian regression formulation that would enable the analyst to use test data more efficiently or to collect it more quickly.

References

[1] Imregun, M. and Visser, W. J., "A Review of Model Updating Techniques," *Shock and Vibration Digest*, Vol. 23, No. 1, January 1991, pp. 9-20.

[2] Allemang, R. J. and Ewins, D. J., "A Correlation Coefficient for Modal Vector Analysis," *Proceedings of the 1st International Modal Analysis Conference*, IMAC-I, SEM, 1983, pp. 110-116.

[3] Lieven, N. A. J and Ewins, D. J., "Spatial Correlation Coefficient of Mode Shapes, the Coordinate Modal Assurance Criterion (COMAC)," *Proceedings of the 6th International Modal Analysis Conference*, IMAC-VI, SEM, Kissimmee, FL, February 1988, pp. 690-695.

[4] Baker, M., "Review of Test/Analysis Correlation Methods and Criteria for Validation of Finite Element Models for Dynamic Analysis," *Proceedings of the 10th International Modal Analysis Conference*, IMAC-X, SEM, San Diego, CA, February 1992, pp. 985-991.

[5] Mottershead, J. E. and Friswell, M. I., "Model Updating in Structural Dynamics: A Survey," *Journal of Sound and Vibration*, Vol. 167, No. 2, 1993, pp. 347-375.

[6] Link, M., "Identification and Correction of Errors in Analytical Models using Test Data," *Proceedings of the 8th International Modal Analysis Conference*, IMAC-VIII, SEM, Kissimmee, FL, February 1990, pp. 570-578.

[7] Dascotte, E., "Practical Applications of Finite Element Model Tuning Using Experimental Modal Data," *Proceedings of the 8th International Modal Analysis Conference*, IMAC-VIII, SEM, Kissimmee, FL, February 1990, pp. 1032-1037.

[8] Natke, H. G., "Updating Computational Models in the Frequency Domain based on Measured Data: a Survey," *Probabilistic Engineering Mechanics*, Vol. 3, No. 1, March 1988, pp. 28-35.

[9] Zhang, L., "A Consistent Derivation and Assessment of Different Model Updating Procedures," *Proceedings of the 14th International Modal Analysis Conference*, IMAC-XIV, SEM, Detroit, MI, February 1996, pp. 769-775.

[10] Guyan, R. J., "Reduction of Stiffness and Mass Matrices," *AIAA Journal*, Vol. 3, No. 2, February 1965.

[11] Kammer, D. C., "Test-Analysis Model Development Using an Exact Modal Reduction," *International Journal of Analytical and Experimental Modal Analysis*, Society for Experimental Mechanics, Vol. 2, No. 4, Bethel, CT, October 1987, pp. 174-179.

[12] Avitabile, P. and Foster, T. J., "Evaluation of Degree of Freedom Based Vector Correlation Methods," *Proceedings of the 14th International Modal Analysis Conference*, IMAC-XIV, SEM, Detroit, MI, February 1996, pp. 1048-1056.

[13] O'Callahan, J., "A Procedure for an Improved Reduced System (IRS) Model," *Proceedings of the 7th International Modal Analysis Conference*, IMAC-VII, SEM, Las Vegas, NV, February 1989, pp. 17-21.

[14] Gordis, J. H., "An Analysis of the Improved Reduced System Modal Reduction Procedure," *Proceedings of the 10th International Modal Analysis Conference*, SEM, IMAC-X, San Diego, CA, February 1992, pp. 471-487.

[15] Freed, A. M. and C. C. Flanigan, "A Comparison of Test-Analysis Reduction Methods," *Proceedings of the 8th International Modal Analysis Conference*, IMAC-VIII, SEM, Kissimmee, FL, 1990, pp. 1344-1351.

[16] Hunt, D. L., "Application of an Enhanced Coordinate Modal Assurance Criterion," *Proceedings of the 10th International Modal Analysis Conference*, IMAC-X, SEM, San Diego, CA, February 1992, pp. 66-71.

[17] Lieven, M. A. J., and D. J. Ewins, "Expansion of Modal Data for Correlation," *Proceedings of the 8th International Modal Analysis Conference*, SEM, IMAC-VIII, Kissimmee, FL, February 1990, pp. 605-609.

[18] O'Callahan, J., Avitable, P., and Rimer, R., "System Equivalent Reduction Expansion Process (SEREP)," *Proceedings of the 7th International Modal Analysis Conference*, IMAC-VII, SEM, Las Vegas, NV, February 1989, pp. 29-37.

[19] O'Callahan, J. and Li, P., "SEREP Expansion," *Proceedings of the 14th International Modal Analysis Conference*, IMAC-XIV, SEM, Detroit, MI, February 1996, pp. 1258-1264.

[20] Baruch, M. and Bar Itzhack, Y., "Optimal Weighted Orthogonalization of Measured Modes," *AIAA Journal*, Vol. 16, No. 4, April 1978, pp. 346-351.

[21] Kabe, A. M, "Stiffness Matrix Adjustment Using Mode Data," *AIAA Journal*, Vol. 23, No. 9, September 1985, pp. 1431-1436.

[22] O'Callahan, J., "Determination of Analytical Model Differences Using Modal Updating," *Proceedings of the 8th International Modal Analysis Conference*, IMAC-VIII, SEM, Kissimmee, FL, February 1990, pp. 999-1003.

[23] Aiad, A., Level, P., and Ravalard, Y., "A Global Updating Procedure to Improve Finite Element Models," *Proceedings of the 10th International Modal Analysis Conference*, IMAC-X, SEM, San Diego, CA, February 1992, pp. 1051-1056.

[24] Conti, P. and Bretl, J., "Mount Stiffness and Inertia Properties for Modal Test Data," *Modal Testing and Analysis, Proceedings of the 11th Biennal Conference on Mechanical Noise and Vibration*, ASME, Vol. 3, December 1987, pp. 11-16.

[25] Ahmadian, H., Ismail, F., and Gladwell, G. M. L., "Acceptable Element Matrices for Finite Element Model Updating," ed. Bui, H. D., et al, *Inverse Problems in Engineering Mechanics* (reprinted from *Proceedings of the 2nd International Symposium on Inverse Problems*, ISIP '94, Paris, November 1994), A. A. Balkema, Rotterdam, 1994, pp. 209-213.

[26] Niedmal, M. and Luber, W., "Updating a Finite-Element Model by Means of Normal Mode Parameters," *Proceedings of the 8th International Modal Analysis Conference*, IMAC-VIII, SEM, Kissimmee, FL, February 1990, pp. 586-592.

[27] Jung, H. and Ewins, D.J., "Error Sensitivity of the Inverse Eigensensitivity Method for Model Updating," *Proceedings of the 10th International Modal Analysis Conference*, IMAC-X, SEM, San Diego, CA, February 1992, pp. 992-998.

[28] Ladeveze, P., Nedjar, D., and Reynier, M., "Updating of Finite Element Models Using Vibrations Tests," *AIAA Journal*, Vol 32., No. 7, July 1994, pp. 1485-1491.

[29] Nobari, A. S. and Ewins, D. J., "On the Effectiveness of Using Only Eigenvalues of Structural Model Updating Problems," *Shock and Vibration*, Vol. 1, No. 4, 1994, pp. 339-348.

[30] Lindholm, B. E. and West, R. L., "Determination of Suspension Effects by Direct Experiments and Comparisons to an Analytical Model," *Proceedings of the 12th International Modal Analysis Conference*, IMAC-XII, Honolulu, February 1994, pp. 262-268.

[31] Farhat, C. and Hemez, F. M., "Updating Finite Element Dynamic Models Using an Element-by-Element Sensitivity Methodology," *AIAA Journal*, Vol. 31, No. 9, September 1993, pp. 1702-1711.

[32] Hemez, F. M., "Closing the Gap Between Modal Parameter Based and Frequency Response Function Based Updating Methods," *Proceedings of the 13th International Modal Analysis Conference*, IMAC-XIII, SEM, Nashville, TN, February 1995, pp. 171-178.

[33] Hemez, F. M., "Advanced Tools for Updating Damped Finite Element Models Using Static, Modal, and Flexibility Data," *Proceedings of the 14th International Modal Analysis Conference*, IMAC-XIV, SEM, Detroit, MI, February 1996, pp. 511-517.

[34] Hasselman, T. K., "A Perspective on Dynamic Model Verification," *Modal Testing and Model Refinement*, ASME, Applied Mechanics Division, Vol. 59, November 1983, pp. 101-118.

[35] Beliveau, J. G., "System Identification of Civil Engineering Structures," *Canadian Journal of Civil Engineering*, Vol. 14, No. 1, January 1987, pp. 7-18.

[36] Link, M., "Requirements for the Structure of Analytical Models Used for Parameter Identification," ed. Tanaka, H. and Bui, H. D., *Inverse Problems in Engineering Mechanics* (from *Proceedings of IUTAM Symposium*, Tokyo, 1992), Springer-Verlag, New York, 1992, pp. 133-146.

[37] Dasacotte, E., Strobbe, J., and Hua, H., "Sensitivity-based Model Updating Using Multiple Types of Simultaneous State Variables," *Proceedings of the 13th International Modal Analysis Conference*, IMAC-XIII, SEM, Nashville, TN, February 1995, pp. 1035-1040.

[38] Hasselman, T. K. and Chrostowski, J. D., "A Recent Case Study in System Identification," *Proceedings of the 32nd AIAA/ASME/ASCE/AHS/ASC Structures, Structural Dynamics, and Materials Conference*, SDM-32, AIAA, Baltimore, MD, April 1991, pp. 2154-2168.

[39] *Engineering Mechanics Associates*, "SSID -- A Computer Code for Structural System Identification," Technical Report No. TR-91-1134-1, Sandia National Laboratories, Albuquerque, NM, March 1991.

[40] Martinez, D. R., Red-Horse, J. R., and Allen, J. J., "System Identification Methods for Dynamic Structural Models of Electronic Packages," *Proceedings of the 32nd AIAA/ASME/ASCE/AHS/ASC Structures, Structural Dynamics, and Materials Conference*, SDM-32, AIAA, Baltimore, MD, April 1991, pp. 2336-2346.

[41] Nefske, D. J. and Sung, S. H., "Correlation of a Coarse-Mesh Finite Element Model using Structural System Identification and a Frequency Response Assurance Criterion," *Proceedings of the 14th International Modal Analysis Conference*, IMAC-XIV, SEM, Detroit, MI, February 1996, pp. 597-602.

[42] Antonacci, E. and Vestroni, F., "Updating of Finite Element Models through Nonlinear Parametric Estimation," ed. Bui, H. D., et al, *Inverse Problems in Engineering Mechanics* (reprinted from *Proceedings of the 2nd International Symposium on Inverse Problems*, ISIP '94, Paris, November 1994), A. A. Balkema, Rotterdam, 1994, pp. 215-222.

[43] Link, M., Rohrmann, R. G., and Pietrzko, S., "Experience with Automated Procedures for Adjusting the Finite Element Model of a Complex Highway Bridge to Experimental Modal Data," *Proceedings of the 14th International Modal Analysis Conference*, IMAC-XIV, SEM, Detroit, MI, February 1996, pp. 218-223.

[44] Alvin, K. F., "Finite Element Model Update via Bayesian Estimation and Minimization of Dynamic Force Residuals," *Proceedings of the 14th International Modal Analysis Conference*, IMAC-XIV, SEM, Detroit, MI, February 1996, pp. 561-567.

[45] Larrson, P. O. and Sas, P., "Model Updating Based on Forced Vibration Testing Using Numerically Stable Formulations," *Proceedings of the 10th International Modal Analysis Conference*, IMAC-X, SEM, San Diego, CA, February 1992, pp. 966-974.

[46] Fritzen, C. P. and Kiefer, T., "Localization of Correction of Errors in Analytical Models," *Proceedings of the 10th International Modal Analysis Conference*, IMAC-X, SEM, San Diego, February 1992, pp. 1064-1071.

[47] Zimmerman, D. C., Simmermacher, T., and Kaouk, M., "Structural Damage Detection using Frequency Response Functions," *Proceedings of the 13th International Modal Analysis Conference*, IMAC-XIII, SEM, Nashville, TN, February 1995, pp. 179-184.

[48] Berger, H., et al, "Parametric Updating of Finite Element Models Using Experimental Simulation -- A Dynamic Reaction Approach," *Proceedings of the 8th International Modal Analysis Conference*, IMAC-VIII, SEM, Kissimmee, FL, February 1990, pp. 180-184.

[49] Yang, M. and Brown, D., "An Improved Procedure for Handling Damping During Finite Element Modal Updating," *Proceedings of the 14th International Modal Analysis Conference*, IMAC-XIV, SEM, Detroit, MI, February 1996, pp. 576-584.

[50] Schulz, M. J. and Thyagarajan, S. K., "Inverse Dynamic Design Technique for Model Correction and Optimization," *AIAA Journal*, Vol. 33, No. 8, August 1995, pp. 1486-1491.

[51] Schulz, M. J., Pai, P. F., and Abdelnaser, A. S., "Frequency Response Function Assignment Technique for Structural Damage Detection," *Proceedings of the 14th International Modal Analysis Conference*, IMAC-XIV, SEM, Detroit, MI, February 1996, pp. 105-111.

[52] Friswell, M. I. and Penny, J. E. T., "Updating Modal Parameters Directly from Frequency Response Function Data," *Proceedings of the 8th International Modal Analysis Conference*, IMAC-VIII, SEM, Kissimmee, FL, February 1990, pp. 843-849.

[53] Conti, P. and Donley, M., "Test-Analysis Correlation Using Frequency Response Functions," *Proceedings of the 10th International Modal Analysis Conference*, IMAC-X, SEM, San Diego, CA, February 1992, pp. 724-729.

[54] Imregun, M., "Three Case Studies in Finite Element Model Updating," *Shock and Vibration*, Vol. 2, No. 2, 1995, pp. 119-131.

[55] Zhang, Q., et al, "A Complete Procedure for the Adjustment of a Mathematical Modal from Identified Complex Modes," *Proceedings of the 5th International Modal Analysis*

Conference, IMAC-V, SEM, London, February 1987, pp. 1183-1190.

[56] Visser, W.J. and Imregun, M., "A Technique to Update Finite Element Models Using Frequency Response Data," *Proceedings of the 9th International Modal Analysis Conference*, IMAC-IX, SEM, February 1991, pp. 462-468.

[57] Imregum, M., Visser, W. J., and Ewins, D. J., "Finite Element Model Updating Using Frequency Response Function Data — I. Theory and Initial Investigation," *Mechanical Systems and Signal Processing*, Vol. 9, No. 2, March 1995, pp. 187-202.

[58] Imregum, M., Sanliturk, K. Y., and Ewins, D. J., "Finite Element Model Updating Using Frequency Response Function Data — II. Case Study on a Medium-Sized Finite Element Model," *Mechanical Systems and Signal Processing*, Vol. 9, No. 2, March 1995, pp. 203-213.

[59] Cogan, S., et al, "An Improved Frequency Response Residual for Model Correction," *Proceedings of the 14th International Modal Analysis Conference*, IMAC-XIV, SEM, Detroit, MI, February 1996, pp. 568-575.

[60] Reix, C., et al, "Updating the Damping Matrix using Frequency Response Data," *Proceedings of the 14th International Modal Analysis Conference*, IMAC-XIV, SEM, Detroit, MI, February 1996, pp. 585-590.

[61] Mottershead, J. E., and Foster, C. D., "On the Treatment of Ill-conditioning in Spatial Parameter Estimation from Measured Vibration Data," *Mechanical Systems and Signal Processing*, Vol. 5, No. 2, March 1991, pp. 139-154.

[62] Ibrahim, S. R., "Direct Updating on Non-Conservative Finite Element Models using Measured Input/Output Data," *Proceedings of the 10th International Modal Analysis Conference*, IMAC-X, SEM, San Diego, CA, February 1992, pp. 202-210.

[63] Bronowicki, A. J., Likich, M. S., and Kuritz, S. P., "Application of Physical Parameter Identification to Finite Element Models," *Proceedings of the 1st NASA/DOD CSI Technology Conference*, NASA, Norfolk, VA, November 1986, pp. 187-206.

[64] Koh, C. G. and See, L. M., "Identification and Uncertainty Estimation of Structural Parameters," *Journal of Engineering Mechanics*, Vol. 120, No. 6, June 1994, pp. 1219-1237.

[65] Brown, R. G. and Hwang, P. Y. C., *Introduction to Random Signals and Applied Kalman Filtering, 2nd Edition*, John Wiley & Sons, Inc., New York, NY, 1983.

[66] Mahnken, R. and Stein, E., "Gradient-Based Methods for Parameter Identification of Viscoplastic Materials," ed. Bui, H. D., et al, *Inverse Problems in Engineering Mechanics* (reprinted from *Proceedings of the 2nd International Symposium on Inverse Problems*, ISIP '94, Paris, November 1994), A. A. Balkema, Rotterdam, 1994, pp. 137-144.

[67] Yoshimura, T. and Nagamatsu, A., "Estimation of Variance of the Frequency Response Function and its Application to the Curve Fit," *Japanese Society of Mechanical Engineering International Journal*, JSME, Series III, Vol. 34, No. 2, 1991, pp. 227-232.

[68] Montgomery, D. M. and West, R. L., "Identification of Estimated Error Variance in Time Signal Coefficients of Laser Doppler Vibrometer Data," *Proceedings of the 13th International Modal Analysis Conference*, IMAC-XIII, SEM, Nashville, TN, February 1995, pp. 728-734.

[69] Montgomery, D. E., Lindholm, B. E., and West, R. L., "Monte Carlo Verification of the Multivariate Delta Method Variance Estimation of Harmonic Dynamic Response Coefficients," *Symposium on Optical Methods in Vibration and Noise*, 15th ASME Biennial Conference on Mechanical Vibration and Noise, Boston, MA, 1995.

[70] Zeng, X. and Wicks, A. L., "A Comparison of Two Methods for Estimating the Magnitude and Phase Angle of a Harmonic Wave," *Proceedings of the 11th International Modal Analysis Conference*, IMAC-XI, SEM, Kissimmee, FL, February 1993, pp. 906-912.

[71] Lopez Dominguez, J. C., *Reconstruction of 3-D Structural Dynamic Response Fields: an Experimental, Laser-Based Approach with Statistical Emphasis*, Department of Mechanical Engineering Ph.D. dissertation, Virginia Polytechnic Instititue and State University, Blacksburg, VA, August 1994.

[72] Bendat, J. S., "Statistical Errors in Measurement of Coherence Functions and Input/Output Quantities," *Journal of Sound and Vibration*, Vol. 59, No. 3, August 1978, pp. 405-421.

[73] Cobb, R. E., *Confidence Bands, Measurement Noise, and Multiple Input - Multiple Output Measurements Using the Three-Channel Frequency Response Function Estimator*, Department of Mechanical Engineering Ph.D. dissertation, Virginia Polytechnic Institute and State University, Blacksburg, VA, May 1988.

[74] Deaton, M. L., Reynolds, M. R., and Myers, R. H., "Estimation and Hypothesis Testing in Regression in the Presence of Nonhomogeneous Error Variances," *Communications in Statistics: Simulation and Computation*, Vol. 12, No. 1, March 1983, pp. 45-66.

[75] Williams, J. S., "The Variance of Weighted Regression Estimators," *Journal of the American Statistical Association*, Vol. 62, 1967, pp. 1290-1301.

[76] Jacquez, J. A. and Norusis, M, "Sampling Experiments on the Estimation of Parameters in Heteroscedastic Linear Regression," *Biometrics*, Vol. 29, No. 4, December 1973, pp. 771-779.

[77] Walpole, R. E. and Myers, R. H., *Probability and Statistics for Engineers, 4th Edition*, Macmillan Publishing Co., New York, 1989.

[78] Myers, R. H., *Classical and Modern Regression with Applications, 2nd Edition*, PWS-Kent Publishing Co., Boston, MA, 1990.

[79] Beck, J. V. and Arnold, K. J., *Parameter Estimation in Engineering and Science*, John Wiley & Sons, New York, NY, 1977.

[80] Golub, G. H. and Van Loan, C. F., *Matrix Computations, 2nd Edition*, Johns Hopkins University Press, Baltimore, MR, 1989.

[81] Bendat, J. S. and Piersol, A. G., *Random Data, Analysis and Measurement Procedures*, John Wiley & Sons, New York, NY, 1986.

[82] Ewins, D. J., *Model Testing: Theory and Practice*, Research Studies Press, Letchworth, Hertfordshire, England, 1984.

[83] Rubinstein, R. Y., *Simulation and the Monte Carlo Method*, John Wiley & Sons, New York, NY, 1981.

[84] Przemienicki, J. S., *Theory of Matrix Structural Analysis, 2nd Edition*, McGraw-Hill Book Publishing Co., New York, NY, 1985.

[85] Bathe, K., *Finite Element Procedures in Engineering Analysis*, Prentice-Hall, Inc., Englewood Cliffs, NJ, 1982.

[86] Rocklin, G. T., Crowley, J., and Vold, H., "A Comparison of H_1, H_2, and H_v Frequency Response Functions," *Proceedings of the 3rd International Modal Analysis Conference*, IMAC-III, SEM, February 1985, pp. 272-278.

[87] Mitchell, L. D. and Deel, J. C., "An Unbiased Frequency Response Function Estimator," *Proceedings of the 5th International Modal Analysis Conference*, IMAC-V, SEM, London, February 1987, pp. 364-373.

[88] Dongarra, J., et al, *LAPACK Users' Guide -- Release 2.0*, Society for Industrial and Applied Mathematics, Philadelphia, PA, 1995.

[89] Grace, A., *MATLAB Optimization Toolbox, version 1.0b*, The Mathworks, South Natick, MA, 1991.

[90] *MATLAB 4.2c Users Manual, for UNIX Workstations*, The Mathworks, Inc., Natick, MA, 1994.

[91] Woon, C. E. and Mitchell, L. D., "Variations in Structural Dynamic Characteristics Caused by Changes in Ambient Temperatures: I. Experimental," *Proceedings of the 14th International Modal Analysis Conference*, IMAC-XIV, SEM, Detroit, MI, February 1996, pp. 963-971.

[92] Lindholm, B. E., *Reconciliation of a Rayleigh-Ritz Beam Model with Experimental Data*, Department of Mechanical Engineering M.S. thesis, Virginia Polytechnic

Institute and State University, Blacksburg, VA, September 1994.

[93] Budinski, K. G., *Engineering Materials: Properties and Selection, Third Edition*, Prentice-Hall, Englewood Cliffs, NJ, 1989.

[94] Mitchell, L. D., et al, *BEAM VI* (software), Department of Mechanical Engineering, Virginia Polytechnic Institute and State University, Blacksburg, VA, 1992.

[95] Zeng, X., Mitchell, L. D., and Agee, B. L., "A Laser Position Determination Algorithm for an Automated Mechanical Mobility Measurement System," *Proceedings of the 11th International Modal Analysis Conference*, IMAC-XI, Kissimmee, FL, February 1993, pp. 122-129.

[96] Montgomery, D. E. and West, R. L., "Position Registration of Scanning Lasers for Experimental Spatial Dynamics Modeling," *Proceedings of the ASME Conference on Design Automation*, ASME, 1994.

[97] Zeng, X., *The Estimation and Statistical Inferences of the Position and Orientation of a Scanning Laser Doppler Vibrometer*, Department of Mechanical Engineering Ph.D. dissertation, Virginia Polytechnic Institute and State University, Blacksburg, VA, November, 1994.

[98] Lindholm, B. E., "Three-Dimensional Position Registration of a Laser Doppler Vibrometer," *Proceedings of the 14th International Modal Analysis Conference*, IMAC-XIV, Detroit, MI, February 1996, pp. 830-836.

Appendices

Appendix A: Estimation Methodologies

MAXIMUM LIKELIHOOD (ML) ESTIMATION

In a regression problem, we typically have a data vector y that we are trying to fit using a parameter vector p. If the measurements errors are additive and come from a known multivariate normal distribution described by the variance-covariance $\mathrm{Var}[\hat{p}]$, we can define a probability distribution function (PDF) for the data as a function of the parameter vector p_{true} (which provides the true data vector y_{true}). This PDF is given in Eq. (A.1), where $W_y = \mathrm{Var}^{-1}[y]$. The notation $f(y|p)$ indicates a conditional probability, where we have the PDF of y given a fixed p [79].

$$f(y|p_{true}) = \sqrt{\frac{\det(W_y)}{(2\pi)^{n_y}}} \exp\left(-\frac{1}{2}(y - y_{true})^{\mathrm{T}} W_y (y - y_{true})\right) \tag{A.1}$$

In regression, we approach this problem in reverse. Instead of knowing the true parameter vector p_{true} and looking for possible data sets, we try to find an estimated parameter vector $\hat{p}$ using only the single data set that we have measured. We are therefore looking for the vector $\hat{p}$ that is *most likely* to have given us the actual data that was measured, i.e., we want to maximize the likelihood function $L(\hat{p}|y_{meas})$ (which has the same form as $f(y|p)$, except that $\hat{p}$ is variable while y is fixed). Equation (A.2) gives the appropriate likelihood function, where $\hat{y}$ is a function of $\hat{p}$.

$$L(\hat{p}|y_{meas}) = \sqrt{\frac{\det(W_y)}{(2\pi)^{n_y}}} \exp\left(-\frac{1}{2}(y_{meas} - \hat{y})^{\mathrm{T}} W_y (y_{meas} - \hat{y})\right) \tag{A.2}$$

Maximizing Eq. (A.2) is not an easy task because it contains a matrix exponential and is very poorly conditioned in regions away from the solution. However, we can find the maximum of $L(\hat{p}|y_{meas})$ by instead maximizing the natural logarithm of $L(\hat{p}|y_{meas})$. Equation (A.3) shows this simplified objective function.

$$\ln(L(\hat{p}|y)) = -\frac{1}{2}\left(n_y \ln(2\pi) - \ln(\det(W_y)) + (y_{meas} - \hat{y})^{\mathrm{T}} W_y (y_{meas} - \hat{y})\right) \tag{A.3}$$

Most of the terms of Eq. (A.3) are constant. To maximize $L(\hat{p}|y_{meas})$, it is only necessary to minimize $(y_{meas} - \hat{y})^{\mathrm{T}} W_y (y_{meas} - \hat{y})$, which is the term minimized in standard weighted least-squares. Because W_y is positive definite (always the case in statistics problems), the minimization can be easily accomplished using a number of different optimization algorithms. The estimated parameter vector $\hat{p}$ is known as the *maximum likelihood* estimate.

MAXIMUM A POSTERIOR (MAP) ESTIMATION

If we have prior knowledge concerning the parameters, we can combine this information with the data-based PDF to obtain results with Bayesian statistics. The fundamental theorem used to derive Bayes' rule is the conditional probability statement given in Eq. (A.4). If we rearrange Eq. (A.4), we can generate an alternate form of $f(\hat{p}|y_{meas})$ which includes prior knowledge $f(\hat{p})$, as opposed to using the likelihood function of Eq. (A.2). This results in the PDF of Eq. (A.5). Instead of

assuming a fixed parameter vector, we assume that it is a random variable, just as we do with the data vector. The "reversal" in thinking used with the maximum likelihood approach is no longer necessary.

$$f(\hat{p}|y_{meas})f(y_{meas}) = f(y_{meas}|\hat{p})f(\hat{p}) \tag{A.4}$$

$$f(\hat{p}|y_{meas}) = \frac{f(y_{meas}|\hat{p})f(\hat{p})}{f(y_{meas})} \tag{A.5}$$

Again, the PDF $f(y_{meas}|\hat{p})$ has the exact same form as Eq. (A.2). The PDF $f(\hat{p})$ (representing our knowledge of the parameters *before* analyzing any data) is given below in Eq. (A.6), where $W_p = \mathrm{Var}^{-1}[p_0]$. The parameters are assumed to come from a multivariate normal distribution. The vector p_0 and matrix $\mathrm{Var}[p_0]$ specify a set of estimated means and variances that comprise our prior knowledge. This is also called *a priori* knowledge.

$$f(\hat{p}) = \sqrt{\frac{\det(W_p)}{(2\pi)^{n_p}}}\exp\left(-\frac{1}{2}(p_0-\hat{p})^{\mathrm{T}}W_p(p_0-\hat{p})\right) \tag{A.6}$$

Bayes' theorem combines information coming from the data with the prior knowledge to form the *a posterior* distribution. If we find the parameter vector that maximizes the values of this PDF, we will have found the *maximum a posterior* estimate. Again, this can be accomplished most easily by taking the natural logarithm of Eq. (A.5), as shown in Eq. (A.7).

$$\begin{aligned}\ln(f(p|y)) = &-\frac{1}{2}\big[(n_y+n_p)\ln(2\pi) - \ln(\det(W_y)) - \ln(\det(W_p)) \\ &+ (y_{meas}-\hat{y})^{\mathrm{T}}W_y(y_{meas}-\hat{y}) + (p_0-\hat{p})^{\mathrm{T}}W_p(p_0-\hat{p})\big] - \ln(f(y))\end{aligned} \tag{A.7}$$

And again, most of the terms in this expression are constant with respect to the parameters. Therefore, to maximize $f(\boldsymbol{p}|\boldsymbol{y})$, we need to minimize only the expression $(\boldsymbol{y}_{meas} - \hat{\boldsymbol{y}})^{\mathrm{T}} \boldsymbol{W}_y (\boldsymbol{y}_{meas} - \hat{\boldsymbol{y}}) + (\boldsymbol{p}_0 - \hat{\boldsymbol{p}})^{\mathrm{T}} \boldsymbol{W}_p (\boldsymbol{p}_0 - \hat{\boldsymbol{p}})$, which can be readily accomplished using a number of different optimization algorithms.

Appendix B: FFT Orthogonality

INTRODUCTION

In Chapter 6, a statement was made that the FFT algorithm was equivalent to an orthogonal least-squares fit of sine and cosine terms. This subject was also addressed by Zeng and Wicks [70], who reached the same conclusion. A MATLAB [90] script file that shows this equivalency is given below in Table B.1.

Table B.1: FFT / Least-Squares Equivalency Script

```
% perform fft on random data using fft and least-squares

n = input('length of vector?  ');
y = randn(n,1)    % time series data

X = zeros(n,n);
X(:,1) = ones(n,1);
x = [0:(2*pi/n):((2*n-2)*pi/n)]';
X(:,2) = cos(n*x/2);
for i = 1:(n/2-1)
  X(:,2*i+1) = cos(i*x);
  X(:,2*i+2) = sin(i*x);
end
outfft = fft(y), % basic fft result
outls = X\y,     % least-squares coefficients

% rearrange each result to get the other

outls2 = zeros(n,1);
outls2(1) = real(outfft(1)/n);
outls2(2) = real(outfft(n/2+1)/n);
for i = 1:(n/2-1);
  outls2(2*i+1) = real(outfft(i+1))*2/n;
  outls2(2*i+2) = -imag(outfft(i+1))*2/n;
end
outls2,          % least-squares coefficients coming from fft results

outfft2 = zeros(n,1);
outfft2(1) = outls(1)*n;
outfft2(n/2+1) = outls(2)*n;
for i = 1:(n/2-1);
  outfft2(i+1) = (outls2(2*i+1) - sqrt(-1)*outls2(2*i+2))*n/2;
  outfft2(n+1-i) = (outls2(2*i+1) + sqrt(-1)*outls2(2*i+2))*n/2;
end
outfft2,         % fft results coming from least-squares coefficients
```

In MATLAB, the apostrophe mark indicates a matrix transpose, and the expression "`p = X\y`" is equivalent to "`p = inv(X'*X)*X'*y`", except that a more efficient and accurate QR-decomposition based algorithm (described by Golub and Van Loan [80] and in Chapter 8) is used.

The coefficients coming from the least-squares analysis (vector `outls`) do not initially look like the numbers coming from the FFT (vector `outfft`). However, if the numbers are rearranged and rescaled as given by vectors `outls2` and `outfft2`, they are shown to be equivalent. Sample output of the MATLAB script for a four point data vector is shown in Table B.2.

Table B.2: Equivalency Script Output

```
y =
   -0.6965
    1.6961
    0.0591
    1.7971

outfft =
   2.8558
  -0.7556 + 0.1009i
  -4.1307
  -0.7556 - 0.1009i

outls =
    0.7139
   -1.0327
   -0.3778
   -0.0505

outls2 =     % based on outfft
    0.7139
   -1.0327
   -0.3778
   -0.0505

outfft2 =    % based on outls
   2.8558
  -0.7556 + 0.1009i
  -4.1307
  -0.7556 - 0.1009i
```

If the matrix `inv(X'*X)` is computed, it *always* comes out to be a diagonal matrix. This implies that the coefficients coming from the least-squares fit are

statistically independent, meaning that potential errors from one coefficient to the next are uncorrelated. This, in turn, means that terms coming from an FFT analysis will also have uncorrelated errors, even between real and imaginary parts.

Because FFT results corresponding to a given frequency are never recombined with results corresponding to any other frequency during the signal processing computations, each spectral line bin of the resulting FRF remains statistically independent from all other spectral lines. This argument cannot be applied to the real and imaginary parts from a single spectral line, since they are multiplied together during the signal processing computations. However, using arguments from Bendat [81], it can be shown that the final real and imaginary components of the FRF are statistically independent for the H_1 FRF estimator, as was done in Chapter 6.

Appendix C: Model Update Algorithm

INTRODUCTION

Chapters 3 and 8 together in effect describe an algorithm for estimating design parameters using a Bayesian regression approach. This appendix lists pseudo-code extracted from the actual MATLAB [90] script file used for this purpose. The pseudo-code is given below in Table C.1.

Table C.1: Bayesian Regression Parameter Estimation Algorithm

```
input: z_input (input parameter vector)
       y_meas  (measured data vector)
       C_y     (cholesky decomposition of data weighting matrix)
       C_p     (cholesky decomposition of prior weighting matrix)
       alpha   (data downweighting coefficient)
subroutines: FEM (compute response vector y_hat)
             FEM_grad (compute response sensitivity matrix X)
             SSE (compute Bayesian sum-of-squares error)
Copyright:   Brian E. Lindholm, 1996.

z_old = z_input;
y_hat = FEM(z_input);
X = FEM_grad(z_input);
I_n = eye(num_vars); % identity matrix
zeros_n = zeros(num_vars, 1); % vector of zeros
y_meas_star = [alpha * C_y * y_meas; zeros_n];

while (not done) and (count < maxiters)

  X_star = [alpha * C_y * X_old * inv(C_p); I_n];
  y_hat_star = [alpha * C_y * y_hat; z_old];
  step = X_star \ (y_meas_star - y_hat_star);

  if (norm(step) > sqrt(num_vars))
    step = step / norm(step) * sqrt(num_vars); % restrict initial step
  endif
  z_new = z_old + step; count = count + 1;
  done = (norm(step) < tolerance);
  reduced = (SSE(z_new) < SSE(z_old);

  while not (reduced or done)
    step = step / 2;
    z_new = z_old + step; count = count + 1;
    done = (norm(step) < tolerance); % test for convergence
    is_reduced = (SSE(z_new) < SSE(z_old); % test for SSE reduction
  endwhile

  z_old = z_new;
  y_hat = y_new;
  X = FEM_grad(z_new);

endwhile
return(z_old, X_star'*X_star);
```

As mentioned in Appendix B, in MATLAB the apostrophe mark indicates a matrix transpose, and expressions similar to "`step = X\y`" are equivalent to the least-squares "`step = inv(X'*X)*X'*y`", except that MATLAB uses a more efficient and accurate QR-decomposition based algorithm (described by Golub and Van Loan [80] and used in Chapter 8) instead of matrix inversion.

The algorithm given in Table C.1 utilizes line searches, parameter rescaling, and the QR decomposition algorithm. It is quite robust and will always converge to a solution, although the solution can sometimes be a non-optimal local minimum rather than the global minimum.

Appendix D: Using the Scanning LDV

SCANNING LDV REGISTRATION

In order to use the scanning laser-Doppler vibrometer (LDV) for data acquisition purposes (as was done in Chapter 13), it is necessary to *register* the location of the LDV unit in space *relative* to the test structure. Without this information, it is impossible to determine at what point on the structure data is being acquired or at what angle the laser beam is striking the structure. This information is required if predictions are to be made of what the laser beam "sees."

To locate the LDV in space, the laser beam was "manually" aimed at seven different points of *known* location on the structure. The scanning angle pair for each point was carefully recorded and used to estimate the location of the LDV in space relative to the structure. This was accomplished with a MATLAB-based implementation of a registration algorithm developed by Lindholm [98]

Once this was done, it became possible to use the registration information to compute the scanning angles required to hit *other* points on the structure, as also described by Lindholm [98]. In Chapter 13, this procedure was used to acquire data at points on the structure corresponding a subset of the FE model nodal points. Table D.1 below shows the results of the LDV registration procedure.

Table D.1: LDV Registration Results

location parameter	value	C.I.
x_0	0.003 m	±0.009 m
y_0	0.587 m	±0.013 m
z_0	2.013 m	±0.005 m
ϕ_1	-0.189 rad	±0.013 rad
ϕ_2	2.781 rad	±0.006 rad
ϕ_3	2.962 rad	±0.012 rad

As can be seen in Table D.1, the position and rotation the LDV assembly (as measured in the structural coordinate system given in Figure 13.1 and Figure 13.2) has been measured quite accurately. There were no perceptible errors in where rays hit when aimed at points on the beam.

Appendix E: Cantilevered Beam Priors

INTRODUCTION

In Chapter 13, priors for several parameters had to be obtained. These included the effective translational stiffness k_t and rotational stiffness k_r of the clamp, beam thickness t and width w, the effective mass m_0 and rotatory inertia I_0 of the transducers, and the effective rotational stiffness k_s of the stinger.

EFFECTIVE CLAMP STIFFNESSES

To find the effective translational stiffness of the clamp, k_t, the clamp was crudely modeled as a pinned-pinned beam (length 0.1 m, width 0.05 m, thickness 0.015 m) with a load applied in the center. For a material modulus of elasticity of 2.0×10^{11} N/m^2, an effective translational stiffness of 1.35×10^8 N/m is obtained.

For the effective rotational stiffness of the clamp, k_r, the clamp was crudely modeled as a cantilever beam of the same dimensions. In this case, an effective rotational stiffness of 2.8×10^4 N·m/rad was obtained. These results were summarized below in Eq. (E.1). It should be noted that these estimates are quite rough and probably cannot be trusted to be accurate within even a factor of 10. Thus, confidence interval sizes of $\pm 10000\%$ were assigned to these parameters.

$$\begin{aligned} k_t &= 1.35 \times 10^8 \text{ N/m } (\pm 10000\ \%) \\ k_r &= 2.8 \times 10^4 \text{ N·m/rad } (\pm 10000\ \%) \end{aligned} \tag{E.1}$$

Beam Thickness and Width

The thickness of the beam (nominally 0.25 in.) was carefully measured with a micrometer at a number of locations, while the width of the beam (nominally 1.50 in.) was measured with a tape measure. The results are given in Eq. (E.2), with confidence interval sizes assumed to be half the size of the smallest increment on the measuring devices.

$$\begin{aligned} t &= 0.00640 \text{ m } (\pm 0.00002 \text{ m}) \\ w &= 0.0381 \text{ m } (\pm 0.0002 \text{ m}) \end{aligned} \tag{E.2}$$

Tip Mass And Rotatory Inertia

The mass of the force gauge was measured to be 23.1 ± 0.1 g, while the mass of the accelerometer was measured to be 2.3 ± 0.1 g. In a standard test configuration, half of the force gauge mass is *isolated* from the system because it is on the other side of the piezoelectric core of the transducer. Thus, only half of the force gauge mass is added to the tip of the beam, while the entire mass of the accelerometer is added. Out of these considerations comes the prior estimate given in Eq. (E.3) below. The broad confidence interval of $\pm 20\%$ was arbitrarily picked as a safe estimate of how far the true effective mass of the force gauge might be away from a perfect 50% effective mass.

$$m_0 = 0.01385 \text{ kg } (\pm 20\%) \tag{E.3}$$

A small experiment was performed (after the model update of Chapter 13 was complete) to obtain an independent measure of the tip mass. The test configuration of Figure E.1 was used.

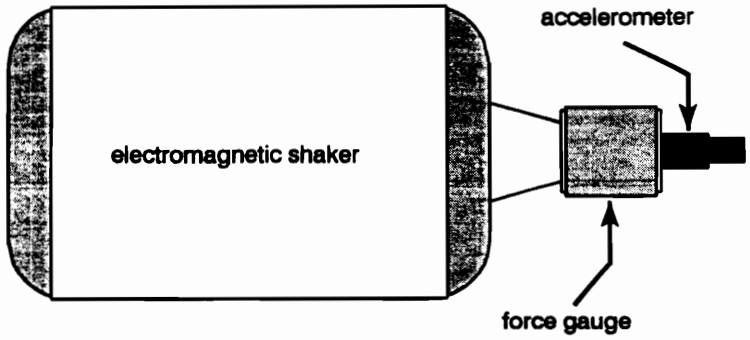

Figure E.1: Test Configuration for Effective Mass Testing

This test yielded a effective mass (of force gauge and accelerometer combined) of $m_0 = 0.0132$ kg. This is somewhat lower than the estimate given in Eq. (E.3), but compared well with the estimate given in Table 13.4 of Chapter 13.

The rotatory inertia was computed by assuming that the force gauge (radius 8 mm and height 8 mm) and accelerometer (radius 4 mm and height 9 mm) were cylinders of uniform density rotating about the neutral axis of the beam. Each cylinder rested on the surface of the beam, separated from the neutral axis by a distance of 3 mm), which yielded the effective rotatory inertia given in Eq. (E.4).

$$I_0 = 4.25 \times 10^{-6}\ \text{kg}\cdot\text{m}^2\ (\pm 20\%) \qquad \textbf{(E.4)}$$

Again, a fairly broad confidence interval was assigned to the rotatory inertia estimate, primarily because of uncertainty about how mass is actually distributed within the transducers, as opposed to the assumption of uniform density. The

assumptions of perfectly cylindrical geometry and the rough dimension measurements were also potential sources of error in the estimate.

STINGER STIFFNESS

For purposes of estimating rotational stiffness, the metallic stinger used to attach the electromagnetic shaker to the force gauge was modeled as a cantilever beam with a moment applied at the end. With a cylindrical cross-section (diameter 1 mm) and a length of 32 mm, the estimated rotational stiffness of the stinger was computed, yielding the result given in Eq. (E.5). Again, a confidence interval size of $\pm 20\%$ was assigned.

$$k_s = 0.328 \text{ N}\cdot\text{m/rad } (\pm 20\ \%) \tag{E.5}$$

Vita

Brian Eric Lindholm was born November 8, 1967 in Jacksonville, Arkansas. His early childhood was spent in Chattanooga, Tennessee, while his later childhood years were spent in Midlothian, Virginia. He graduated from Clover Hill High School in June of 1986.

He then enrolled at Virginia Tech, where he completed his B.S. degree in Mechanical Engineering in May of 1991. He continued at Virginia Tech and completed his M.S. degree in Mechanical Engineering in September of 1994 and his Ph.D. degree in Mechanical Engineering in August of 1996. Later that month, he began work with the Corporate Research and Development division of the General Electric Company in Schenectady, New York.

Brian E. Lindholm